Molecular actors of Chloroplast-Mitochondrion energetic interactions in the marine diatom Phaeodactylum tricornutum

Davide Dal Bo

▶ **To cite this version:**

Davide Dal Bo. Molecular actors of Chloroplast-Mitochondrion energetic interactions in the marine diatom Phaeodactylum tricornutum. Vegetal Biology. Université Grenoble Alpes, 2019. English. NNT : 2019GREAV048 . tel-02902971

HAL Id: tel-02902971

https://theses.hal.science/tel-02902971

Submitted on 20 Jul 2020

THÈSE

Pour obtenir le grade de

DOCTEUR DE LA COMMUNAUTE UNIVERSITE GRENOBLE ALPES

Spécialité : **Biologie Végétale**

Arrêté ministériel : 25 mai 2016

Présentée par

Davide DAL BO

Thèse dirigée par **Gilles CURIEN, Chargé de Recherche, CNRS** codirigée par **Giovanni FINAZZI, Directeur de Recherche, CNRS**

préparée au sein du **Laboratoire de Physiologie Cellulaire et Végétale** dans **l'École Doctorale Chimie et Sciences du Vivant**

Acteurs moléculaires des interactions énergétiques entre le chloroplaste et la mitochondrie chez la diatomée marine *Phaeodactylum tricornutum*

Thèse soutenue publiquement le **29 Novembre 2019** devant le jury composé de :

M, David, MACHEREL
Professeur, Université d'Angers, Président
Mme, Claire, REMACLE
Professeur, Université de Liège, Rapporteur
M, Tomas, MOROSINOTTO
Professeur, Università degli Studi di Padova, Rapporteur
M, Robert BLANVILLAIN
Professeur Associé, Université Grenoble Alpes, Examinateur
M, Olivier LEROUXEL
Maitre de Conférence, Université Grenoble Alpes, Examinateur

Index

Abstract

Molecular actors of Chloroplast-Mitochondrion energetic interactions in the marine diatom *Phaeodactylum tricornutum*

To produce the energy needed for cell metabolism, eukaryotic photosynthetic organisms rely on two organelles: the chloroplast and the mitochondrion. The former converting light energy into chemical energy, the latter performing cell respiration. Since both organelles have overlapping function, their activities need to be regulated. In Diatoms the direct exchange of ATP and reducing equivalents between these two organelles are essential for the cell's survival. Although the physiology of this energetic crosstalk is well established, the molecular actors of this process are still unknown. During this PhD project, I have selected four candidate proteins from the diatom model *Phaeodactylum tricornutum*, which turned out to play a role in the organelles' cross talk mechanisms. These are transporters predicted to be located within the chloroplast envelope and the inner membrane of the mitochondrion. To understand their physiological role, we compared the photosynthetic performances of the wild type and the mutant strains with spectroscopic and fluorescence approaches, while the respiration was quantified measuring the oxygen evolution rates. The observed differences suggest that the selected transporters play a role the chloroplast-mitochondrion crosstalk and that other proteins might be involved in this regulative process.

The further characterization of these transporters might also validate them as possible targets to improve algal biomass productivity for biotech, promoting the simultaneous use of respiration and photosynthesis (mixotrophy).

Résumé

Acteurs moléculaires des interactions énergétiques entre le chloroplaste et la mitochondrie chez la diatomée marine *Phaeodactylum tricornutum*

Pour produire l'énergie nécessaire au métabolisme cellulaire, les eucaryotes photosynthétiques se servent de deux organites : le chloroplaste et la mitochondrie. Le premier est capable de convertir l'énergie lumineuse en énergie chimique et le deuxième est le lieu de la phosphorylation oxydative. Puisque les deux organites partagent la même fonction de production d'énergie, leurs activités doivent être régulées. Chez les diatomées, l'échange direct de ATP et de pouvoir réducteur entre ces organites est essentiel pour assurer la survie de la cellule. Bien que cette interaction énergétique ait été caractérisée d'un point de vue physiologique, les acteurs moléculaires responsables de ce processus restent encore inconnus. Dans le cadre de mon projet de thèse, quatre protéines candidates ont été sélectionnées et étudiées chez la diatomée *Phaeodactylum tricornutum* pour déterminer leur implication dans les échanges énergétiques entre ces deux organites. Ces protéines sont des transporteurs localisés au niveau de l'enveloppe chloroplastique et de la membrane interne de la mitochondrie. Pour comprendre leur rôle physiologique, les souches mutantes correspondantes ont été générées. La capacité photosynthétique et la respiration cellulaire de ces mutants ont été évaluées par des approches de fluorescence, de spectroscopie, ou de mesure du taux d'évolution de l'oxygène. Ces mesures suggèrent que les transporteurs sélectionnés contrôlent en partie les mécanismes des échanges énergétiques entre le chloroplaste et la mitochondrie bien que d'autres protéines (non identifiées) semblent aussi impliquées dans cette régulation. Une caractérisation plus avancée de ces transporteurs pourrait permettre d'augmenter la production de biomasse des microalgues dans le cadre d'applications biotechnologiques, en favorisant l'utilisation simultanée de la respiration et de la photosynthèse (mixotrophie).

Chapter 1

1.1   Introduction

After the first appearance of oxygenic phototrophs, the oxygen concentration in the atmosphere largely increased, challenging the survival of most living organisms due to the strong oxidising properties of this molecule. This event shaped life as we know it today, since the vast majority of non-photosynthetic species currently rely on oxygen of photosynthetic origin for their metabolic processes. Unlike land plants, where 99% of species belong to Embryophyta, photosynthetic microalgae are a very diverse group of organisms, divided in twelve different phyla (Decelle et al., 2015) and they contribute almost as much to the global oxygen production and carbon assimilation as the land forests, despite representing only 1% of photosynthetic global biomass (Field et al., 1998). Even if all photosynthetic eukaryotic species share the same building blocks of photosynthesis (photosystems to harvest and photochemically convert light energy, a cytochrome complex for proton to electron coupling, the ATP synthase, etc), they present distinct light harvesting accessory pigments, peculiar thylakoid membrane topologies (Flori et al., 2017) and have developed different strategies to regulate and optimize photosynthesis according to their evolutionary history and their living environment.

Photosynthesis is a series of reactions converting light into chemical potential, which is used in downstream cell metabolism. Absorbed photons provide the energy needed to start a linear electron flow across the photosynthetic (thylakoids) membrane, eventually generating NADPH, the redox currency of the cell. This process is coupled with pumping of protons from the stroma to the thylakoid lumen, driving the production of ATP. In oxygenic photosynthesis, photosystems (PS) I and II contain special pairs of chlorophylls, called P700 and P680 respectively, which, when at the oxidised state, are able to oxidise stable molecules. The absorbed photons provide the energy needed to modify the redox potential of these chlorophylls. Once at the excited state, these molecules are able to reduce electron carriers with

a positive redox potential (Em), and thus allowing the production of NADPH at the expense of H_2O oxidation. The overall process occurs via several steps collectively called "linear electron flow" (LEF). Besides the two PS, cytochrome b_6f is involved in LEF, contributing to the acidification of the thylakoid lumen while oxidising plastoquinols, membrane embedded electron carriers reduced by PSII. By consuming the proton gradient, ATP synthase CF_O-F_1 complex produces ATP, which together with NADPH derived from LEF will be exploited by further reactions during the cell metabolism, notably for CO_2 assimilation during the Calvin-Benson-Bassham Cycle.

1.2 Photosynthesis slows light energy down to make it stable enough to be exploited by the cell metabolism

A major problem faced by photosynthetic cells is how to deal with the different time scales of the processes mentioned above. While light harvesting and photochemical utilisation occur in a time window of 10^{-12}-10^{-9} seconds, the limiting step of electron flow, meaning the oxidation of cytochrome b_6f, takes place in around 10^{-3} seconds. Kinetics of downstream processes could be even slower: CO_2 assimilation is catalysed by Rubisco, which has a catalytic rate of only 0.5 molecule per second (reviewed in Ellis 2009). This means that, in theory, by the time a single CO_2 molecule is fixed, the light harvesting complexes could have absorbed approximately 10^{12} photons. If all light energy were converted in one single reaction, most of it would be lost or might lead to photodamage. To overcome these problems, photosynthetic organisms evolved two types of strategies: *i.* increasing the cell concentration of the enzymes downstream to photosynthetic electron flow, to increase metabolic utilisation of ATP and NADPH and *ii.* split the photosynthetic electron transfer process into a set of reactions with different kinetics, gradually slowing down the rate of light energy conversion into chemical energy, to introduce

regulatory mechanisms (Fig 1.1), which for instance, allow dissipating excess of electrons under conditions where downstream metabolism limits the overall CO_2 assimilation capacity.

1.3   Electron flow processes

1.3.1 Electrochromic Shift: a probe to measure the kinetics of the main components of the photosynthetic apparatus

The kinetics of the different protein complexes involved in photosynthetic electron flow can be easily visualised *in vivo* by measuring the time course of the Electro-Chromic Shift (ECS) upon illumination of a photosynthetic organism with a single turnover flash (Fig 1.2). The ECS is a Stark effect, *i.e*. a modification of the absorption spectrum of thylakoid embedded molecules (chlorophyll and carotenoids) when exposed to an external electric field (Bailleul et al., 2010). During photosynthesis, this electric field stems from light driven generation of an electrochemical potential, or proton motive force, across the thylakoid membranes ($\Delta\mu H^+$). The pmf comprises a proton concentration gradient (ΔpH) and the electric potential ($\Delta\Psi$). The latter stems from the peculiar topology of the electron transfer complexes, where all the electron donors are localised toward the luminal side while acceptors are located at the stromal side of the membranes. Electron transfer thus lead to asymmetric distribution of charges across the thylakoids, leading to a shift of the absorption maxima of specific pigments that can be followed at appropriate wavelengths along time.

Upon exposure of photosynthetic cells to a single turnover flash, the ECS signal displays a multiple phase kinetic: the first fast phase (phase "a" according to Joliot and Delosme 1974), reflects the rapid onset of the electric field due to charge separation by the PSs. This phase comprises photon absorption, energy transfer to the reaction centre and primary photochemistry (10^{-15}-10^{-9} s) and it is followed by a slower phase ("b" phase), occurring in the ms time range

(10^{-3} s), which mirrors the oxidation of plastoquinols by cytochrome b_6f (Joliot & Delosme, 1974). Afterwards, a much slower decay of the ECS signal is seen (''c'' phase, Joliot and Delosme 1974), due to the relaxation of the light induced pmf: in native systems, this process corresponds essentially to the H^+ flux through the ATP-synthase complex.

Figure 1.1 | Electrochromic shift measurements allow visualising the different time frames of photosynthetic linear electron flow. The kinetics of the electrochromic shift measured in dark adapted Chlamydomonas cells (top) display different phases. After exposure to a single turnover saturating laser flash (intensity 2 mJ, duration 5 ns), a rapid increase of the ECS signal (< 100 µs) is observed (red), which is related to the turnover of the two photosystems working in series: PSII and PSI (also in red in lower panel). The following slower phase (in the millisecond time range, blue) reflects electron transfer within the cytochrome b_6f complex (in blue in the lower panel). The kinetics of the ECS signal also allows visualising proton fluxes across the photosynthetic membranes. This is shown by the slow signal decay (in the tens of ms time range, green), which is associated with proton flux through the ATP synthase CF_O-F_1.

1.3.2 Constant regulation: alternative electron flow and CO_2 assimilation

1.3.2.1 ATP and NADPH are needed for CO_2 fixation during the Calvin cycle

In theory, focusing on the photosynthetic reactions, the ATP/NADPH ratio of 9/7 generated by linear electron flow is thought not to be sufficient to fuel CO_2 assimilation process, since the one required during the Calvin cycle is 9/6 (Reviewed in Alric 2010, see however Petersen et al. 2012). Moreover, the ratio between the two molecules requires continuous adjustment according to light availability and the cell's metabolic demands. Under adverse environmental condition (*e.g.* for example in the case of nutrient starvation, where photosynthetic proteins are degraded to mobilise nutrients toward other metabolic activities) the CO_2 assimilation capacity is further reduced. Because of that, light absorption and electron flow can overcome the utilisation of CO_2 by the Calvin-Benson-Bassham (CBB) cycle, and part of the photosynthetic electrons must be redirected towards alternative sinks other than $NADP^+$. In plants and microalgae alternative electron flows comprise cyclic electron flow (CEF) around PSI (Shikanai, 2007) and the water to water cycles (WWCs). WWCs include the photoreduction of O_2 by PSI, called Mehler reaction (Mehler, 1951; Asada, 2000) and the non-photochemical oxidation of plastoquinols downstream of PSII, catalyzed by the plastoquinone terminal oxidase (PTOX) (Zehr & Kudela, 2009). Photorespiration, *i.e.* the oxygenase activity of Rubisco (reviewed in Ort & Baker, 2002), can also be viewed as a type of WWC. Eventually, the export of reducing equivalents from the chloroplast towards the mitochondrial oxidases, through the malate shuttle (Kinoshita et al., 2011) also leads to reduction of molecular oxygen by electrons generated by PSII, and therefore can be considered as a WWC (Curien et al., 2016).

1.3.2.2   The PTOX and Chlororespiration

Chlororespiratory pathways comprise photochemistry independent oxygen reduction reactions occurring at the level of PSII acceptor site in the dark. The main enzyme involved in this process is the plastid terminal oxidase, PTOX (Kuntz, 2004; Zehr & Kudela, 2009), also reviewed in (Nawrocki et al., 2015), which oxidises plastoquinols and produces water at the stromal side. PTOX was first identified due to its sequence similarity to the mitochondrial Alternative Oxidase AOX (McDonald et al., 2010) and their complementary functions have recently been investigated in plants, where the phenotype of Arabidopsis mutant strains lacking PTOX was recovered when AOX protein was targeted to the plastid (Fu et al., 2012). Besides its role in carotenoid biosynthesis (PTOX is an electron acceptor to phytoene desaturase (Gemmecker et al., 2015), this enzyme is supposed to act as a safety valve for excess of photosynthetic electrons in high light condition, when a high ΔpH would slow down electron transfer at the level of cytochrome b_6f activity potentially leading to photodamage of PSII. Consistent with this idea, the pmf likely promotes the association of PTOX to the thylakoids, thereby enhancing plastoquinols oxidation (Feilke et al., 2016).

1.3.2.3   The ATP/NADPH ratio controls photoprotection of PSI

PSI photoinhibition has been discovered more recently than PSII photoinhibition (reviewed in Sonoike 2011; Li et al., 2018). However, increasing evidence indicates that photoinhibition is more detrimental when occurring at PSI rather than PSII not only in plants (Allahverdiyeva et al., 2014) but also in *C. reinhardtii* (Larosa et al., 2017). One possible reason is that when PSII is photoinhibited, cells can still sustain some ATP synthesis while this is not possible when PSI activity is affected (Huang et al., 2018). Indeed PSI is involved in cyclic electron flow (CEF), in which electrons deriving from the acceptor are not injected into a soluble sink pool, but rather

continuously rerouted to the cytochrome b_6f complex (Finazzi, 2005) (Johnson, 2005). This process is considered as crucial to adjust the ratio between ATP and NADPH generated by the linear electron flow, which as discussed later on is probably insufficient for CO_2 assimilation by the Calvin cycle (J. Petersen et al., 2012; Alric, 2010), and other metabolic processes (Shikanai, 2007; Cardol et al., 2008).

1.3.2.4   Molecular actors of CEF

Despite intensive studies, the mechanism of CEF is still not completely understood and several protein complexes have been proposed to be involved in this process. In the chloroplast of green algae, the Nda2 protein, belonging to the type II NAD(P)H dehydrogenases family, contributes to the nonphotochemical reduction of plastoquinones (Jans et al., 2008). Alternatively, CEF could be mediated by the PGR5- PGRL1 complex (Dal Corso et al., 2008), the function and structure of which are still elusive. Both of the corresponding genes are present in all photosynthetic eukaryotes studied so far, indicating a well conserved role in regulating photosynthetic processes.

However, neither of them seems to fulfil entirely the criteria to support CEF by itself. NDH (2.5 e^{-1} s^{-1} PSI^{-1} in plants, 4 e^{-1} s^{-1} PSI^{-1} in Chlamydomonas) seems to be too slow to account for the CEF rates measured *in vivo* (~100 and ~60 e^{-1} s^{-1} PSI^{-1} in plants and green algae respectively) (Joliot et al., 2004) (Nawrocki et al., 2017). On the other hand, a Chlamydomonas mutant strain lacking PGRL1 is still able of high rates of CEF (Nandha et al., 2007), similarly to what was previously reported in plants. This suggests that these actors play partially overlapping roles, as shown in Arabidopsis, where knock out mutant strains lacking either NDH or PGR5 are viable, while the absence of both activities severely impacts plant growth (Munekage et al., 2004). A third mechanism contributing to CEF may involve the direct

electron donation through the ferredoxin-NADP$^+$ oxidoreductase (FNR) bound to cytochrome-b_6f (H. Zhang et al., 2001) but this process needs further investigation to be better understood.

Besides the nature of the molecular actors, their topological organisation is also unclear. Since CEF and LEF seem to share the same actors to some extent, competition between the two processes is expected. Because CEF requires recycling of electrons around PSI, this process will be outcompeted by LEF every time that an electron is transferred to a terminal LEF sink (no matter whether this is NADP or a WWC sink). To avoid this phenomenon different protein complexes have been propose to regulate the two electron fluxes in the microalga *Chlamydomonas reinhardtii*, such the PSI–LHCI–LHCII– FNR–Cyt bf–PGRL1 complex (Iwai et al., 2010) and the calcium regulated CAS, ANR1, and PGRL1 complex (Terashima et al., 2012).

Despite extensive biochemical investigation, the real occurrence of this complex from a functional point of view has not been proven yet. Recent data in Chlamydomonas either underline the good correlation between CEF occurrence and the observation of a structural CEF supercomplex, or indicate that it performs at its maximal rate regardless of conditions promoting the formation of this supercomplex (Nawrocki et al., 2017).

1.3.3 Transient regulation: The Mehler reaction

The reduction of O_2 in presence of light can occur at different steps of the linear electron transport chain and it is catalysed by multiple enzymes in different species. The pathway was first observed in isolated plant chloroplasts by Alan H. Mehler (Mehler, 1951; Asada, 2000) and was found to generate oxygen superoxide at the level of PSI, which is rapidly converted into H_2O_2 by the enzyme superoxide dismutase (SOD). The chloroplast-associated ascorbate

peroxidase (APX) efficiently oxidises H_2O_2, leading to the formation of monodehydroascorbate radical (MDA) (Miyake & Asada, 1992), which could lead to photodamage. The MDA species can accept electrons from PSI (Forti & Ehrenheim, 1993) thus leading to the 'Mehler-ascorbate reaction' pathway. The MDA reductase can also reduce this radical species by using photosynthetically derived electrons, as it uses NADPH as a substrate (reviewed by Asada 2000). Nowadays, the term "Mehler reaction" comprises all processes able to produce O_2 in presence of light at the level of PSI acceptor site. Since during the Mehler reaction H_2O_2 is produced, it was suggested that this pathway might be also involved in activation of the ROS signalling mechanism (Shao et al., 2008). This process could play different roles and be more or less relevant in different microalgae: while it could oxidise the plastoquinone pool upon illumination of anaerobic cells in the chlorophyte Chlamydomonas, it may represent the main pathway for the alternative electron flow in the dinoflagellate Symbiodinium (Roberty et al., 2014). Recently, Flavodiiron (Flv) proteins discovered in cyanobacteria, (reviewed in Allahverdiyeva et al. 2015; Alboresi et al. 2019) have been proposed to be responsible for the Mehler reaction in microalgae (Peltier et al 2010) despite not producing H_2O_2 but directly reducing oxygen into water. Two FLV genes, called FLVA and FLVB, are found in eukaryotic photosynthetic organisms like mosses and gymnosperms, while they are absent in angiosperms (reviewed in Alboresi et al. 2019). Interestingly FLVs are able to generate a pmf, thus increasing photosynthetic control, *i.e.* the decrease of the cytochrome b_6f activity due to an enhanced ΔpH (Eberhard et al. 2008), and protecting PSI over-reduction and consequent damage. Moreover, under these conditions, FLVs mutants are still able to establish the pmf, suggesting the presence of multiple compensating mechanisms. FLVs are also important under fluctuating light conditions (Chaux et al., 2017; Gerotto et al., 2016; Shimakawa et al., 2017). A sudden change of light intensity causes an imbalance between the NADPH production rate and the capability of the metabolism of consuming it, opening the possibility of photodamage. At first glance,

these proteins seem to play a role similar to PGR5-PGRL1, since mutant strains of the moss *Physcomitrella patens* lacking FLVs show an increased CEF activity and production of PGR5 protein (Gerotto et al., 2016), suggesting that the absence of FLVs is compensated by alternative electron routes. Analysis of *flva pgrl1* double mutant in moss mutant strains (Storti et al., 2019) and Chlamydomonas single KO lines (Jokel et al., 2018) further clarified that despite playing a compensatory role, the two pathways occur with different kinetics. FLVs activity is particularly important during the first seconds of illumination, when electron flow is already occurring while CO_2 assimilation is not fully active, whereas the PGR5-PGRL1 complex takes longer to be activated but remains effective under prolonged intense illumination. The contribution of FLV and PGRL1/PGR5 to the electron transport is marginal in steady state conditions but their role is important to guarantee the presence of extra acceptors for PSI in case of sudden high light exposure.

The apparent overlap of FLVs and PGRL1/PGR5 complex is an example of the advantage of having multiple regulation processes that can take place at the level of a single component of the photosynthetic apparatus, to better regulate them according to specific dynamics of the environment and/or metabolic demands.

Another case of multiple control is the redox state of the cytochrome b_6f, which can be governed by the pH of the thylakoid lumen and various proteins, such as PGR5-PGRL1 complex. In the presence of high light, the accumulation of H^+ in the lumen decreases the kinetics of the cytochrome b_6f in reducing the plastocyanin, preventing the over reduction of P700 chlorophyll in PSI, and therefore its own photoinhibition.
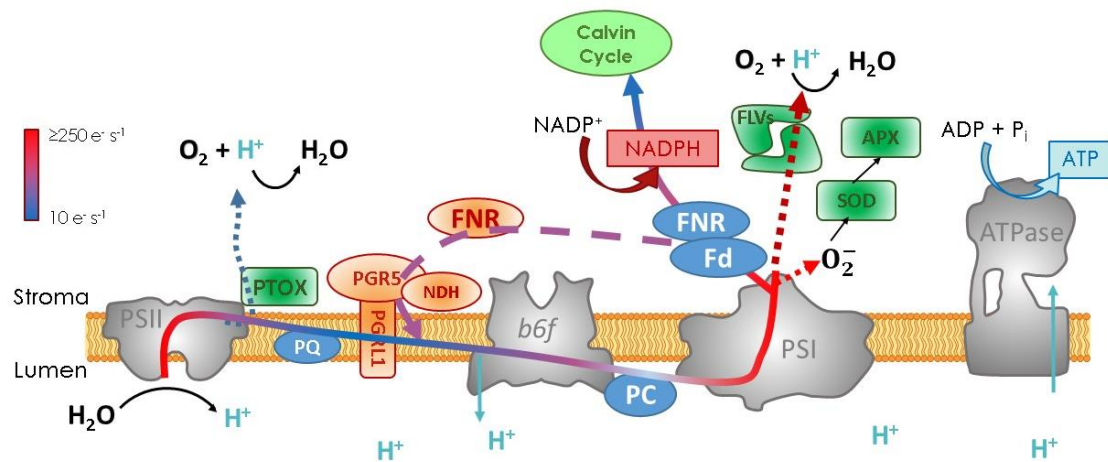
Figure 1.2| Schematic representation of different kinetics of electron transfer chain in the photosynthetic apparatus. Electron flow is progressively slowed down from light driven photochemistry to $NADP^+$ reduction. Electron flow rates from 10 to 250 e^-s^{-1} are represented by different colours. Linear electron flow: solid line; Cyclic electron flow: dashed line; Mehler reaction and chlororespiration: dotted line. Protein complexes involved in different electron transfer reaction are indicated with different colours: LEF in blue; CEF orange; Mehler and WWC in green.

1.4   Metabolic Regulation

1.4.1 Rubisco: quantity over reaction rate

Even if photosynthesis contributes to split the linear electron flow into several steps with lower rates, electron transfer is in principle still too fast compared to those of the cell's metabolism (*e.g.* assimilation of atmospheric CO_2 into organic molecules by Rubisco at a rate of 0.5 s^{-1}). Thus, phototrophs still need to cope at the metabolic level by increasing the cell concentration of the enzymes at the limiting step of the pathway (Bar-Even et al., 2011). In fact, they accumulate high amounts of Rubisco per cell, which consequently turns out to be one of the

most abundant protein on Earth. In microalgae the stoichiometry Rubisco/photosynthetic electron transport chain can reach 1000 (Vandenhecke et al., 2015), meaning that the overall turnover rate of CO_2 assimilation per electron flow chain should be around 200 per second (0.5 s^{-1} * 1000), *i.e.* a value very close to the maximum electron flow rate measured estimated *in vivo* (*e.g.* Joliot et al., 2004). By this mean, therefore, microalgae have matched the two processes at least under optimum environmental conditions. However, these conditions are often not encountered in the natural environments, where biochemical processes are often slowed down by temperature, nutrient availability etc. Thus, most microalgae have improved Rubisco turnover via Carbon Concentration Mechanism (CCM), which increase the local concentration of CO_2 in proximity of this enzyme, thereby reducing its oxygenase activity. By increasing substrate availability, the amount of the enzyme needed to reach sustainable turnover rates can be lowered. The quantity of Rubisco is up to 6% of the total protein concentration per cell in microalgae (Losh et al., 2013), while it is estimated to be 50% in C3 plants (Spreitzer & Salvucci, 2002) and around 35% in C4 plants (Sugiyama et al., 1984; Zhu et al., 2010; Feller et al., 2007).

1.4.2 Photorespiration

Rubisco catalyses both the carboxylation or the oxygenation reaction of ribulose-1,5-bisphosphate, leading to carbon assimilation or photorespiration (reviewed by Wingler et al. 2000). While photorespiration was initially thought to be absent in microalgae (Peltier & Thibault, 1985), later studies indicate that it is active, at least in Chlamydomonas, in stress conditions (Davis et al. 2013). This process requires the cooperation of pathways located in multiple organelles and changes in photorespiration may reflect mechanistic but also subcellular different arrangements of metabolism in plants and algae. In plants, the oxidation

of ribulose-1,5-bisphosphate leads to the generation of 2-phosphoglycolate, which is dephosphorylated before being transferred to the peroxisome and converted to glyoxylate. This reaction involves the glycolate oxidase, exploiting O_2 as electron acceptor, and the activity of a catalase, which converts H_2O_2 in H_2O (Spalding, 2009). In Chlamydomonas and some other microalgae, this reaction is catalysed by a glycolate dehydrogenase in a process where electrons are directly delivered to the mitochondrial ubiquinone (Nakamura et al., 2005). This could prevent the over reduction of the chloroplast and the consequent production of dangerous reactive oxygen species (ROS). Moreover, as glyoxylate is produced, photorespiration participates to the assimilation of external reduced carbon (mixotrophy) in microalgae in high light conditions via the glyoxylate cycle, as the malate synthase condenses photorespiratory derived glyoxylate with external acetate derived acetyl-CoA (Xie et al., 2016). In algae, photorespiration should be largely mitigated by CCM processes (Burnap et al., 2015) and (Wang et al., 2015), since they increase the CO_2 concentration close to Rubisco (*i.e.* the pyrenoid in algae, carboxysome in cyanobacteria). While CCMs consume ATP to actively pump the charged HCO_3- into the pyrenoid then converted in CO_2 by a carbonic anhydrase, they increase CO_2 concentration up to ~1000 times higher compare to the normal aquatic environment, thereby promoting Rubisco carboxylase activity over its oxygenase reaction.

1.4.3 Metabolic interactions between organelles.

In eukaryotic phototrophs, chloroplasts are not the only organelles in charge of the cell energetic metabolism, since mitochondria also produce ATP via oxidative phosphorylation. Some microalgae can in fact grow in presence of an external carbon source in the culture medium, even in absence of light. Because of the coexistence of these two "engines" with overlapping roles within the cell, mutual interactions are expected. In fact, the presence of an active

mitochondrion can sustain the activity of a chloroplast with a defective photosynthetic activity and vice versa. Chlamydomonas KO strains with a single mutation in mitochondrial Complex I, or with altered the cyclic electron flow, do not show a drastic growth phenotype, which was observed only in a double mutant strain, where the activities of both energetic organelles were affected (Cardol et al., 2009; Lemaire et al., 1988). The severe growth phenotype of the Chlamydomonas mutant strain Fud50su, which lacks the chloroplastic ATP synthase, can be rescued by a revertant strain either by an enhanced ATP import from the mitochondria (Lemaire et al. 1988), via the ATP/ADP transporter (Merchant et al., 2007), or thanks to sustained malate shuttle activity. Moreover, not all microalgae rely on chloroplastic CEF to optimise ATP production, therefore, they need to use different strategies. This is the case of diatoms, where energetic exchanges between mitochondria and plastids, meaning the re-routing of reducing power generated in the chloroplast towards mitochondria and importing mitochondrial ATP into the plastid, are no longer optional but play a vital role for the cell's metabolism. In this microalgal group, in fact, cells treated with inhibitors of mitochondrial respiratory complexes (SHAM and Antimycin A) show a lower photosynthetic activity (Bailleul et al., 2015), and the mitochondrial alternative oxidase (AOX) knock-down strain has a higher sensitivity to stress and a more oxidized chloroplast (Murik et al., 2019).

Computational simulations, coupled with experimental analysis, have led to hypotheses on how this organelles' crosstalk can regulate light-dependent metabolic changes in the model diatom *Phaeodactylum tricornutum*. Photorespiration, the ornithine-glutamine shunt and branched-chain amino acid metabolism could act as reductant shuttles to mediate excess light energy dissipation in high light (Broddrick et al., 2019), while CO_2 molecules derived from photorespiration would then be recycled as pyruvate in the chloroplast through multiple pathways possibly involving a serine-ammonia lyase. Overall, optimising energetic metabolism by inter-compartmental exchanges of reductant between organelles might have played an

important role in the evolutionary success of this ecologically important clade in the ocean. This is rather paradoxical since diatoms are secondary endosymbionts, meaning that they originated when a photosynthetic eukaryote was engulfed by an eukaryotic host, and thus its chloroplast is surrounded by four membranes, instead of two as in plants and green algae (Flori et al., 2016). Therefore, mitochondrion derived molecules need to cross a total of six membranes (two of the mitochondrion and four of the secondary plastid) before being exploited in the plastid and thus specific transporters required for this exchange must be membrane proteins localised within both the chloroplast envelope and the mitochondrial membrane. On the other hand, high-resolution tomography of diatoms has pinpointed the existence of physical contacts between the organelles' membranes (nucleus, chloroplast and mitochondria), which could efficiently mediate direct exchanges of relevant molecules, without diluting them in the cytosol (Bailleul et al., 2015).

Besides direct metabolic exchanges, the chloroplast–mitochondria interaction is beneficial for the entire cells metabolism. In fact, the CO_2 derived from oxidative phosphorylation can be directly fixed in the chloroplast (Busch et al., 2013; Riazunnisa et al., 2006) while O_2 generated by photosynthesis can be respired by mitochondria without diffusing out of the cell (Lavergne, 1989). Moreover, organelles' interactions involve also production and regulation of ROS molecules, which are linked to the activities of both the chloroplast and the mitochondrion (reviewed in Sunil et al., 2013).

This is revealed *e.g.* by the responses of *Phaeodactylum tricornutum* under Fe-limited conditions, where cells show a decreased photosynthetic activity while maintaining a functional mitochondrion (with adjustments in the ROS scavenging processes like increased AOX concentration): since PSI is particularly rich in Fe, cells selectively keep mitochondria respiration to provide energy for housekeeping functions (Allen et al., 2008). It is possible that

some of this ATP is imported into the chloroplast and might contribute to the generation of a pmf to protect the remaining photosynthetic complexes (e.g. PSII) from over-reduction and ROS production via Non Photochemical Quenching (NPQ) (Allen et al., 2008).

Kinetics	LEF	FLVs	Photoresp ($\mu mol\ m^{-2}\ s^{-1}$)	Cyt b_6f	Chlororesp (PTOX)	CEF
Arabidopsis	75 ca (Allorent et al., 2015) 200 (Joliot et al., 2004)	/	7 (decarboxylation rate) (in wheat leaf) (F. Busch, 2012)	100 (Joliot & Joliot, 2002)	0,4 ca (Trouillard et al., 2012) (tomato)	130 ca (Joliot et al., 2004)
Physcomitrella	60 (Gerotto et al., 2016)	45 (Gerotto et al., 2016)	not found in literature	50 ca (Meneghesso et al., 2016)	nd	10 (Gerotto et al., 2016)
Chlamydomonas	120 (Nawrocki et al., 2017)	60 (Chaux et al. 2017)	not found in literature	70 ca (Finazzi et al., 1999)	5 (Trouillard et al., 2012)	40 (Trouillard et al., 2012) 70 (Nawrocki et al., 2017)
Phaeodactylum	260 ca (Bailleul et al., 2015)	/	not found in literature	200 ca (Bailleul et al., 2015)	/	~15 (Bailleul et al., 2015)

Table 1.1 | Partition of photosynthetic electron flow between alternative electrons sink in vascular plants, and different microalga. Data are referred as electrons per second unless specified. LEF, linear electron flow; FLVs, flavodiiron proteins, Photoresp, photorespiration; Cyt b_6f, cytochrome b_6f; CEF, cyclic electron flow.

1.5   Questions related to this PhD project.

Photosynthetic organisms exploit light as energy source and convert it into chemical energy. Since light absorption and enzymatic reactions take place with very different kinetics, the photosynthetic pathway is divided in a series of reactions, each occurring at progressively slower rates optimising the assimilation and limiting the loss of energy. Multiple pathways are responsible for efficiently regulating this energy conversion and they can be classified in two main groups: alternative electron transport, which directly reroute electrons in 'excess' from the linear transport chain, and metabolic processes, that take ATP and reduced equivalents

towards other cellular metabolic processes. The former group comprises CEF, FLV mediated Mehler reaction, non FLV Melher and chlororespiration. As summarised in Table 1.1, their simultaneous occurrence in a single cell would largely diminish the efficiency of LEF instead of optimising its ATP/NADPH production for carbon assimilation. Therefore, different processes are likely active at different times in different organisms, to cope with peculiar environmental conditions. An example of a mechanism early activated is the FLV proteins of green algae, which are transiently very active during a dark to light transitions, and then becomes overcome by other processes in steady state. On the other hand, CEF is constantly present in Chlamydomonas. However, this process in enhanced in anaerobic conditions, probably explaining why this strategy was selected to make 'extra' ATP by organisms that often experience this condition in its natural environment. On the other hand, anaerobiosis is likely not to be a relevant condition for other microalgal species like *P. tricornutum,* possibly suggesting why this process is less relevant in diatoms.

Concerning the metabolic processes, the mechanisms that govern the crosstalk between the chloroplast and the mitochondrion might vary in different algal species. In diatoms, the exchange of ATP and reducing equivalent plays a pivotal role for the cell survival, while in Chlamydomonas it becomes relevant in the presence of a defective photosynthetic activity (Cardol et al., 2009). In diatoms, cell division occurs mainly at the end of daytime (Annunziata et al., 2018) and transcriptomic data show a lower expression of mitochondrial genes (Annunziata et al., 2018) during the night. These findings suggest that the energetic contribution of the mitochondrion alone is not sufficient to sustain the whole cell energetic metabolism.

1.6   Aim of the PhD project

Although the energetic crosstalk between these organelles is well established (Bailleul et al., 2015), the molecular actors governing this process are yet to be described. Since the exchange of ATP and NADPH is observed between two different confined compartments, such as the plastid and the mitochondrion, specific transporters embedded in the membrane of each organelle must mediate the export and import of these chemicals either by direct transfer or through shuttle mechanisms. The aim of my PhD project was to characterise proteins involved in the exchange of ATP and reducing equivalents between the chloroplast and the mitochondrion in the marine diatom *Phaeodactylum tricornutum*.

To achieve this goal, I first identified genes coding for putative transporters based on the results of previous transcriptomic data. Using intracellular localisation and 3D structure prediction tools, phylogenetic analysis and a pharmacological approach, I was able to select four candidate genes that turned out to belong the Mitochondrial Carrier Family (MCF), one of the most representative group of organelles' transporters.

To understand their possible role in the exchange mechanism, I applied a mutagenesis protocol and was able to generate knock out and knock down mutant strains. I finally applied non-invasive photophysiology techniques to characterise the mutants' phenotype. I reasoned that if the targeted genes were involved in the transfer of ATP or of reducing equivalents, the photosynthetic and respiration performances should be affected in the mutant algae. This hypothesis was tested using chlorophyll fluorescence analysis, spectroscopy and gas exchange measurements.

I found that two of the four targeted genes (the ones for which I could obtain mutant lines) may in fact play a role in the abovementioned energetic exchanges in diatoms and that the regulation

of this process should involve multiple transporters to guarantee the optimal physiological conditions for the cell to thrive.

Part of this study was done in collaboration with Drs Pierre Cardol, Richard Durrel and Chris Bowler, who helped me with the phylogenetic analysis and Dr Duncan Fitzpatrick (University of Turku, Finland),who helped me to measure gas exchanges using the Membrane inlet Mass Spectrometry (MiMS) approach.

Chapter 2

2.1 Introduction

2.1.1 Endosymbiotic origin of the cellular sub compartments in eukaryotes.

In the eukaryotic cell, the different cellular metabolic processes take place in confined specialized compartments, the organelles. They arose between 1.2 and 2.2 billion years ago, when the first endosymbiotic event started with the engulfment of a proteobacterium by a host eventually providing advantages to both partners (Baurain et al., 2010; Embley & Martin, 2006). Progressively, the bacterium lost its metabolic independence and became part of the host cell. Overall, the new eukaryotic cell had to readjust its metabolic processes to coordinate them with the newborn organelle, a mitochondrion at the beginning and a chloroplast later on in some eukaryotes.

Three major autotrophic lineages then arose, following the chloroplast appearance by this 'primary' endosymbiosis: the glaucophytes, the chlorophytes (including green algae and land plants), and the rhodophytes (red algae).

- **Glaucophytes** consist of a small group of freshwater unicellular algae of 14 species known so far. They feature the presence of phycobilisomes (*i.e.* light harvesting complexes that are not embedded in the photosynthetic membranes, but only interact with the photosystems) as antenna complexes. They are found in the photosynthetic apparatus of cyanobacteria, supporting the model of endosymbiosis. Consistent with their evolutionary origin, Glaucophytes perform CO_2 assimilation via a carbon-concentrating mechanism (CCM) that occurs in structures similar to the cyanobacterial carboxysome (Burey et al., 2007) (for a review on glaucophytes (Keeling, 2004).

- **Rhodophytes** comprise a diverse and large group of uni and multi cellular red algae found in both fresh water and marine environments. As for Glaucophytes, Red algal plastids

contain phycobilisomes as antennas but also membrane embedded antennas similar to plants, providing a paradigm of the evolutionary transition between cyanobacteria and plants (Wolfe et al., 1994).

- Land plants and green algae both belong to **Chlorophytes**. In addition to chlorophyll a, these organisms also contain chlorophyll b as light absorption pigment. They lost the phycobilisomes, which have been replaced by transmembrane protein pigment complexes and carbon concentration mechanisms (if present) occur in more developed structures compared to what happens in cyanobacteria, glauco and rhodophyta, *e.g*. the pyrenoid.

Besides primary plastids, mainly found in land or freshwater settled organisms, some eukaryotic phototrophs contain plastids acquired after secondary endosymbiosis events (for a review see Keeling, 2010). These processes involved the engulfment of a green alga by a primitive mitochondriate eukaryote and led to the appearance of euglenophyta, chlorarachniophyta and dinoflagellate. The acquisition of a red alga gave rise to chromalveolates, which include cryptophytes, the haptophytes, heterokontophyta (e.g., diatoms), and the alveolates (Archibald, 2009; Gould et al., 2008; Keeling, 2010). Additional events contributed to shape the complexity of the eukaryotic cell, like plastid loss, replacement and inactivation as in the red algal-derived apicoplast of apicomplexan parasites (*e.g*. the malaria parasite *Plasmodium*) which is not photosynthetic but still produces fatty acids, haem and isoprene units (Lim & Mcfadden, 2010). After secondary endosymbiosis, the mitochondrion and the nucleus of the guest cell disappeared, with the only exception of cryptophytes, which retain a structure remnant of the

guest cell nucleus called nucleomorph. Consequently, the newborn cell mainly exploits organelles originally deriving from the host.
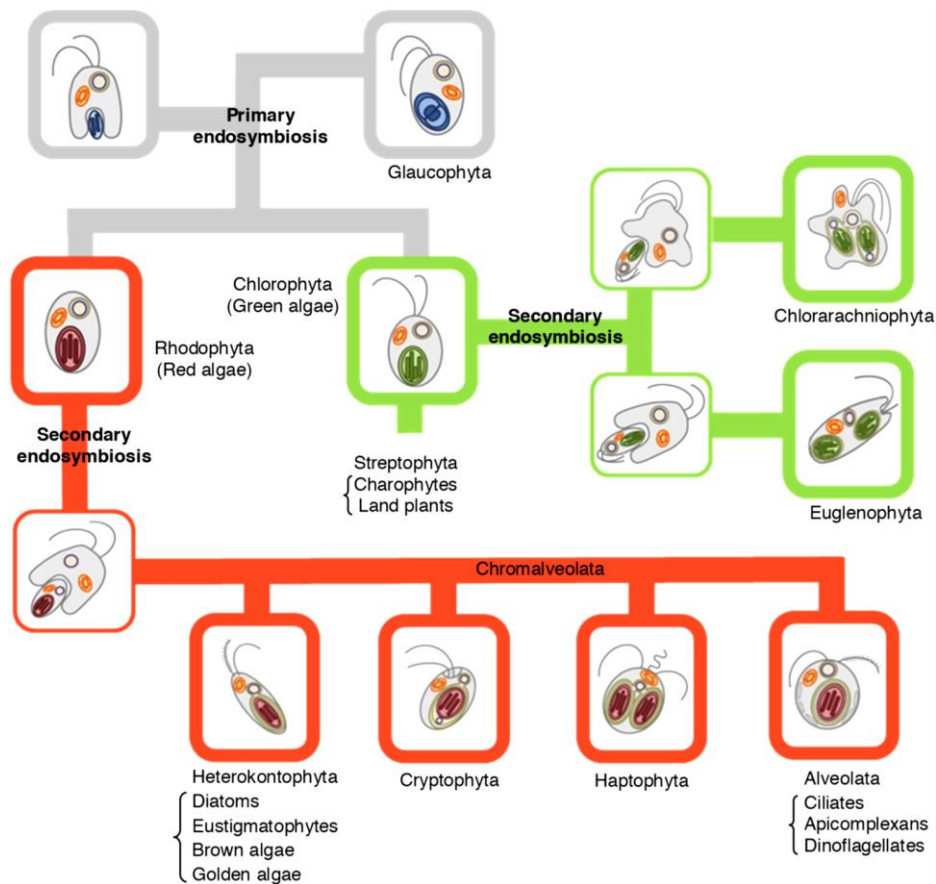
Figure 2.1 | Schematic representation of the phylogenetic tree of the main algal groups (adapted from Marchand et al., 2018). The primary endosymbiosis event (grey line) gave rise to Glaucophyta. Two subsequent events of endosymbiosis allowed the formation of the Chlorophytes (green line), which includes *Chlamydomonas reinhardtii*, when a host eukaryotic cell engulfed a green alga. Diatoms arose after an endosymbiotic event where the guest cell was a red alga (red line).

2.1.2 *Phaeodactylum tricornutum*

Knut Harald Bohlin described this alga for the first time in 1897 as the unique species of the genus Phaeodactylum and it belongs to the Heterokonts group. It is an unusual pennate diatom, possessing an atypical frustule structure that is poorly silicified and therefore it does not require silica for growth (Lewin et al., 1958). Various ecotypes are known (Abida et al., 2015), which can exist in three different morphotypes according to its physiological state and the

31

environmental factors (Fig. 3.2) (De Martino et al., 2007; Borowitzka & Volcani, 1978; reviewed by Tesson et al., 2009). When in their natural environment, cells are in the triradiate
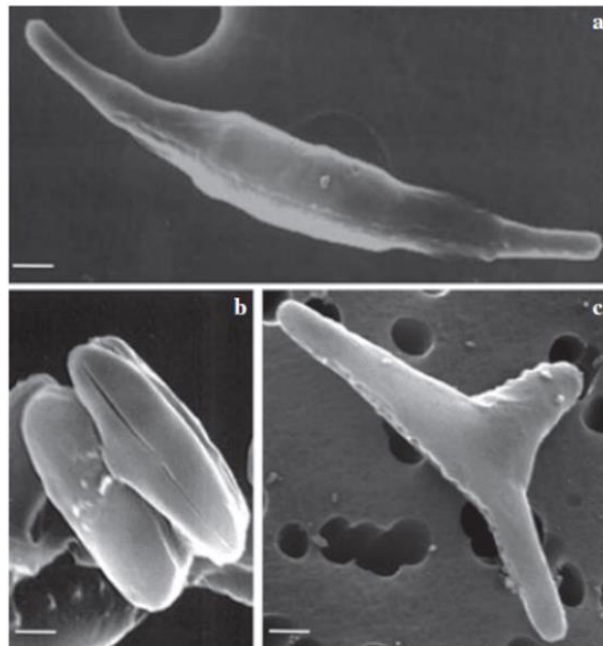
Figure 2.2 | Scan Electron Microscopy (SEM) images of the three morphotypes of *Phaeodactylum tricornutum* (from De Martino et al., 2007). This alga can exist in three different morphotypes: Fusiform cell (**a**), two oval cells (**b**), and triradiate cell (**c**). Scale bar, 1 µm.

conformation (the morphotype that gives the name to this particular species), while when growing in artificial conditions in the laboratory they are fusiform of ∼10 µm in length. When algae are in the ovoidal morphotypes, they are considered to be in stress condition (De Martino et al., 2011).

After the diatom *Thalassiosira pseudonana*, the genome of Phaeodactylum was the second to be fully sequenced from the diatom group (Bowler et al., 2008). Its analysis revealed peculiar and unexpected features: the presence of hundreds of genes from bacteria and a mix of plant and animal metabolic pathways, as exemplified by the presence of the ornithine-urea cycle, which seems to be essential for diatom growth and carbon fixation (Allen et al., 2011). Thanks to the availability of its sequenced genome and of molecular tools, *P. tricornutum* has arisen to the status of model organism for both ecological/photophysiology studies and for biotech

applications, thanks to its capacity to accumulate lipids (Chisti, 2007). Transformation is possible via biolistic method (Apt et al., 1996; Falciatore et al., 1999), electroporation (Zhang & Hu, 2014) and bacterial conjugation (Karas et al., 2015). These methods allow to generate mutant lines, *i.e*. introducing either heterologous or endogenous genes controlled, *e.g*., by the strong light-induced promoters of the FCP proteins (Falciatore et al., 1999). CRISPR_CAS9 genome editing is also available in this organism (Daboussi et al., 2014). Thanks to the development of these molecular tools in Phaeodactylum, and the finding that chloroplast-mitochondria energetic interactions are essential for diatoms photosynthesis (Bailleul et al. 2015, see below), this microalga has immediately appeared to be a promising candidate organism for my PhD project, consisting on the characterization of the molecular actors of these energy exchanges.

2.1.3 Organelles interactions in phototrophs.

After endosymbiosis, most genes of bacterial origin have been transferred to the nuclear genome. Therefore, the organelles rely on nuclear transcription and cytosolic translation to refill their protein pools, which eventually reach the organelles by crossing their external membranes through appropriate import machineries.

On the other hand, both organelles are largely autonomous in their function of contributing to the energetic metabolism of the cell, through either photosynthesis or oxidative phosphorylation. Since both activities rely on the same molecules, (NAD(P)H and ATP), a coordination of these two processes is mandatory to maintain a correct physiological state for proper cell growth and to respond to changes of environmental conditions.

Besides performing photosynthesis and respiration, the two organelles play important roles in multiple metabolic pathways. In fact, the plastid is also involved in amino acids and fatty acids

biosynthesis, nitrogen and sulphur assimilation (Weber and Flügge, 2002; Weber et al., 2006; Weber and Fischer, 2007) while the mitochondrion is responsible for other functions *e.g.* ROS signalling (Marchand et al., 2018). In addition to the energetic activities, these pathways must also be coordinated and this regulation is likely to have a vital role in the case of diatoms, because of the energetic interactions between chloroplasts and mitochondria (Bailleul et al., 2015).

In photosynthesis, the efficient conversion of CO_2 into organic matter requires the optimization of the ATP/NADPH ratio (Allen, 2002). In *Viridiplantae*, the most studied photosynthetic organisms so far, this optimization mainly relies on processes localized within the plastid. The first one is cyclic electron flow (CEF), where electrons derived by the activity photosystem I are reinjected into the plastoquinone pool, which in turn are oxidised by the cytochrome b_6f complex, without the involvement of PSII photochemistry (Shikanai, 2007) (see also introduction). The second one is the water-to-water cycles (Allen, 1975) (review in Curien et al., 2016), where flows of electrons resulting from the oxidation of water at PSII are routed to reduce O_2 through an oxidase activity. The latter reactions include the Mehler reaction at the PSI acceptor side (Asada, 2000; Radmer & Kok, 1976; Badger et al., 2000), the activity of the plastoquinone terminal oxidase downstream of PSII (Cardol et al., 2008), and the oxygenase activity of RuBisCO (photorespiration) (Ort & Baker, 2002). Although genes encoding the majority of components for these processes appear to be present in diatoms (Prihoda et al.,

2012; Bowler et al., 2008; Grouneva et al., 2011) none of the mechanisms described so far seems to be relevant to balance the ATP/NADPH.

In a previous work from our laboratory, it was shown that diatoms regulate the ATP/NADPH ratio for proper photosynthesis through interactions between plastids and mitochondria (Bailleul et al., 2015). The hypothesis suggested by this study is that optimization of carbon fixation in *P. tricornutum* occurs via the re-routing of reducing power (NADPH) generated in the plastid towards mitochondria (the site of respiration) and the import of mitochondrial ATP into the chloroplast, compensating for the extra need of ATP in the Calvin cycle. This assumption implies that exchanges between the two organelles should occur via specific transporters, possibly located in the physical contacts between the two organelles that were
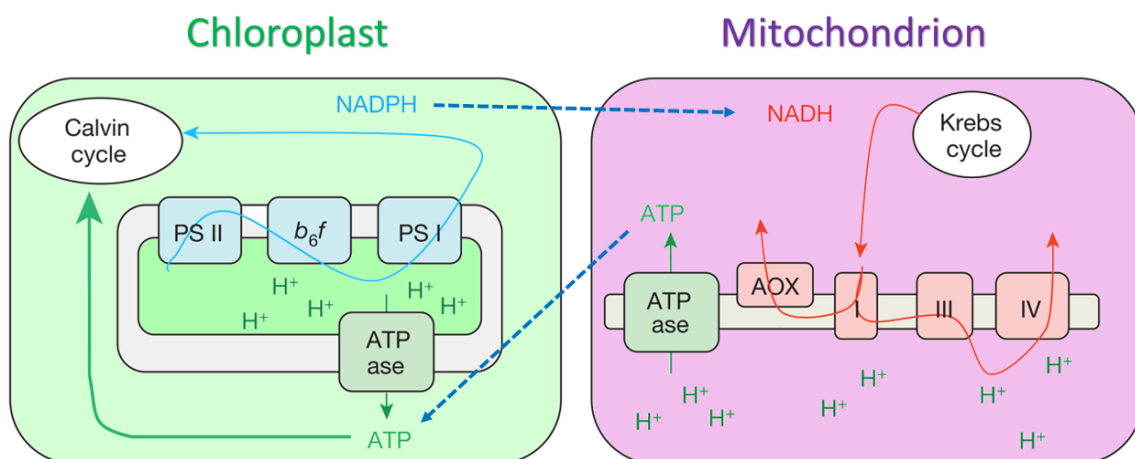
Figure 2.4 | Schematic representation of energetic interaction between the mitochondrion and the chloroplast. According to the model, the optimum ATP/NADPH needed for carbon fixation is achieved through the import of ATP produced by the mitochondrion. Light blue lines: photosynthetic linear electron transport chain; red lines: respiratory electron flow; dark blue dashed lines: putative ATP/ADP and reducing equivalents exchange pathway between the organelles.

identified when observing the structure of chloroplast and mitochondria in intact *P. tricornutum* cells (Fig. 2.5) (Bailleul et al., 2015; Flori et al., 2017). These transporters should be located in

35

the mitochondrial inner membrane, the most selective barrier for solutes, and the plastid envelope.
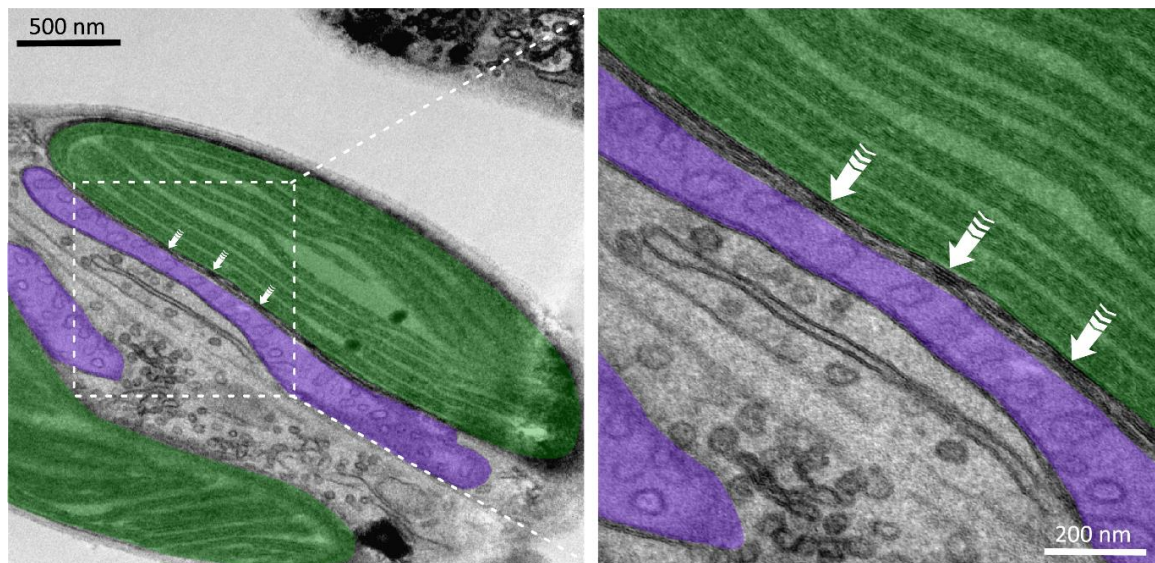
Figure 2.5 | Electron micrographs of *Phaeodactylum tricornutum* (from Bailleul et al., 2015). The arrows indicate the putative physical contacts between the chloroplast (upper structure in green) and mitochondrion (in violet).

2.1.4 Membrane organisation of the mitochondrion

Mitochondria of eukaryotic cells arose after a unique endosymbiotic event involving an α-proteobacterium. In secondary endosymbiotic species, where both the host and the guest cell happened to be eukaryotes, only mitochondria derived from the host where retained. Moreover, the general properties of diatom mitochondrial genomes are more similar to animal than to plant mitochondrial genomes and no red algal mitochondrial genes was found in the *T. pseudonana* or *P. tricornutum* nuclear genomes, reinforcing the conclusion that the mitochondrion derived from the endosymbiont was lost (Secq & Green, 2011). As a product of an endosymbiotic event, two membranes surround this organelle:

- The **outer membrane** derives from the host cell membrane invagination process during the symbiosis event, as indicated by the similar protein-to-phospholipid ratio between the mitochondrial and the cell membrane (about 1:1 by mass) (Müller et al., 2008). It is permeable to a large variety of solutes and the most common transporters are porins and the voltage-dependent anion channel (VDAC), which is the primary transporter of nucleotides, ions and metabolites (Blachly-Dyson & Forte, 2001). In addition, the outer membranes also present enzymes catalysing different reactions, like fatty acid Co-A ligase and carnitine acetyltransferase.

- The **inner membrane** is a selective barrier since it is impermeable to most small molecules and ions, including H^+. Thus, the presence of specific transporters allows the import and export of certain solutes. It has a higher protein/phospholipid ratio (>3:1 by weight) compared to the outer membrane, a similar lipid composition to bacterial membrane and it contains cardiolipin (McMillin & Dowhan, 2002). It harbours the protein complexes involved in the electron transfer reaction and the ATP synthase. This membrane forms numerous invaginations called *cristae*, which significantly increase the total membrane's surface area and thereby the capacity for ATP generation. The region enclosed by the inner membrane is called matrix, while the intermembrane space is comprised between the two membranes. In the matrix are localised the pyruvate dehydrogenase complex and the enzymes of the citric acid cycle, the fatty acid β-oxidation pathway, and the pathways of amino acid oxidation.

After the gene transfer process, occurred following the endosymbiosis event, hundreds of mitochondrial proteins are now encoded by nuclear genes. Once translated, mitochondrial pro-proteins are imported through specialised translocation complexes localised at the outer (TOM) and the inner membrane (TIM) and, once in the matrix, are sorted and folded thanks to the presence of chaperone proteins.

The contribution of this organelle to the cell energy metabolism mainly relies on the production of ATP via the Krebs cycle and oxidative phosphorylation, thanks to the presence of specific enzymes in the matrix. From the metabolic point of view, the mitochondrion of diatoms differ from the one present in green algae as it harbours ornithine-urea cycle, which is similar to that of metazoans but is absent in green algae and plants. This pathway is believed to coordinate the metabolic response of diatoms to episodic nitrogen availability and to play a role in the regulation of tricarboxylic acid cycle and the glutamine synthetase/glutamate synthase cycles (Allen et al., 2011). Moreover, beside the regular cytosolic localisation, the six last enzymes of glycolysis in *P. tricornutum* are also present in the mitochondrion, as demonstrated by cellular localisation of GFP fused with mitochondrion targeting signals of glycolytic enzymes, suggesting that this algal species likely have a branched glycolysis (Río Bártulos et al., 2018).

2.1.5 Membrane organisation of secondary plastids

The envelope of primary plastids comprises two membranes: the outer, mainly deriving from the invagination of the host cell membrane during the acquisition process, as remarked by the presence of galactolipids and β-barrel proteins (Jarvis et al., 2000; Schleiff et al., 2003), and the inner, which still shows similarities with the ancestral cyanobacterial one. The different lipid and protein composition of these two membranes influence their permeability. The same classes of lipids found in thylakoid membranes of higher plants and green algae are also present in diatom, even if the most abundant species of galactolipids is anionic sulfoquinovosyl diacylglycerols (SQDG) rather than monogalactosyldiacylglycerol (MGDG) (Vieler et al., 2007; Goss et al., 2007).

In the chloroplast of Chlorophytes, the outer membrane allows the passage of solutes with a molecular mass of less than 4–5 kDa (Ludwig et al., 1986) thanks to the presence of porin-like transporters (Benz et al., 1990). Even if it has always been considered as a low selectivity filter for solutes, the existence of specific channels suggests a more active regulatory role of this membrane (Duyet al., 2007; Inoue, 2011). Moreover, it presents proteins that regulate various biological processes such as components of the protein translocation and organelle division machines and lipid biosynthetic enzymes.

The inner membrane serves as a barrier for the metabolites associated with the carbon cycle and presents a high concentration of transporters involved in their transfer. These are membrane proteins, typically presenting four or more α-helices spanning across the lipid bilayer and are present in high concentration in the inner membrane. The most common kind of transporter proteins are antiporters, which associate the import of a certain metabolite with the export of another one. This mechanism confers a higher control on the metabolic homeostasis between the organelle and the rest of the cell (Weber & Linka, 2011). Phylogenetic studies show that the host cell has been responsible for the connection with the uprising organelle, as in Arabidopsis only 12% of the metabolite transporters are derived from the endosymbiont while 58% are of host origins (Tyra et al., 2007), reflecting the importance for the host to take advantage of the guest's metabolism.

On the other hand, the plastids of secondary endosymbionts are surrounded by more than two membranes, as shown by electron microscopy studies. In *Phaeodactylum tricornutum*, four membranes separate the stroma of the chloroplast from the rest of the cell (Flori et al., 2016; Tanaka et al., 2015). These membranes are likely derived from a "rearrangement" of structures inherited from both the host and the symbiont.

From the cytosol toward the stroma of the chloroplast the four membranes are:

- Chloroplastic Endoplasmic Reticulum (cERM): likely derived from the host phagocytic structures and thus possibly rich in phospholipids (Petroutsos et al., 2014), it's the outermost membrane (Cavalier-Smith, 2003; Mcfadden, 2014). The cERM of diatoms is continuous with the host Endoplasmic Reticulum (ER) and the outer nuclear envelope membrane.

- Periplastidial Membrane (PPM): it is likely what remained from the symbiont plasma membrane after the endosymbiosis event (Grosche et al., 2014). The region confined within the PPM is referred to as Periplastidial Compartment (PPC), reminiscent of symbiont reduced cytoplasm (Grosche et al., 2014);

- Outer Envelope Membrane (oEM): is reminiscent of the galactolipid-rich chloroplast envelope of the symbiont;

- Inner Envelope Membrane (iEM): developed from the inner envelope membranes of the symbiont's chloroplast.
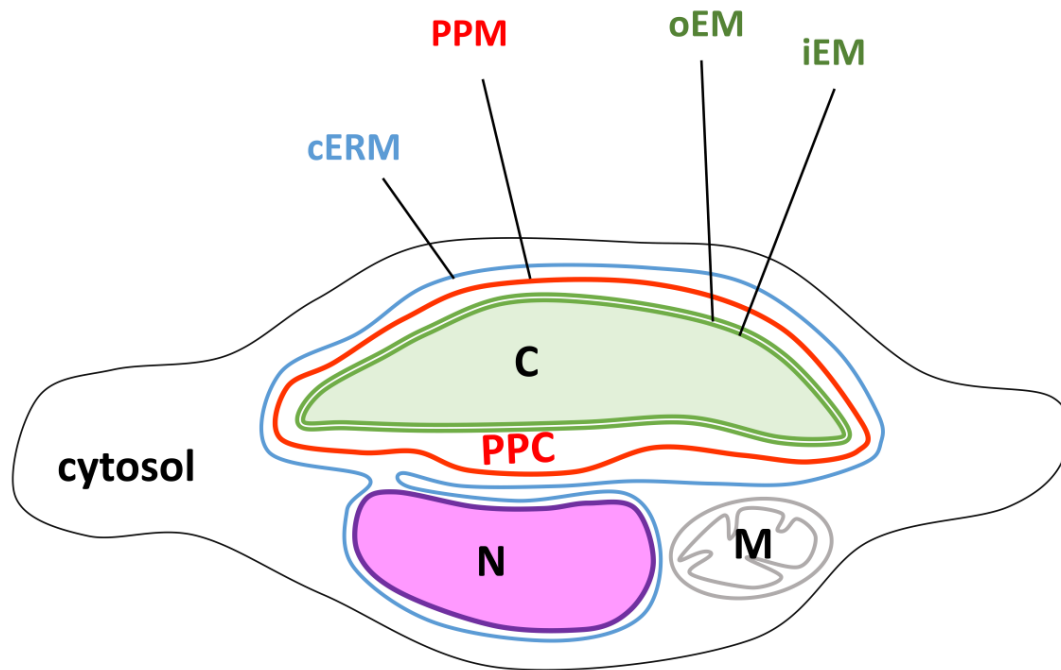
Figure 2.6 | Structural organisation of organelles' membrane in *Phaeodactylum tricornutum* (adapted from Flori et al., 2016). Scheme of the four membranes surrounding the Chloroplast of secondary endosymbionts; from the outside, Chloroplastic ER (cERM) also surrounding the nucleus, Periplastidial Membrane (PPM), outer Envelope Membrane (oEM), inner Envelope Membrane (iEM). The Periplastidial space (PPC) is the region comprised between the PPM and oEM. M: Mitochondrion N: Nucleus.

Due to the peculiar structure of their envelope, secondary endosymbionts have evolved peculiar mechanisms to mediate for the import of nuclear encoded-cytosol synthesized proteins into the plastid. In addition to the plant TOC and TIC related complexes, localised at the oEM and iEM respectively, the diatom *Phaeodactylum tricornutum* evolved a series of protein complexes derived from the ER-associated degradation (ERAD) machinery called SELMA (symbiont-specific ERAD-like machinery) to catalyse the transport of newly synthetised proteins across the PPM (Lau et al., 2016). The high similarity of the TIC-TOC import machinery within primary endosymbiont and the SELMA-dependent system among red complex plastids are both evidence of the occurrence of a single endosymbiotic event for each group during their evolutionary history. Since most of chloroplastic proteins in *P. tricornutum* are encoded by

nuclear genes, they present a bipartite targeting peptide at the N-terminus that allow them to cross the secondary plastid membranes. It comprises a pre-sequences that consist of an ER-type signal peptide and a conserved cleavage ASAFAP motif (Gould et al., 2006; Kilian & Kroth, 2005; Gruber et al., 2015). Even if the length of the amino acid sequence does not seem to be a critical feature for plastid import, this transit peptide is characterized by the presence of a high proportion of hydroxylated residues, few negatively charged residues, and a net positive charge. The cleavage site is localised at the level of the phenylalanine present in the ASAFAP motif in several secondary endosymbionts, including diatoms (Kilian & Kroth, 2005; Gruber et al., 2007). Once the mature protein is imported, the transit peptide is cleaved off, likely by a specific peptidase localised in the stroma (Huesgen et al., 2013).

2.1.6 Characteristics of the molecular actors involved in the crosstalk between the chloroplast and the mitochondrion

In diatoms, the transfer of ATP and reducing equivalents has been well documented but the proteins involved in this exchange are yet to be identified. Even if the cell metabolism comprises numerous and diverse reactions that can influence and regulate one another, the candidate transporters must have precise characteristics. The ATP can be exported from the mitochondrion via specific transporters, already described in different species (Bamber et al., 2007; Pebay-Peyroula et al., 2003), in order to be exploited by the whole cell metabolism. In diatoms, mitochondrial ATP needs to cross the four membranes of the secondary plastid before reaching the chloroplastic stroma and this mechanism has not been characterised so far. This must involve some specific transporters that need to be localised in at least one of the four chloroplastic membranes. Concerning the exchange of NADPH, transporters that likely mediate redox exchanges between the organelles also exists in diatoms (Prihoda et al., 2012). They

remind of the machineries involved in the export of reducing equivalents from the plastids towards mitochondria (*i.e.* the malate shunt, see Kinoshita et al., 2011) which serves as a valve to dissipate excess electrons in plants and green algae. However, because of the different topologies of the envelopes, their nature might be different. One of the most represented group of transporters comprises the mitochondrial carriers (MCs). These are nuclear-coded membrane-embedded proteins that are localized in the inner membranes of mitochondria but also in the inner membrane of chloroplasts. They catalyse the selective transport of specific essential metabolites (di- and tricarboxylates, keto acids, amino acids, nucleotides, and coenzymes/cofactors) across the inner mitochondrial membrane providing a connection between mitochondria and cytosol. This link is of vital importance, as many physiological processes require the cooperation of both intra- and extramitochondrial pathways. All MCs of known function exhibit a tripartite sequence structure, consisting of three tandemly repeated homologous domains of about 100 amino acids in length (Satre et al., 2007). Each domain contains two hydrophobic stretches, separated by hydrophilic regions and every repeat contains the signature sequence motif PX[DE]XX[RK] (PROSITE PS50920 and PFAM PF00153) by which MCs members are recognized.

Amongst the different families of mitochondria carriers, those belonging to the "Mitochondrial Carrier Family" (MCF) (Palmieri et al., 2011) catalyse the translocation across the mitochondrial membranes of a large variety of solutes, connecting numerous metabolic pathways occurring in different cell compartments where specific enzymes are localised (Palmieri, 2013). It is likely that the transporters mediating the energetic crosstalk might belong to this family or at least share some features.

Figure 2.7 | Schematic representation of Mitochondrial Carriers (MCs) localised across the mitochondrial inner membrane (from Palmieri, 2013). So far, 16 MCs have been functionally identified (in green) and their roles in transporting catalyzing metabolites, nucleotides or coenzymes transport regulate multiple pathways of the mitochondrial metabolism. AAC, ADP/ATP carrier; AGC, aspartate glutamate carrier; APC, ATP-Mg/Pi carrier; CAC, carnitine-acylcarnitine carrier; CIC, citrate (tricarboxylate) carrier; CoA, coenzyme A carrier; DIC, dicarboxylate carrier; GC, glutamate carrier; ODC, oxoadipate carrier; OGC, oxoglutarate carrier; ORC, ornithine carrier; PiC, phosphate carrier; PNC, pyrimidine nucleotide carrier; SAMC, S-adenosylmethionine carrier; TPC, thiamine pyrophosphate carrier; UCP, uncoupling protein.

2.2 Results

2.2.1 Identification of putative transporters involved in chloroplast-mitochondria energetic interactions

This PhD project aimed to identify and characterise the molecular actors involved in the energetic exchanges between the plastid and the mitochondrion in diatoms. As a first step to find possible candidates, we started by looking at previous transcriptome analysis, where the gene expression profile of *Phaeodactylum tricornutum* was compared when glycerol was present or absent in the growth medium. In fact, in addition to light as energy supply, this sugar acts as an external carbon source for algal cells, thus enhancing their growth rate when compared to cells grown in a minimum medium (Villanova et al., 2017). We reasoned that, if growth depends on the activity of the two organelles, the activities of which are linked to one another, any modifications of photosynthesis/respiration should have a consequence on the other process, likely mediated by changes in the interactions between the two organelles. Thus, starting from the above mentioned transcriptomic dataset, we focused on the genes encoding for putative transporters, *i.e.* proteins with multiple transmembrane domains and sequence/structure reminiscences of known transmembrane transporters.

Based on these criteria, we were able to identify three candidates, the characteristic of which are listed in the table below.

Gene ID (Ensembl)	Gene Name	Gene Expression Log2(+gly/-gly)	Subcellular Localization ASAFind	BLAST (first annotated gene)	Transmembrane prediction (TMHMM)	I-Tasser 3D prediction)
Phatr3_J46742	Mitochondrial Carrier Family (**MCF**)	-0,50 (±0,08)	Plastid (high conf.)	Mitochondrial Carrier [Fragilariopsis cylindrus] (Diatom)	7	
Phatr3_J35625	Dicarboxylate/ tricarboxylate carrier (**DTC**)	+0,18 (±0,18)	plastid (low conf.)	Mitochondrial Carrier [Fragilariopsis cylindrus] (Diatom)	8	
Phatr3_J15797	**AAC1**	-0,62 (±0,27)	/	ADP,ATP carrier protein 2-like [Nilaparvata lugens] (brown planthopper)	7	
Phatr3_J22873	AAC2	+0,14 (±0,14)	/	ADP/ATP Carrier [Thalassiosira pseudonana]	6	

Table 2.1 | List of selected transporters, putatively involved in the energetic crosstalk between the chloroplast and the mitochondrion in *Phaeodactylum tricornutum*. Gene names are indicated as reported in the Ensemble Protists Gene Browser (protists.ensembl.org). The first two genes have been selected from previous transcriptome analysis (light blue background), comparing algal gene expression profile in presence or absence of glycerol. Additional transporters (orange background) were chosen since they were considered to be a possible targets of bongkrekic acid. Differential gene expression is reported as the logarithm of the ratio of the two growth conditions (+/- glycerol). The webtool ASAFind (Gruber et al., 2015) was used for subcellular localisation prediction in secondary endosymbionts and TMHMM for the number of transmembrane domain (Krogh et al., 2001). Online service I-TASSER provided a 3D model prediction (Roy et al., 2010) (https://zhanglab.ccmb.med.umich.edu/I-TASSER/).

We focused on genes that were differentially transcribed in the presence of glycerol and that were predicted to present multiple transmembrane domains in their amino acid sequence. Moreover, we looked for transcripts coding for proteins that presented a putative secondary plastid target sequence according to ASAFind. This web tool identifies nuclear-encoded plastid-localised proteins in red algae lineage based on the output of SignalP (Petersen et al., 2011) and the recognition of conserved "ASAFAP"-motifs and transit peptides. Finally, we also considered the sequence homology with other characterised proteins from other related species implied in the transport of ATP or reducing equivalent. According to these criteria, we selected three genes out of the list of transcripts derived from the transcriptomic data: DTC (Phatr3_J35625), ACC1 (Phatr3_J15797) and MCF (Phatr3_J46742). A fourth candidate was also chosen through a pharmacological approach that will be described at the end of this section.

2.2.2 Phatr3_J46742 is a peculiar member of the MCF family

According to Ensembl Protists Gene Browser (protists.ensembl.org), the Phatr3_J46742 is located on Chromosome 11 and encodes for the protein B5Y3N0 (UniProt). To investigate the possible function of the protein, we looked for the homologs using the using Basic Local Alignment Search Tool (BLAST) (Altschul et al., 1990) and we found proteins in species closely related or to other diatoms (Table 2.1), such as *Fistulifera solaris* (Oleaginous diatom), *Pseudo-nitzschia multistriata* (bilaterally symmetrical Pennate diatom), *Thalassiosira oceanica* (centric diatoms), *Vitrella brassicaformis* (Alveolate related to parasitic phylum of Apicomplexa, which includes *Plasmodium*, the agent of malaria) and *Fragilariopsis cylindrus* (cold-water diatom found in Arctic and Antarctic sea water and sea ice). The first BLAST hit not related to diatoms or red algae is a gene present in *Chlamydomonas reinhardtii*, coding for the uncharacterized predicted protein XP_001697915.1 (UniProt: A8J8K5) with 54 % of

identity and 72 % coverage. This gene corresponds to the Cre16.g658850.t1.1 sequence in JGI Phytozome database (https://phytozome.jgi.doe.gov), reporting the functional annotation of PFAM mitochondrial carrier protein (PF00153), mitochondrial solute carrier protein (KOG0752), mitochondrial carnitine-acylcarnitine carrier protein (KOG0758) and Mitochondrial oxoglutarate/malate carrier proteins (KOG0759).

Description	Total Score	Query Cover	E-value	Per. Ident	Accession
predicted protein [Phaeodactylum tricornutum CCAP 1055/1]	791	100%	0	100,00%	XP_002185866.1
hypothetical protein FisN_10Hu003 [Fistulifera solaris]	448	85%	2,00E-154	70,57%	GAX21425.1
unnamed protein product [Pseudo-nitzschia multistriata]	399	93%	2,00E-133	57,78%	VEU42048.1
hypothetical protein THAOC_09594 [Thalassiosira oceanica]	389	89%	1,00E-130	61,19%	EJK69176.1
unnamed protein product [Vitrella brassicaformis CCMP3155]	339	75%	1,00E-111	56,61%	CEM36155.1
mitochondrial carrier [Fragilariopsis cylindrus CCMP1102]	342	87%	8,00E-111	62,85%	OEU17374.1
predicted protein [Chlamydomonas reinhardtii]	308	72%	3,00E-99	54,09%	XP_001697915.1

Table 2.2 | Homolog proteins of the Phatr3_J46742 corresponding amino acid sequence (BLAST output). The first hits appear to be proteins belonging to other species of diatoms (*Fistulifera solaris, Pseudo-nitzschia multistriata, Thalassiosira oceanica, Fragilariopsis cylindrus*), suggesting the possible specific physiological role of this protein in this group of organisms.

Using ASAFind web tool (Gruber et al., 2015), we investigated the intracellular localisation of Phatr3_J46742 gene product. A secondary plastid targeting peptide was found, which corresponded to the first 21 AA at the N-terminal portion of the protein sequence.

To understand whether the selected protein was indeed a membrane protein, we used secondary and tertiary structure prediction tools. Transmembrane domains prediction with the server TMHMM (Krogh et al., 2001) (http://www.cbs.dtu.dk/services/TMHMM-2.0/), indicates that it should present 7 hydrophobic alpha helices, suggesting its membrane localisation. We then used the I-TASSER web tool (see Materials and Methods) to predict the tertiary structure from the sequence to obtain more hints regarding the possible membrane localisation of this protein. For this prediction studies, we removed the first 21 AA corresponding to the chloroplastic target polypeptide, since it is cleaved once the protein reaches its final conformation. The output of the program showed that the best predicted model (c-score = -0.55, see Materials and Methods) appeared to be related to the known structures of well-characterised transporters: the mitochondrial ADP-ATP carriers in *B. taurus* (PDB: 2C3E) (Fig. 2.8) and *S. cerevisiae* (PDB: 4C9Q). Overall, the prediction of intracellular localisation, secondary and tertiary structure of the protein encoded by the Phatr3_J46742 gene make it a good candidate to be a plastid membrane protein with a possible role as a transporter.

We gained more information by investigating the evolutionary history of the Phatr3_J46742 gene. In collaboration with Pierre Cardol, from the University of Liège (Belgium), and Richard Durrel, from Institut de Biologie de l'Ecole Normale Supérieure (IBENS) in Paris, we generated a phylogenetic tree showing distribution of the gene of interest and its closest homologs Phatr3_J46612 and Phatr3_J42874 (see Table 2.3) among other species.
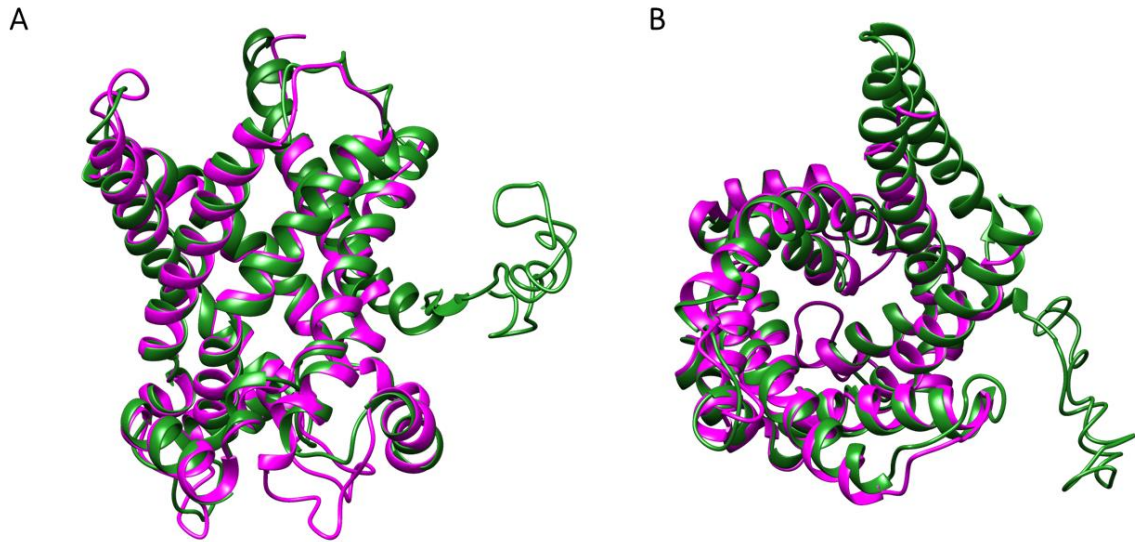
Figure 2.8 | Protein structure prediction derived from the amino acid sequence of the Phatr3_J46742 gene product with I-TASSER. The best model of MCF (in green) and the most similar crystal structure present in the PDB, corresponding to the mitochondrial ADP/ATP carrier (purple) (Pebay-Peyroula et al., 2003). **A**, side view of the carriers, top corresponds to the intermembrane space, bottom to mitochondrial lumen, according to the topology of the ADP/ATP carrier (Pebay-Peyroula et al., 2003). **B**, Top view of the channel, from the intermembrane space.

Description	Total Score	Query Cover	E-value	Per. Ident	Accession	UniProt ID	Ensemble protists ID	ASAFind
predicted protein	791	100%	0	100.00%	XP_002185866.1	B5Y3N0	Phatr3_J46742	High confidence
predicted protein	268	73%	1.00E-88	46.32%	XP_002181098.1	B7G1V3	Phatr3_J46612	No
predicted protein	221	73%	1.00E-69	42.46%	XP_002176773.1	B7FPV3	Phatr3_J42874	No
predicted protein	33.5	43%	0.07	21.08%	XP_002185141.1	B7GDJ7	Phatr3_J23908	No
predicted protein	26.6	14%	8.7	25.00%	XP_002179307.1	B7FXB0	Phatr3_J11634	No

Table 2.3 | Homolog proteins of Phatr3_J46742 in *P. tricornutum*. The closest related proteins, encoded by Phatr3_J46612 and Phatr3_J42874 genes, were selected for further phylogenetic studies. The results of the ASAFind software indicates whether the gene product is likely to be targeted to the secondary plastid, which was predicted only for Phatr3_J46742.

50

The resulting tree (Fig. 2.9) derived from the analysis of composite genome and transcriptome library of the entire tree of life, using reciprocal BLAST best hit and previously defined methodology (Rastogi et al., 2018; Dorrell et al., 2019).

We observed that Phatr3_J46742 belongs to the MCF family and that this protein is related to other diatom chloroplast-targeted proteins, consistent with its predicted plastidial localisation. The Mitochondrial Carrier Family" (MCF) (Palmieri et al., 2011) comprises a variety of transporters responsible for the translocation across biological membranes of a wide range of substrate, including ATP and reducing equivalents. Even if a large fraction of these transporters are localised in the mitochondrial inner membrane, some members of this family are also found in other organelles, thus contributing to the complex cell metabolic network (Palmieri, 2013). Additionally, Phatr3_J46742 (named from now on Pt-MCF) and the related Phatr3_J42874 are shared between photosynthetic organisms, primarily in lineages with a history of secondary endosymbiosis (*e.g.* the diatoms *Fistulifera solaris*, *Pseudo-nitzschia multistriata* and *Thalassiosira oceanica*, the alveolate *Chromera velia*, the dinoflagellate symbiodinium, the Eustigmatophyceae Nannochloropsis etc.), and in species that have lost their chloroplast during evolution (*e.g. Toxoplasma gondi*), while they are absent in non-photosynthetic organisms.

These findings, plus the presence of a plastid-targeting signal strongly support the hypothesis of a possible plastidial localization. Moreover, this assumption was supported by Pr Hanhua Hu from the Chinese academy of Science, who recently purified intact chloroplast from *P. Tricornutum*. After investigating the plastid's proteome by mass spectrometry (unpublished), they were able to find also the protein encoded by Pt-MCF gene. Overall these data point to a peculiar chloroplast localisation of this gene product compared to other members of the MCF family that have been characterised so far, which were mainly found in mitochondria, some in

chloroplasts (as reviewed in Haferkamp, 2007) and (in a very few cases) in the peroxisomes (Satre et al., 2007).

Figure 2.9 | Phylogenetic tree of Phat 46274 and its closest relatives. The tree topology shown is the consensus inferred using MrBayes with three substitution matrices (GTR, Jones, WAG) and RAxML with three matrices (GTR, JTT, WAG). Branches are coloured by taxonomic affiliation. Taxon names are coloured by the inferred subcellular localisation of the protein (for lineages containing four-membrane bound plastids), or in grey (for lineages that do not contain four membrane-bound plastids). Circles at each node are shaded by consensus support for the topology shown. Three evolutionarily distinct families of homologues identifiable in the *Phaeodactylum* genome are labelled with circular brackets.

2.2.2.1   Generation of Pt-MCF Knock-Out Mutant Strains.

The transporter features and the putative plastid localisation of the Pt-MCF protein prompted us to investigate its possible role in the chloroplast-mitochondria energy interactions. To this aim, we generated KO strains using the CRISPR-Cas9 technology: we modified a specific plasmid previously used (Falciatore et al., 1999), which now includes the vector for transformation and the zeocin resistance cassette (see Material and Methods). After transformation, we obtained 31 zeocin resistant *P. tricornutum* (Pt1) colonies. Sequencing analysis revealed that two independent clones were carrying mutations in the Phatr3_J46742 gene, introducing a stop codon predicted after 90 amino acids. These two clones were further tested for their content of Pt-MCF protein by western blot. For this purpose, the corresponding gene was expressed in *E. coli*, and the gene product was purified and sent to a private company for the generation a specific polyclonal antibody (see Chapter 3: Material and Methods). Western blot analysis revealed that the antibody recognises a band of around 40 kDa in the WT, corresponding to the predicted molecular weight of the Pt-MCF protein. The band is absent in the two selected colonies, confirming that we successfully generated knocking out lines of the Phatr3_J46742 gene. To confirm that the altered phenotype observed in these mutant strains, later described in the text, is indeed associated to the lack of the gene of interest, we proceeded by complementing the KO algae. We transformed these cells with a second plasmid carrying the original WT copy of gene with altered sequence at the level of the region recognised by the Cas9 endonuclease, to avoid digestion. However, even if the new inserted gene appeared to be amplified through PCR, the transformation finally proven unsuccessful, as none of the recovered lines expressed the Pt-MCF protein, as indicated by the absence of the band in the western blot after incubation with the correspondent antibody (see *e.g.* an example in Fig 2.10).
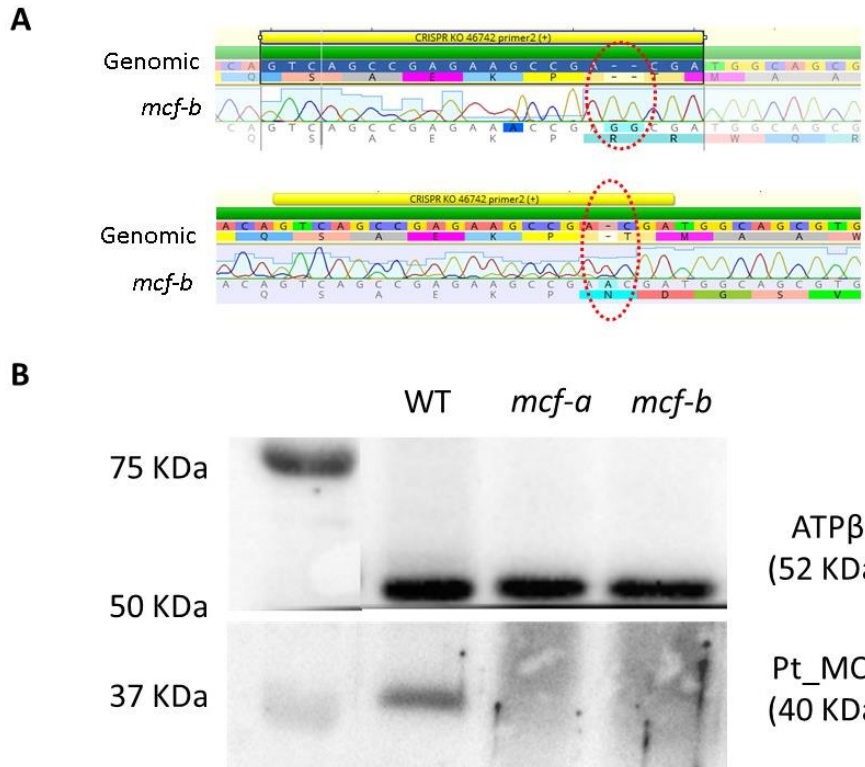
Figure 2.10 | Molecular characterisation of the Pt_MCF KO mutants. A, Sequencing of the Phatr3_J46742 gene in *mcf-a* and *mcf-b* indicates that both clones bear a stop codon after 90 codon triplets due to the insertion of 2 and 1 base pair, respectively. Western blot analysis (**B**) confirm the successful knocking out of the Pt-MCF gene by revealing the absence of a specific protein at around 40 KDa in the two mutant lines. Note that mutant complementation did not proved successful, as the MCF protein was still missing in putative complemented lines (data not shown).

2.2.2.2   Functional Phenotype of Pt-MCF KO mutant strains

To investigate the possible role of Pt-MCF in diatoms energetic exchange between the plastid and the mitochondrion, we first evaluated the photosynthetic capacity of the two generated mutant strains. Thanks to an *in vivo* imaging approach, it is possible to measure the quantum yield of PSII derived from chlorophyll fluorescence and consequently calculate the Electron Transfer Rate (ETR) (see Material and Methods). Our analysis revealed that both KO lines display lower photosynthetic performances when compared to the wild type (WT) cells. In fact,

even if the ETR signal reached its maximum value at the same light intensities as for the wild-type strain, we observed that this parameter was decreased by 40% and 20% for the *mcf-a* and *mcf-b* respectively, suggesting that the loss of Pt-MCF has a detrimental impact on photosynthesis. We next measured the establishment of Non Photochemical Quenching (NPQ), a parameter that reflects the ability of the cells to cope with a high light stress, also deduced by chlorophyll fluorescence analysis. If the cells are in favourable environmental conditions most of the absorbed light is exploited for carbon assimilation. However, a significant portion is dissipated under excess illumination, thanks to the onset of protective mechanisms that enhance thermal emission. As observed in the case of the ETR, mutant strains show a lower (around 25%) NPQ capacity after exposure at high light, but a similar induction and relaxation kinetics as the WT.
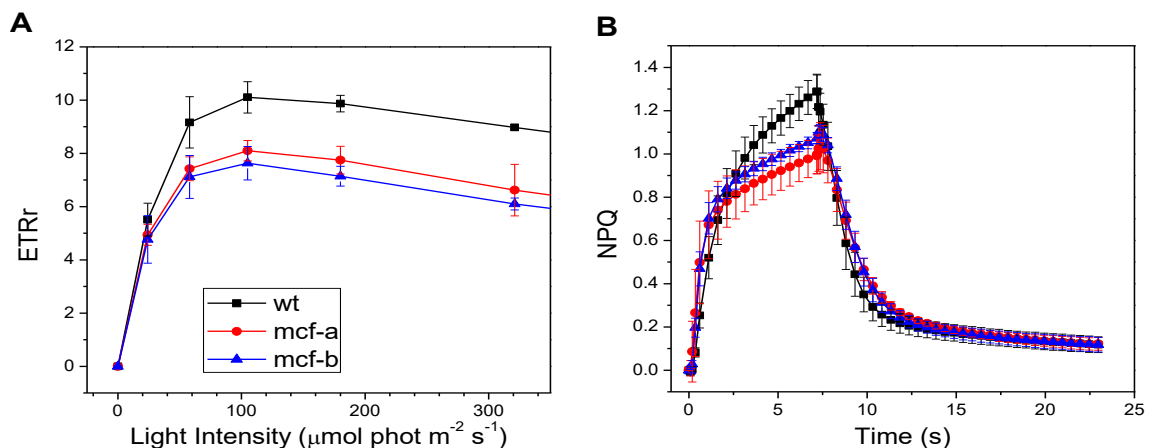
Figure 2.11 | Photosynthetic phenotype of two PT_MCF knockout mutant strains. Measurements were performed on *P. tricornutum* cells in exponential growth phase (between 1 and $3 \cdot 10^6$ cell ml^{-1}). After centrifugation (3500g, 5', 19°C) cells were distributed on a 96-well plate at $20 \cdot 10^6$ cell ml^{-1} concentration in 150 µL volume of growth medium. For both ETR (**A**) and NPQ (**B**) data correspond to average +SD of 3 replicate independent experiments, each comprising 3 technical replicates. ETR and NPQ were calculated according to Maxwell and Johnson 2000 (see Materials and Methods).

To complete the physiological characterisation of the mutant lines, we tested their capability to maintain a proton motive force ($\Delta\Psi_d$) in the dark. Previous studies conducted by researchers

from the host laboratory have revealed that diatoms are capable of generating a PMF in the dark across thylakoids membranes, thanks to the hydrolysis by the chloroplast CFo-FI ATPase/ATPsynthase of ATP generated by mitochondrial respiration (Bailleul et al., 2015). Thanks to the peculiar spectroscopic properties of the pigments embedded in the thylakoid membranes of *Phaeodactylum tricornutum*, it is possible to quantify the absolute value of the electric field across the photosynthetic membranes through the deconvolution of the Electrochromic shift (ECS) signal. The ECS is the Stark effect observed in photosynthetic pigments after light exposure, meaning the shifting of their absorption spectra in the presence of a transmembrane electric field in the thylakoids (see Material and Methods). In diatoms, two components displaying different spectra (Fig. 2.12A) constitute the ECS signal and their intensities respond to changes of the membrane $\Delta\Psi$ with a linear (at 520 nm) and quadratic (at 565 nm) dependence (Bailleul et al., 2015; Joliot & Joliot, 1989). They likely correspond to the presence of polar and polarizable pigments, in particular to their relative ECS responses to the electric field (Fig. 2.12B). When plotting the amplitude of the quadratic versus linear ECS components during the relaxation of a light-induced $\Delta\Psi$, a parabolic function is obtained (Fig. 2.12C): the $\Delta\Psi$ corresponds to the difference between the recorded signals and the vertex of the curve. As demonstrated by Bailleul and colleagues, in WT *Phaeodactylum tricornutum* cells, the minimum measured value does not correspond to the minimum of the parabola, indicating the presence of the $\Delta\Psi$ also in the dark ($\Delta\Psi_d$). The $\Delta\Psi_d$ can be depleted only when algae are treated with uncouplers (carbonyl cyanide-4-(trifluoromethoxy)phenylhydrazone, FCCP) and by blocking the mitochondrial activity. The latter is achieved either through anaerobiosis or by adding a combination of specific inhibitors, notably antimycin A (AA) plus salicylhydroxamic acid (SHAM) (Fig. 12D). These two molecules are responsible for the inactivation of the cyanide-sensitive (complex III) and the cyanide-insensitive (alternative oxidase, AOX) respiratory pathways respectively (Fig. 2.12E). This indicates that the mitochondrial activity is

responsible for the residual $\Delta\Psi_d$ measured in plastids, likely through the hydrolysis of the ATP

imported from the mitochondrion by chloroplast ATPase, as proposed above.

Figure 2.12 | ECS signal observed in *Phaeodactylum tricornutum*. A, The ECS spectrum (black) is constituted by two different components and their association to polar and polarizable pigments embedded in the thylakoid membranes (**B**) exhibiting a linear (blue) and quadratic (red) growth relationship to the $\Delta\Psi$ (r.u., relative units). The relationship between quadratic and linear ECS fitting a parabolic function in control conditions (**C**), with addition of the uncoupler (FCCP, black squares), anaerobiosis (red circles) and respiratory inhibitors (AA and SHAM; blue circles) (**D**). The green arrow indicates the proton motive force in the dark ($\Delta\Psi_d$). **E**, Putative model of the energetic crosstalk between chloroplasts (left) and mitochondria (right) in the dark. Red arrows: oxidative phosphorylation electron flows. Green dashed line: possible ADP/ATP transfer mechanism between the organelles. ATPase, ATPase/ synthase; b6f, cytochrome b6f; I/III/IV, respiratory complexes I, III and IV. Adapted from (Bailleul et al., 2015).

To test the implication of Pt-MCF in this process, we evaluated the extent of $\Delta\Psi_d$ in the WT and mutant lines. We reasoned that mutant strains with altered organelle crosstalk mechanism should show a similar repercussion on the PMF to the one caused by inhibitors, meaning a quadratic VS linear ECS minimum closer to the vertex of the parabola. This effect would reflect the affected ATP exchange mechanisms in an alga lacking a transporter involved in this crosstalk process. This was indeed the case, since the $\Delta\Psi_d$ signal appeared to be 25% and 50% lower in the mutant strains with respect to the WT strain. The fact that these photosynthetic parameters are affected in the mutant lines despite Pt-MCF is not predicted to be part of the photosynthetic apparatus implies that this transporter might in fact be involved to some extent in the energetic interactions between the two organelles in diatoms.

Figure 2.13 | Effect of the lack of the Pt-MCF gene on the proton motive force in the dark ($\Delta\Psi_d$) in *P. tricornutum* cells. Measurements were performed on *P. tricornutum* cells in exponential growth phase (between 1 and $3\cdot10^6$ cell ml^{-1}). After centrifugation (3500g, 5', 19°C) cells were placed in a 2 ml plastic cuvette at $20\cdot10^6$ cell ml^{-1} concentration in 1.5 ml volume. ECS measurements were conducted using a Joliot Type Spectrophotometer (JTS). Data ± SE form 3 independent experiments, the $\Delta\Psi_d$ in the control sample was set to 100%. ECS Linear and quadratic components of P. tricornutum cells were deconvoluted and $\Delta\Psi_d$ calculated as described in Chapter 3: Materials and Methods.

2.2.2.3   MCF contributes to the synergy between photosynthesis and respiration in *P. tricornutum*.

The results obtained so far from the analysis of the different photosynthetic parameters indicate that the absence of Pt-MCF modifies the interactions between the two energetic organelles in the dark. Previous results by Bailleul and colleagues (Bailleul et al., 2015) suggest that these exchanges of molecules between the plastid and the mitochondrion also occur in presence of light, since they are believed to optimise CO_2 assimilation by the cells. This is indicated by the fact that the photosynthetic activity linearly increases with the cell respiration rate, as revealed by oxygen evolution and consumption analysis, either by polarographic approaches (*e.g.* with a Clark electrode) or Membrane inlet Mass Spectrometry (MiMS). This linear relationship would reflect the export of reducing power in excess from the plastid to the mitochondria, its consumption to produce ATP, and the concomitant import of ATP into the chloroplast to fuel CO_2 assimilation (Fig. 2.14).

Since Pt-MCF appeared to be involved in the regulation of photosynthesis (ETR and NPQ), we decided to further investigate its possible role in the relationship between photosynthesis and respiration. First, we used a Clark Oxygen Electrode system to measure oxygen evolution and consumption in light and dark conditions respectively. We performed a titration of different concentrations of SHAM and Antimycin A, inhibitors of mitochondrial respiratory pathway, in order to progressively decrease the activity of this organelle and observe the consequences on the photosynthetic performances. By plotting the oxygen evolution rate against oxygen
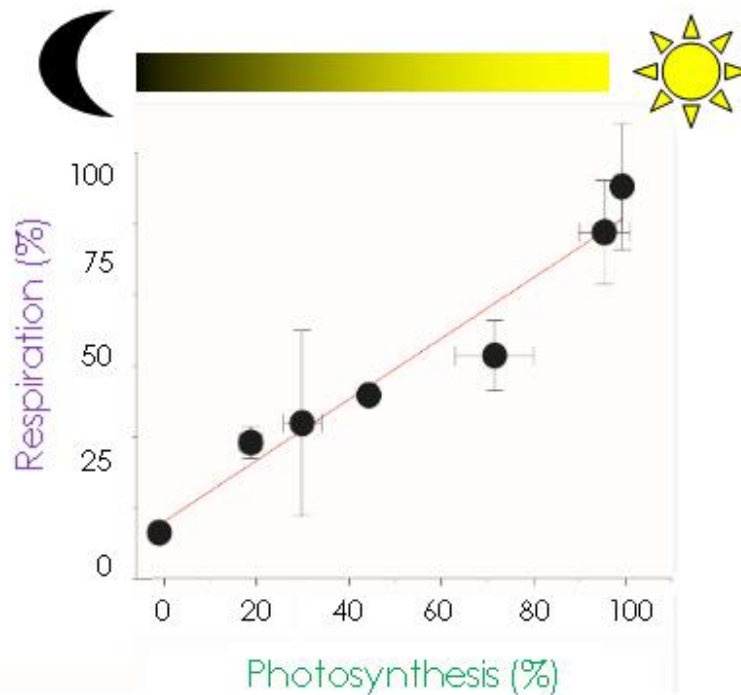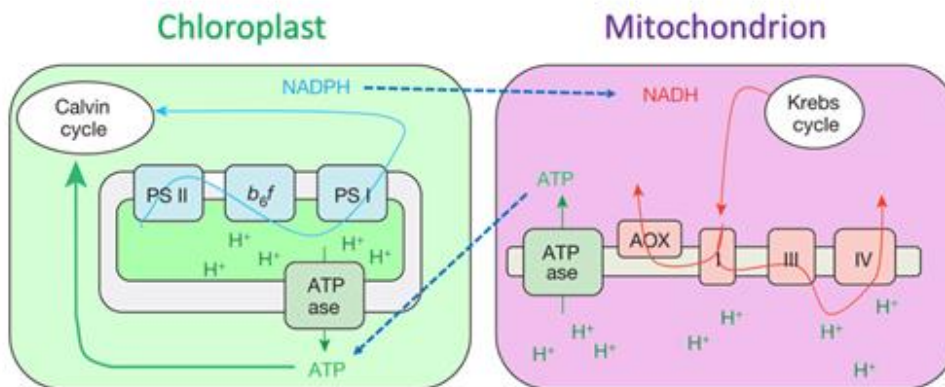
Figure 2.14 | Photosynthesis/respiration relationship. A, Linear relationship between the photosynthetic and the mitochondrial respiration activities (adapted from Bailleul et al., 2015). **B**, Schematic representation of the energetic exchanges model connecting the mitochondrial and chloroplastic activities.

consumption rate, we established the relation between photosynthesis and respiration. Coherently with the results previously published (Bailleul et al., 2015), the two mechanisms show a linear dependence in the WT, meaning that the increase activity of one pathway contributes to the enhancement of the other. This linearity was also observed in the mutant

strain. However, the steepness of oxygen evolution over consumption was less pronounced in the KO strain (Fig. 2.15), suggesting that the crosstalk between the two organelles was modified upon removal of Pt_MCF. In particular, the photosynthetic activity increased more slowly at higher rate of oxygen consumption in the dark.

Figure 2.15 | Analysis of photosynthesis/respiration relationship. *P. tricornutum* cells in exponential growth phase (between 1 and $3 \cdot 10^6$ cell ml^{-1}) were centrifuged (3500g, 5',19°C) and placed in a specific 2 ml cuvette at $20 \cdot 10^6$ cell ml^{-1} concentration in 1 ml volume. Photosynthetic activity was measured as O_2 evolution in light and cellular respiration rate as O_2 uptake in the dark. The mitochondrial activity was titrated with increasing amount of the respiratory inhibitors SHAM and Antimycin A (SHAM+AA: 0; 0,4mM+2μM; 0,66mM+3,33μM; 1mM+5μM; 2mM+10μM; 4mM+20μM). Data ± SD from 3 independent experiments.

As we recorded low O_2 evolution signals at the Clark electrode, we obtained relatively scattered and noisy data, which did not allow us to accurately quantify the effect of the Pt-MCF mutation on the relationship between photosynthesis and respiration. Therefore, we decided to measure this parameter using the more powerful MiMS approach, in collaboration with Dr. Duncan Fitzpatrick form the laboratory of Prof. Eva-Mari Aro, at the University of Turku, Finland.

Molecular oxygen evolution and uptake of algae grown in minimum ESAW 10NP medium were recorded in the dark, at two different light intensities (low light: 25 µmol phot $m^{-1}s^{-2}$; high light: 250 µmol phot $m^{-1}s^{-2}$) and again dark, for four minutes per condition (Fig 16A). Thanks to the addition of ^{18}O and ^{13}C isotopes, we were able to record the rates of photosynthesis and cellular respiration simultaneously upon different light conditions (see Materials and Methods). When analysing photosynthesis, O_2 evolution and $^{13}CO_2$ fixation rates displayed similar trend between the mutant and the WT strain, showing an approximate linear relationship to the light intensity (data not shown). Unfortunately, we did not have enough time to optimize the protocol for the CO_2 production during my stay at the Plant Molecular Biology laboratory in Turku, so we focused on the $^{18}O_2$ uptake signal to evaluate the activity of the mitochondrion. Cellular respiration showed no relevant activity in any sample during the dark and low light phase (Fig. 2.16). However, the $^{18}O_2$ uptake rate presented an increment upon high light illumination in all samples. Moreover, the signal of *mcf-a* strain displayed a spike after low to high light transition of about 10 seconds before attaining at a lower steady state activity and overall the ratio of O_2 evolution over uptake rate turned out to be significantly lower in mutant strain compared to the WT at high light.
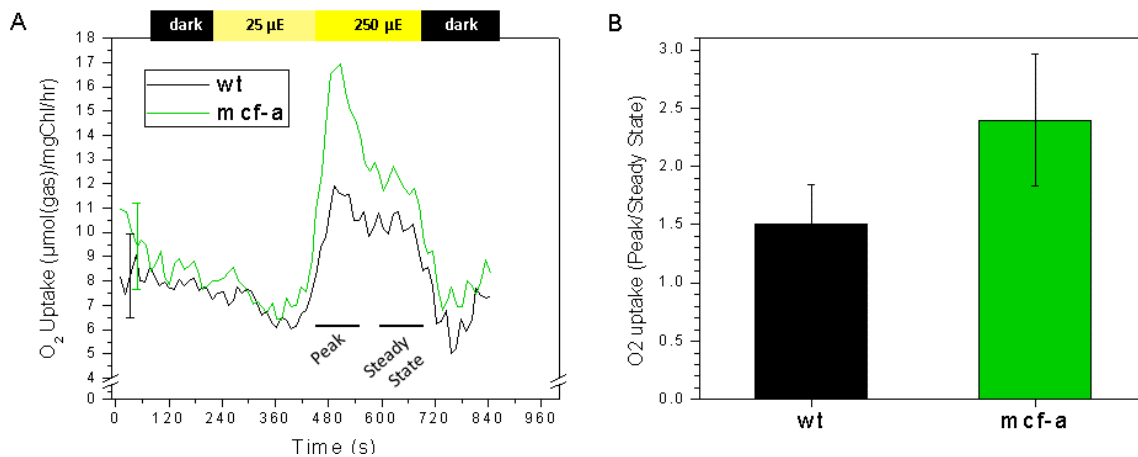
Figure 2.16 | O$_2$ uptake rates of *P. tricornutum* cells at different light intensities (dark, 25µEm^{-2}s^{-1}, 250 µEm^{-2}s^{-1}, dark). **A**, After dark adaptation, cells were kept for four minutes in each condition. Data correspond to the average + SD of 4 independent replicates. **B**, Ratio between O$_2$ uptake peak from low (25 µEm^{-2}s^{-1}) to high (250µEm^{-2}s^{-1}) light transition and the Steady State (see Fig. A). Net values of both Peak and Steady State were obtained by subtracting the average value of O$_2$ consumption in the dark.

This trend was confirmed when comparing the data obtained from our measurements at the MiMS to what was previously published (Fig. 2.17), the relationship between photosynthesis and respiration appeared to be the same in both mutant and wt strain at low light intensity, while it differs at saturating light conditions. We tentatively interpret this higher O$_2$ consumption in terms of an increased mitochondrial performance or the occurrence of photo/chloro respiration in the mutant strain, likely to compensate for the unbalanced redox/ATP exchanges. If the MCF protein is indeed involved, either directly or indirectly, in the ATP exchange mechanisms between the mitochondrion and the plastid, especially in the import of this molecule in the chloroplast, the transitory high O$_2$ consumption might reflect a stronger Chlororespiration activity due to the over-reduction of PSII.
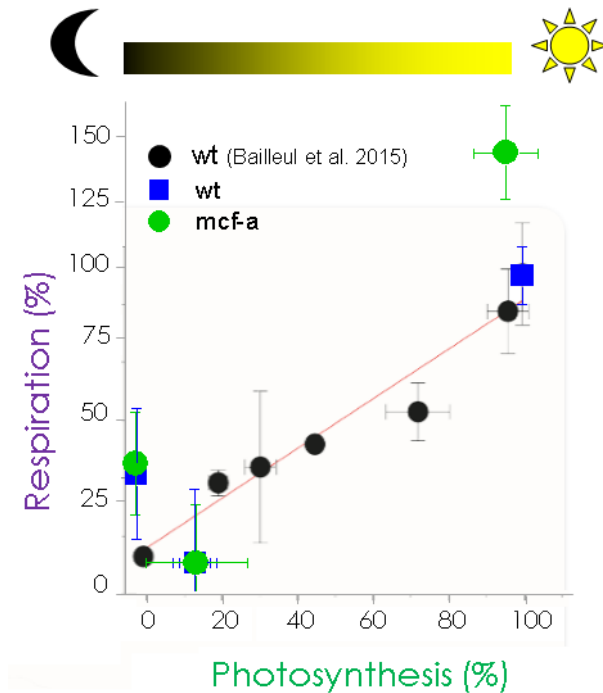
Figure 2.17 | Comparison of the measured O₂ evolution and ¹⁸O₂ uptake rates with previously published data (Bailleul et al., 2015). Respiration values correspond to the peak phase after low (25 µEm⁻²s⁻¹) to high light transition (250 µEm⁻²s⁻¹). Data correspond to the average + SD of four independent replicates.

2.2.2.4   Substrate specificity of Pt-MCF.

As indicated above, the functional characterisation of MCF mutants suggests that this protein may be involved in the crosstalk processes involving the chloroplast and the mitochondrion in *Phaeodactylum tricornutum*, possibly by playing a role in the exchanges of ATP or NADPH. Transporters belonging the MCF group have been described to transport a large variety of substrates, including ATP and reducing equivalents, such as di-/tri-carboxylates like malate and oxoglutarate (Palmieri et al., 2011; Palmieri, 2013). To further investigate the mechanisms by which Pt-MCF regulates the photosynthetic and respiration activities, we decided to test the Pt-MCF specificity in collaboration with the laboratory of Pr. Ferdinando Palmieri at the University of Bari, Italy. Pr. Palmieri's research group has conducted many studies where they

identified and characterised membrane transporters, often focusing on proteins belonging to the Mitochondrial Carrier Family in both animals and plants.

By optimising the protocol employed to produce the Pt-MCF protein for antibody synthesis, in the lab we have been able to obtain higher amounts of protein with a purity that was enough to include into lipid micelles and test substrate specific with radioactive compounds.
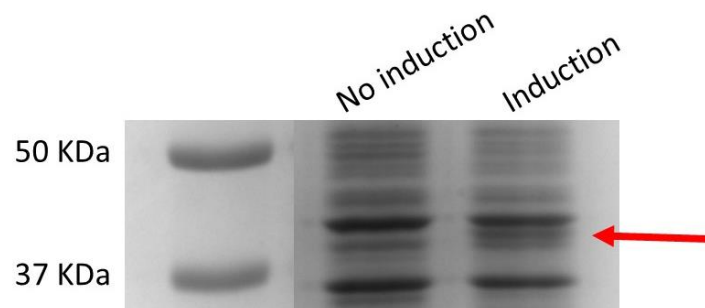
Figure 2.18 | SDS-PAGE confirming the expression of Pt-MCF protein in Rosetta2 *E.coli* competent cells. The two lines correspond to protein extractions performed on samples before and after induction of protein expression, which was carried out by incubation with 0,4 mM IPTG over night at 37 °C. The red arrow indicates the band at 40 kDa corresponding to the predicted molecular weight of Pt-MCF.

Despite several attempts, no activity of MCF could be detected by this approach so far. This negative result could either reflect a misfolding of the protein during micelle incorporation or an inhibition of activity by the micelle environment. These experiments were performed indeed prior to the identification of Pt-MCF as a plastid protein, thus the lipid composition of the micelles reflected therefore those of mitochondrial membranes (*i.e.* enriched in cardiolipin), which might affect the correct folding of proteins specific for plastid membranes.

Based on the recent information concerning its plastidial localisation, we have agreed to repeat these experiments after incorporation of Pt-MCF in micelles produced using plastid-derived lipids.

2.2.2.5 Consequences of Pt-MCF on growth

Even if we were able to address the influence of Pt-MCF in coordinating photosynthesis and respiration, we could not observe major differences in growth between WT and mutant cells. On average, the cell division rates appeared to be similar (around 1 per day) in both strains under normal growth condition (19°C, 40 µmoles photons m^{-2} s^{-1}). This evidence suggest that the activity of other transporters involved in the regulation of the organelles crosstalk might be sufficient to compensate for the negative consequences derived by the lack of Pt-MCF.

In order to test this possibility, we examined the consequences of altering the activity of the other candidates pinpointed by our transcriptomic analysis on *P. tricornutum* photosynthesis.
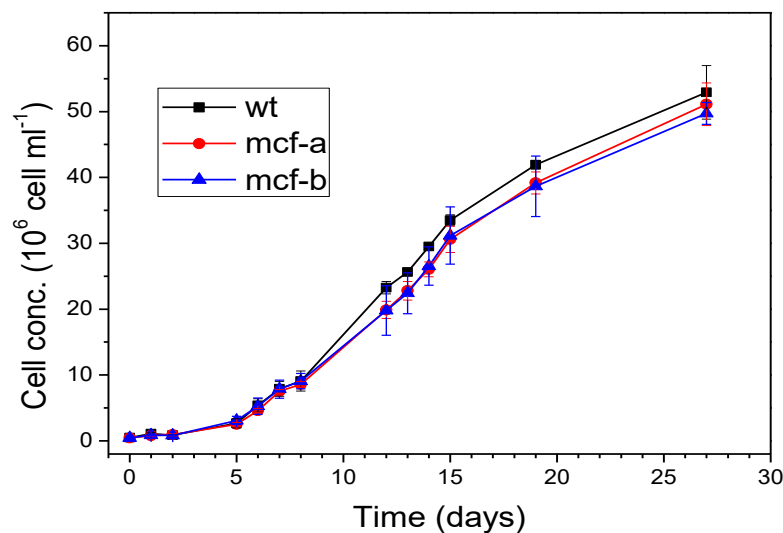
Figure 2.19 | Growth curve of *Phaeodactylum tricornutum* knock-out mutant strains lacking the gene Phatr3_J46742 coding for Pt-MCF. Cells cultures of $0.5 \cdot 10^6$ cells ml^{-1} were cultivated in ESAW10NP medium and growth was followed for 27 days during weekdays. Data ± SD from 3 biological replicates.

2.2.3 Are there other transporters involved in the chloroplast mitochondria interactions?

Out of the list of genes derived from transcriptomic data, we then focused on the candidate gene Phatr3_J15797 annotated as ADP/ATP Carriers (AAC), which, like Pt-MCF, also belongs to the Mitochondrial Carrier Family (Palmieri, 2013). AAC are in fact the best-characterised members of this group and they catalyse the ADP/ATP exchange across biological membranes. Since ATP synthesis occurs in the mitochondrial matrix, it needs to be exported toward the cytosol in order to be exploited in multiple metabolic processes while the import of ADP into the mitochondrial matrix is required for the synthesis of new ATP. Different studies show that the exchange of ADP and ATP is accomplished by AACs localised in the inner membrane of the mitochondrion, the selective barrier for solutes. The structure of this protein was first solved from the bovine orthologous in 2003 (Pebay-Peyroula et al., 2003) and it still is the reference for structural studies on other mitochondrial carriers (*e.g.* Palmieri et al., 2011) while the corresponding PET9 (or Anc2) (UniProt: P18239) in yeast is used for physiological characterization (Zeman et al., 2003).

The structure of AAC comprises six transmembrane α-helices that form a barrel around the cavity, with both C-end and N-end protruding toward the intermembrane space (Fig 2.20). The region located at the matrix side presents a typical six amino acids peptide (RRRMMM), a consensus sequence generally shared by nucleotide carrier. The 3D structure of this protein also indicates that the equal molar ADP/ATP exchange relies on the interchange between the "cytosolic-open" (Ruprecht et al., 2014) and the "matrix-open" conformation (Ruprecht & Kunji, 2019), which can only bind and transport ADP and ATP respectively (Klingenberg, 2008; Robinson et al., 2008).
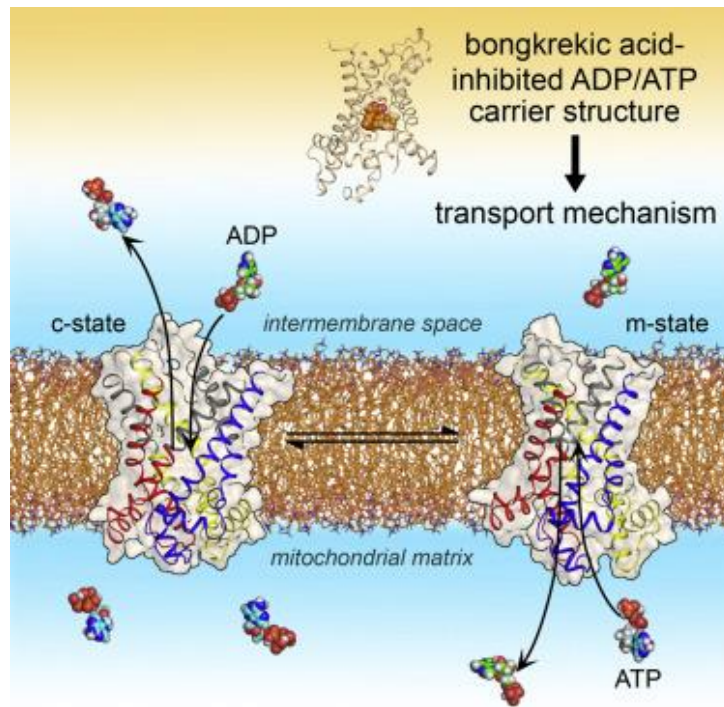
Figure 2.20 | ADP/ATP Carrier transport mechanism (from Ruprecht & Kunji, 2019)). The "cytosolic open" state (c-state) allows either the binding of ADP or the release of mitochondrial ATP. The transition to the "matrix open" state (m-state) conformation consists on the rotation of six mobile transmembrane helices around a central substrate-binding site, allowing the release of ADP and the binding of ATP.

More details describing the structural organization and conformational changes of AAC have been investigated through Molecular Dynamics Simulations, suggesting that the ability of the carriers to transport two different substrates might derive from the asymmetric structural organization of this transporter at the level of the pocket of the "cytosolic-open" state (Yi et al., 2019).

The possible ADP/ATP carrier nature of the protein encoded by the Phatr3_J15797 gene was also suggested by BLAST analysis, as it appeared to align to other members of the AAC group (Table 2.4) in different organisms. Since multiple members of this protein family exist in yeast and mammals, we looked for more possible AACs homologs in *P. tricornutum*. Therefore, we searched for other putative intraspecific homologs of Phatr3_J15797genes by running a BLAST against the genome of *P. tricornutum*, 7 and other putative AAC genes were found. We chose

the best hit, encoded by the gene Phatr3_J22873, presenting the highest sequence identity and named therefore the two genes AAC1 and AAC2, respectively.

Description	Total score	Query cover	E-value	Ident	Accession
predicted protein [Phaeodactylum tricornutum CCAP 1055/1]	591	92%	0	87.83%	XP_002184022.1
hypothetical protein THAOC_04708 [Thalassiosira oceanica]	274	95%	3.00E-86	44.23%	EJK73656.1
predicted protein [Thalassiosira pseudonana CCMP1335]	250	97%	5.00E-77	41.14%	XP_002289981.1
unnamed protein product [Pseudo-nitzschia multistriata]	223	89%	2.00E-65	45.27%	VEU41805.1
ADP,ATP carrier protein 2-like [Nilaparvata lugens]	207	96%	7.00E-61	35.16%	XP_022196757.1
ADP,ATP carrier protein 2 [Anopheles darlingi]	207	93%	1.00E-60	36.68%	ETN61769.1
adenine nucleotide translocase insect1 [Planococcus kraunhiae]	207	96%	2.00E-60	34.71%	BAV14133.1
PREDICTED: ADP,ATP carrier protein 2 [Habropoda laboriosa]	206	93%	3.00E-60	35.41%	XP_017791641.1
ADP,ATP carrier protein 2 [Athalia rosae]	206	93%	3.00E-60	36.26%	XP_012261845.1
ADP/ATP translocase [Nilaparvata lugens]	205	96%	5.00E-60	34.89%	AGI96985.1

Table 2.4 | Homologs proteins of the Phatr3_J15797 corresponding amino acid sequence. First hits BLAST output with E-value lower than 10^{-10} are listed. The presence of other AAC protein from different species suggest the AAC nature of the selected protein in *P. tricornutum*.

Description	Total Score	Query Cover	E value	% Ident	Accession	
predicted protein	615	100%	0	100.00%	XP_002184022.1	AAC1 (Phatr3_J15797)
predicted protein	176	97%	8,00E-54	35.43%	XP_002183547.1	AAC2 (Phatr3_J22873)
predicted protein	115	94%	2,00E-30	28.04%	XP_002184712.1	
predicted protein	135	61%	2,00E-15	28.57%	XP_002181224.1	
predicted protein	70.9	100%	2,00E-14	23.66%	XP_002185715.1	
predicted protein	67.8	99%	4,00E-13	25.72%	XP_002177113.1	
predicted protein	61.2	63%	3,00E-11	23.92%	XP_002179991.1	
predicted protein	60.8	63%	5,00E-11	23.92%	XP_002179990.1	
predicted protein	59.7	79%	1,00E-10	20.16%	XP_002186328.1	

Table 2.5 | Homolog proteins of Phatr3_J15797 in *P. tricornutum*. First hits from BLAST output with E-value lower than 10^{-10} are listed. The best hit was selected for further physiological analysis.

To investigate the possible involvement of the selected AAC transporters in the energetic interactions between chloroplast and mitochondria in diatoms, we first tested the effect of known inhibitors of mitochondrial AAC called carboxyatractyloside (CATR) and bongkrekic acid (BKA).

The two molecules have the same inhibitory effect but bind to different sites within the AAC structure and block the protein in different conformations. Moreover, the mitochondrial inner

membrane is impermeable to CATR but not to BKA. CATR is a diterpene glycoside which binds to the substrate-binding site of AAC and blocks it in the "cytosolic open" state (c-state), with the ADP-binding site accessible to the intermembrane space, which is confluent with the cytosol (Vignais et al., 1973). BKA is a polyunsaturated methoxy tricarboxylic acid, a lethal toxin produced by the gram-negative bacterium *Burkholderia gladioli pathovar cocovenenans* found in fermented coconuts. This molecule locks the AAC in the "matrix-open" state, with the ATP-binding site accessible to the mitochondrial matrix (Henderson & Lardy, 1970; de Bruijn et al., 1973). The structure of ADP/ATP Carrier in presence of either carboxyatractyloside (CATR) (Pebay-Peyroula et al., 2003) and BKA (Ruprecht & Kunji, 2019) has been solved, confirming the different binding sites and effect on the conformation of these transporters.

During *in vivo* spectroscopic measurements, the $\Delta\Psi_d$ of P. tricornutum appeared to be affected when in presence of BKA, while this was not the case for the samples treated with CATR (Fig. 2.21). We reasoned that cell membrane of *P.tricornutum* is permeable to BKA while it is probably impermeable to CATR. Since the $\Delta\Psi_d$ probes the import of mitochondrial ATP in the thylakoids, we deduced that this inhibitor affects to some extent the exchange of this molecule between the organelles, as the respiratory activity of the mitochondrion was not directly compromised. Because BKA is a known inhibitors of ADP/ADP carriers, these data suggest that members of the AAC family could be involved to some extent in the regulation of energetic exchanges.

Figure 2.21 | Effect of bongkrekic acid (BKA) and Carboxyatractyloside (CATR) on the $\Delta\Psi_d$ in _P. tricornutum_. Cells were incubated with either 20 µM BKA, 100 µM CATR or 1 mM SHAM and 5 µM Antimycin A for at least 15 minutes before performing the measurements. Note that to provide efficient inhibition of $\Delta\Psi_d$ BKA has to be employed at acid pH (pH 5). The potential negative effects of the non-physiological pH were investigated and resulted negligible in the dark. The $\Delta\Psi_d$ in the control sample was set to 100%; Data ± SD from 5 independent experiments for measurements with BKA, 3 replicates with CATR.

To test this hypothesis, we adapted the same CRISPR-Cas9 approach described above for MCF to generate knockout mutants of ACC1. One KO clone was isolated, presenting a 2 base pair deletion, which led to the appearance of a premature stop in the protein sequence after 177 amino acids. Although we were not able to generate a specific antibody to test if the truncated protein was still accumulating in the cells, we hypothesize that the protein should be absent in this mutant, since the mutation was deleting half of the transmembrane helices that are required for nucleotide translocation. Nonetheless, the mutant line did not show any clear phenotypic traits when observing the growth rate, the $\Delta\Psi_d$, photosynthetic electron flow and NPQ features, all resulting comparable to those of the WT.

We conclude that either ACC1 is not a target of BKA or that other actors can compensate for its absence in this mutant strain, as in the case of Pt-MCF.
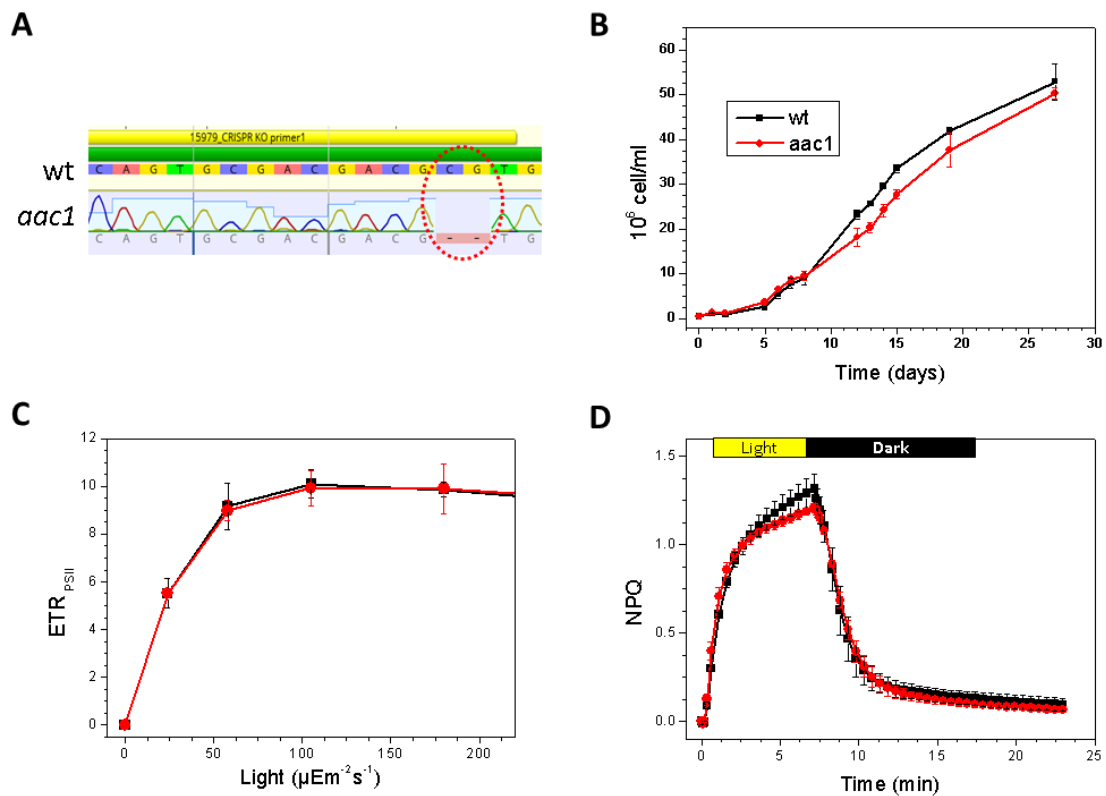
Figure 2.22 | Molecular and photosynthetic characterisation of *aac1* knock out mutant strain. A, After CRISPR-Cas9 mutagenesis and biolistic transformation, gene sequencing revealed a 2 bp deletion in one colony, which was selected for further analysis. **B**, Measurement of growth rates (starting concentration: $0.5 \cdot 10^6$ cell ml^{-1}). **C**, Analysis of chlorophyll fluorescence parameters, ETR and NPQ (**D**). *P. tricornutum* cells at exponential growth phase were distributed on a 96-well plate at $20 \cdot 10^6$ cell ml^{-1} concentration in 150 μL volume and measurements were performed with an imaging system.

The second AAC candidate, encoded by the gene Phatr3_J22873 and named AAC2, corresponded to the first hit when looking for the orthologous of the bovine mitochondrial AAC in *P. tricornutum* genome and when searching for interspecific homologs for Pt_AAC1. Furthermore, no secondary plastid target sequence was predicted by ASAFind for Phatr3_J22873 (named AAC2). Thus, we reasoned that this gene product might in fact be the mitochondrial transporter sensitive to BKA. Despite the apparently low sequence identity, corresponding to 53 %, we assumed that it was still a promising candidate since also the yeast and the bovine proteins share a 50% sequence identity but are both sensitive to BKA and play the same ADP/ATP transport role.

73

Description	Total Score	Query Cover	E value	Per. Ident	Accession	Ensemble
predicted protein	300	98%	2,00E-102	53.36%	XP_002183547.1	Phatr3_J22873 (AAC2)
predicted protein	188	96%	1,00E-58	37.01%	XP_002184022.1	Phatr3_J15797 (AAC1)
predicted protein	202	93%	1,00E-38	29.26%	XP_002184712.1	
predicted protein	98.2	91%	2,00E-24	28.87%	XP_002177405.1	
predicted protein	87.8	95%	2,00E-20	25.59%	XP_002185141.1	
predicted protein	79.7	94%	4,00E-17	22.69%	XP_002177113.1	
predicted protein	77.0	96%	1,00E-16	24.18%	XP_002185715.1	
predicted protein	73.6	96%	3,00E-15	23.15%	XP_002184938.1	
predicted protein	72.8	80%	4,00E-15	25.20%	XP_002179990.1	
predicted protein	67.8	88%	2,00E-13	22.68%	XP_002179991.1	

Table 2.6 | Homologs proteins of the bovine AAC (PDB: 1OKC) in *P. tricornutum*. First five hits from BLAST output are listed. A total of 17 proteins with E-value lower than 10^{-10} were found. The best hit corresponds to the already selected AAC2 gene (Phatr3_J22873), making it a promising candidate to be the target for the BKA in *P. tricornutum*.

Description	Total Score	Query Cover	E value	Per. Ident	Accession
predicted protein	620	100%	0	100.00%	XP_002183547.1
solute carrier family 25 (mitochondrial adenine nucleotide translocator), member 4/5/6/31 [Fistulifera solaris]	545	100%	0	86.14%	GAX21040.1
hypothetical protein THAOC_30677 [Thalassiosira oceanica]	545	97%	0	88.85%	EJK50366.1
adenine nucleotide translocator; ADP/ATP translocase [Thalassiosira pseudonana CCMP1335]	544	97%	0	88.81%	XP_002286255.1
solute carrier family 25 (mitochondrial adenine nucleotide translocator), member 4/5/6/31 [Fistulifera solaris]	541	100%	0	85.81%	GAX12355.1
putative mitochondrial ADP/ATP translocase [Pavlova lutheri]	460	95%	8.00E-161	76.29%	ABV25598.1

Table 2.7 | Homologs proteins of AAC2 (Phatr3_J22873). First five hits from BLAST output appear to belong to other ADP/ATP transporter present in other species of diatoms.

Despite several attempts to make KO mutants using CRISP-CAS9, we could not obtain any transformed clones in this case. We hypothesize therefore that this negative result could reflect the fact that the mitochondrial ADP/ATP carrier may be essential for cell survival and thus a KO mutant would show a lethal phenotype. Therefore, we adopted another strategy and generated knock-down (KD) lines by the insertion of antisense (AS) sequences: through this approach, we aimed to reduce the amount of proteins produced in the cell in order to lower the function of AAC2 rather than abolishing it. After antibiotic selection, we isolated two AS mutant colonies and, by using a specific antibody, we were able to verify the lower amount of AAC2 protein in these lines by western blot (Fig. 2.23). The AAC2 antibody was obtained after the heterologous expression of the AAC2 gene in *E.coli*, protein extraction and purification (same protocol followed for the production of Pt-MCF antibodies) and further injection into guinea pig (performed by Charles River Biologics). Western blot analysis revealed the successful silencing of the AAC2 gene in two Anti-Sense mutants. Moreover, we also validated the generation of an overexpressing line with the same approach. This last strain was generated by insertion of WT copy of the AAC2 gene regulated by the light-inducible promoter fcpA through biolistic transformation (see Materials and Methods).
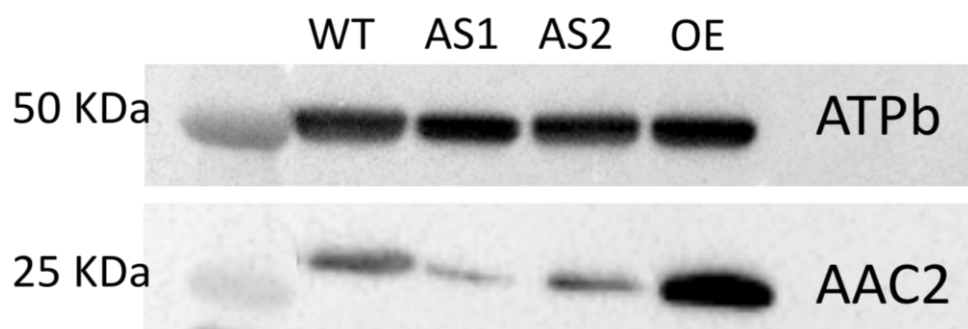
Figure 2.23 | Western blot analysis of AAC2 knock-down (AS1 and AS2) and overexpressor (OE) mutant strains. Total cell extracts were blotted with a specific antibody. ATPb was used as a loading control.

Chlorophyll fluorescence analyses revealed a small decrease of the photosynthetic electron transfer rate in one of the two AAC2-AS strains, while we did not observe any significant phenotype in the overexpressing line. According to the hypothesis presented above, where we considered AAC2 a vital gene for the alga since we could not obtain any KO mutant colony, we interpreted the AAC2-AS mild phenotype as the fact that the decreased amount of the transporter left in the mutant is still sufficient to catalyse the energetic exchanges required for a functional photosynthesis. This would imply that the protein amount is not limiting for the exchange itself, and therefore even small quantities are sufficient for a useful ATP transport. Although speculative, this possibility is consistent with the finding that when the AAC2 quantity is increased in our OE line, no specific phenotype is observed (Fig 24).
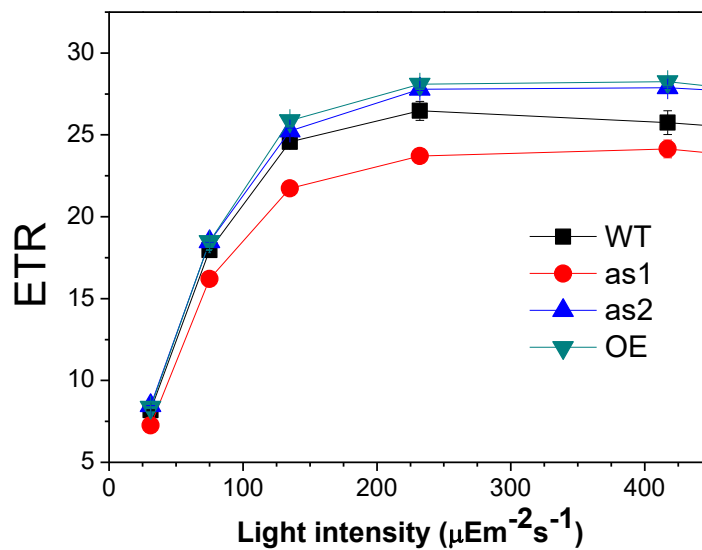
Figure 2.24 | Electron Transfer Rate phenotype of AAC2 Antisense and Over Expression lines. Measurements were performed on *P. tricornutum* cells in exponential growth phase (between 1 and $3 \cdot 10^6$ cell ml^{-1}). After centrifugation (3500g, 5', 19 °C) cells were distributed on a 96-well plate at $20 \cdot 10^6$ cell ml^{-1} concentration in 150 µL volume. Data correspond to average + SD of 3 independent experiments, each comprising 3 technical replicates.

We decided to test this assumption by titrating the AAC activity in the WT and the AAC2-AS mutant strains with BKA, and investigate the consequences on the photosynthetic performances. Unfortunately, we faced a technical problem that made this experiment difficult to interpret. As explained in Figure 2.25, in order to observe an effect of BKA in diatoms, cells have to be incubated at pH 5. This treatment turned out to have severe consequences on photosynthetic activity even in the absence of the inhibitor, while this was not the case during the ECS measurements that were performed in dark conditions. Therefore, even if an effect is seen on photosynthesis upon BKA addition (which is stronger in the two AAC2 KD lines), it is difficult to draw firm conclusions regarding the real effect of this inhibitor in the light.
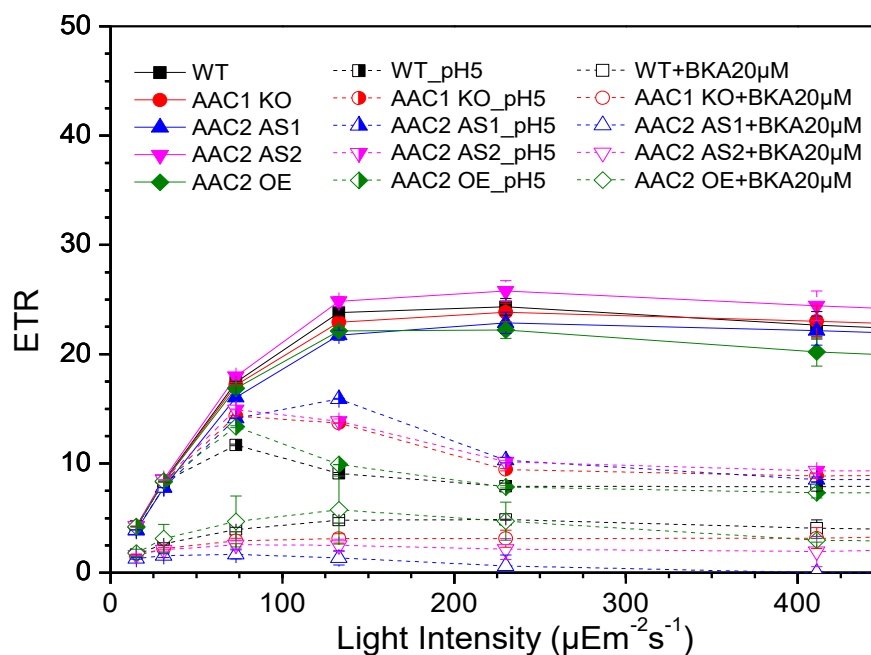
Figure 2.25 | ETR measurements of AAC2-AS and OE lines in presence of BKA. Measurements were performed on *P. tricornutum* cells in exponential growth phase (between 1 and $3 \cdot 10^6$ cell ml^{-1}). After centrifugation (3500g, 5', 19 °C) cells were distributed on a 96-well plate at $20 \cdot 10^6$ cell ml^{-1} concentration in 150 µL volume. Since BKA is effective only at acidic pH (pH 5). The potential negative effects of the non-physiological pH were also investigated. Data ± SE from 3 independent experiments.

2.2.4 DTC, the carboxylic transporter

The last candidate selected from transcriptomic data was the gene Phatr3_J35625. It was chosen since the bioinformatics analysis showed 8 predicted transmembrane domains by TMHMM and a putative secondary plastid target sequence at the beginning of the protein (see Table 2.1) by ASAFind, with the cleavage site located after 22 amino acids. The BLAST analysis shows that this putative transporter also belonged the Mitochondrial Carrier family (Palmieri et al., 2011) and it also appeared to be the homolog in *P. tricornutum* for the citrate/oxoglutarate carrier protein of yeast (UniProt: YHM2). This made us wonder whether it could be a candidate for the export of reducing equivalents from the chloroplasts in diatoms. Within the MCF group, a dicarboxylate–tricarboxylate carrier (DTC) subgroup exists. DTCs catalyse an electroneutral transport of a broad spectrum of single protonated tricarboxylate (citrate, isocitrate, and aconitate) in exchange with unprotonated dicarboxylates (oxoglutarate, oxaloacetate, malate, maleate, succinate, and malonate), but not phosphoenolpyruvate. As DTCs transport a large variety of dicarboxylates and tricarboxylates molecules, it has been suggested that these carriers may play a role in a number of important metabolic functions in photosynthetic organisms, which require organic acid flux to or from the mitochondria. The malate/oxaloacetate exchange (as showed by homology analysis with the correspondent protein in Chlamydomonas) catalysed by DTC can enable the export of redox equivalents from the mitochondrial matrix that can act as reductants for the production of glycerate during photorespiration in photosynthesizing cells. As indicated by the BLAST analysis (Table 2.8) DTC (Phatr3_J35625) (dicarboxylate/tricarboxylate carrier) has a low degree of conservation in stramenopiles and Chlamydomonas, suggesting that it could be specific of Phaeodactylum.

Also in the case of this candidate, no KO mutant strain was obtained after CRISPR-Cas9 transformation, as previously observed for the AAC2 gene. We designed the mutagenesis

protocol in order to target three different regions in the gene sequence (see Materials and Methods). After the antibiotic selection, we obtained between 50 and 150 colonies for each of the 12 constructions (3 constructions for each of the 4 selected genes) and sequenced an average of 50 per transformation but none of them appeared to have any frameshift mutation. As for what observed in the case of AAC2, we deduce that the lack of the DCT might be detrimental for the cell and thus a KO mutation could be lethal. This made us speculate that the lack of this protein might be a lethal condition for the cell. In fact, it appeared to be a unique gene in P. tricornutum genome, as showed by BLAST analysis (Table 2.9), where only one possible homolog was identified with a low sequence identity. Because of lack of time, I could not attempt to generate KD mutant strains.

Description	Total Score	Query Cover	E-value	Per. Ident	Accession
predicted protein [Phaeodactylum tricornutum CCAP 1055/1]	702	100%	0	100.00%	XP_002180033.1
mitochondrial carrier [Fragilariopsis cylindrus CCMP1102]	338	90%	9.00E-112	54.57%	OEU17160.1
hypothetical protein DD238_000649 [Peronospora effusa]	149	73%	1.00E-38	35.61%	RMX67668.1
unnamed protein product [Albugo candida]	148	73%	1.00E-38	35.61%	CCI41766.1
Mitochondrial Carrier (MC) Family [Achlya hypogyna]	147	73%	6.00E-38	34.22%	OQR83879.1
hypothetical protein CCR75_005119 [Bremia lactucae]	144	73%	9.00E-37	34.47%	TDH65510.1
Mitochondrial Carrier (MC) Family putative [Albugo laibachii Nc14]	143	73%	1.00E-36	35.98%	CCA15079.1

Table 2.8 | Homologs proteins of the Phatr3_J35626 corresponding amino acid sequence. First six hits BLAST output are listed.

Description	Total Score	Query Cover	E value	Per. Ident	Accession
predicted protein	702	100%	0.0	100.00%	XP_002180033.1
predicted protein	53.1	44%	3.00E-08	27.71%	XP_002180536.1
predicted protein	32.7	62%	0.10	26.43%	XP_002186029.1
predicted protein	32.3	17%	0.15	35.29%	XP_002185715.1

Table 2.9 | Homologs proteins of Phatr3_J35625 (DTC) in *P. tricornutum*. The closest related protein shares only 44% of coverage and 27% of homology, possibly making the DTC protein a unique transporter for its substrate.

Chapter 3: Materials and Methods

3.1 *Phaeodactylum tricornutum* cultivation

Phaeodactylum tricornutum (Pt1, CCAP 1055/3) cells were grown in glass flasks, in a volume ranging from 25 to 250 ml. The growth medium, named ESAW 10NP, contains a concentration of N and P ten times higher compared to the regular ESAW medium (Harrisonet al., 1980) modified in (Berges et al., 2001), added copper and removed silicate.

Salt Solution 1 (Anhydrous salts)	Final (M)
NaCl	3.63×10^{-1}
Na_2SO_4	2.50×10^{-2}
KCl	8.03×10^{-3}
$NaHCO_3$	2.07×10^{-3}
KBr	7.25×10^{-4}
H_3BO_3	3.72×10^{-4}
NaF	6.67×10^{-5}

Salt Solution 2 (Hydrated salts)	Final (M)
$MgCl_2\ 6H_2O$	4.71×10^{-2}
$CaCl_2\ 2H_2O$	9.14×10^{-3}
$SrCl_2\ 6H_2O$	8.18×10^{-5}

Nitrate and Phosphate	Final (M)
$NaNO_3$	5.49×10^{-3}
$NaH_2PO_4.H_2O$	2.24×10^{-4}

Trace Metal Solution A	Final (M)
$Na_2EDTA.2H_2O$	8.30×10^{-6}
$ZnSO_4.7H_2O$	2.54×10^{-7}
$CoSO_4.7H_2O$	5.69×10^{-8}
$MnSO_4.4H_2O$	2.42×10^{-6}

Trace Metal Solution B	Final (M)
$Na_2MoO_4.2H_2O$	6.12×10^{-9} M
Na_2SeO_3	1.00×10^{-9} M
$NiCl_2.\ 6H_2O$	6.27×10^{-9} M
$CuSO4.\ 5H_2O$	3.92×10^{-8} M

Iron	Final (M)
Fe-EDTA	6.55×10^{-6}

Vitamins	Final (M)
thiamine HCl (vit. B_1)	2.96×10^{-7}
biotin (vit. H)	4.09×10^{-9}
cyanocobalamin (vit. B_{12})	1.48×10^{-9}

Table 3.1 | ESAW 10NP components and their concentration in the final medium. Salts solutions were made as 10x stock solutions; vitamins, trace metal and Fe EDTA at 1000x, nitrate and phosphate as 100x stock solutions. Individual stock solutions were sterilised either by autoclave treatment or through 2 μm filters under flow hood before use.

Liquid cell cultures were kept in glass flasks, in Infors Multitron incubators (Infors, Switzerland) at 22 ± 1 °C, agitating at 90 rpm, in continuous 40 µE m^{-2} s^{-1} light intensity provided by white LEDs. Cells were diluted with fresh medium every 3-4 days, to keep the cultures in the exponential growth phase. Algae concentration of a given culture were measured by collecting a 15 µL sample, algae were counted using a LUNA Automated Cell Counter (Logos Biosystems, USA). In this manuscript cell concentration are indicated as $10^6 \cdot$cells mL^{-1}. Stock cultures were kept in solid ESAW 10NP medium with the addition of Agar at 1% (w/v).

3.2   Gibson Assembly

This approach allowed the assembly of various overlapping DNA sequences in a single isothermal reaction thanks to the combined activity of 5′ exonuclease, a DNA polymerase and a DNA ligase (Gibson et al., 2009). This technique is used for the creation of the plasmids needed for protein expression.

Before the isothermal reaction, a Polymerase Chain Reaction (PCR) step with proof-reading enzyme without terminal transferase activity (3'A tag) is needed to amplify the fragments of interest and to add new DNA sequences of 15 bp to 30 bp at the 5' and at the 3', which are overlapping to the previously digested (NdeI and XhoI) vector's ends.

For the reaction, 15 fmol of each fragment are dissolved in 5 µL of distilled water and are then added to 15 µL of isothermal reaction mix. After incubation at 50°C 60', sample are used to transform usual competent cells through heat shock treatment.

GA 5X
5mL Tris HCl 1M pH 7.5
500µL MgCl$_2$ 1M
100µL dATP 100mM
100µL dCTP 100mM
100µL dGTP 100mM
100µL dTTP 100mM
500µL DTT 1M
2.47g PEG-8000
500µL NAD 100mM (dissolved at pH 7.5)
Complete to 10mL and aliquot in 160µL

Store at -80°c

GA mix
160µL GA 5X
0.2µL T5 exonuclease NEB (M0363S) 10u/µL (minimum 200 bp fragments; if less, use only 0.1µL)
10µL Phusion High fidelity DNA polymerase NEB (M0530S) 2u/µL
80µL Taq DNA ligase NEB (M0208S) 40u/µL
Complete to 600µL with sterileH$_2$O

Table 3.2 | List of components for the Gibson Assembly reaction and their concentrations in the final mix.
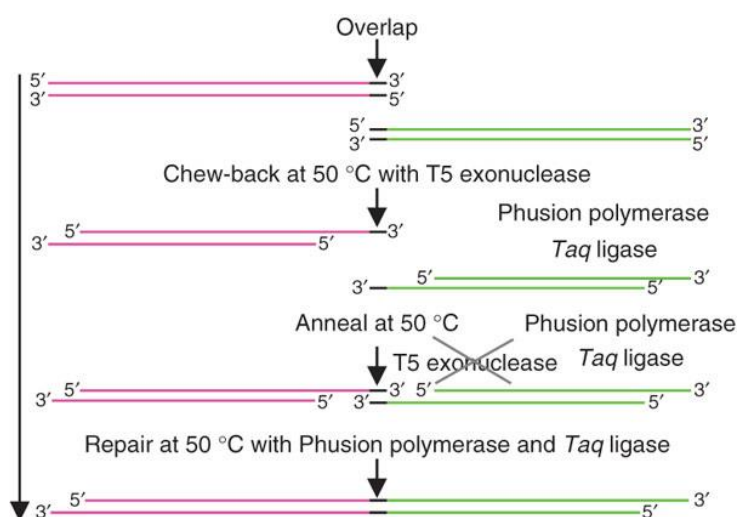
Fig 3.1 | Schematic representation of Gibson Assembly steps. The simultaneous presence of the exonuclease, the DNA polymerase and the DNA ligase allows the fusion of multiple fragment of DNA.

3.2.1 Plasmids

The pET-28a(+) was used for the heterologous expression of the AAC2 and the MCF genes. It presents a sequence coding for an His-Tag either at the C-terminal or at the N-terminal of the insert. The T7 terminator can be used for sequencing. It contains a kanamycin resistance cassette for the selection of transformed bacteria.
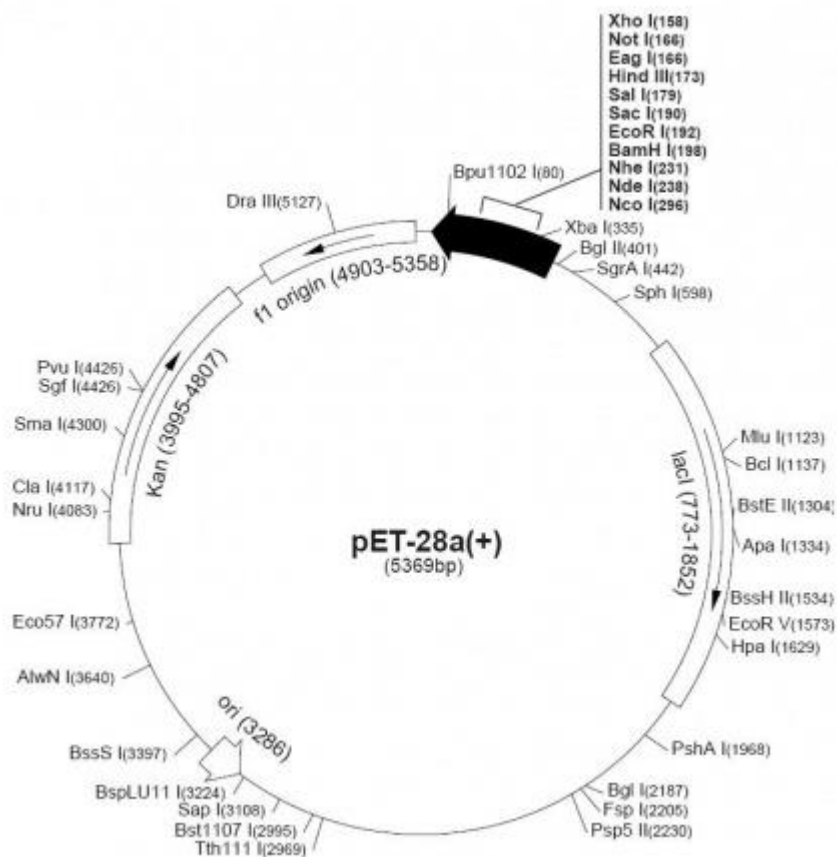
Figure 3.2 | pET-28a(+) presenting a sequence coding for an His-Tag either at the C-terminal or at the N-terminal of the insert. Unique restriction sites are reported and the black arrow indicates the Multicloning site. The plasmid presents a gene conferring the resistance to the antibiotic kanamycin to transformed cells. The T7 terminator can be used for sequencing.

Coding sequence of AAC2 (Phatr3_J22873) was amplified using primers NdeIFwd (CCTACTCTTCATTCCCCCCCATATGTCCAGTTCTA) and SacIRev (GGGTATTT TTCTCAGGGGAGCTCCCGTACTTATTT), cut by NdeI/SacI (NEB) and cloned into a

pET28b(+) plasmid, also previously digested with NdeI/SacI. The MCF (Phatr3_J46742) gene was inserted in the expression plasmid using Gibson Assembly method using the 46742for (CTGGTGCCGCGCGGCAGCCATATGAGGACTTCCTTCGGTATGC) and 46742rev (AG TGGTGGTGGTGGTGGTGCTCGAGCAATGCCTCATACCC) primers. The vector sequence contains a resistance cassette to Kanamycin for the selection of transformed bacteria. The expression of the inserted gene was induced by adding Isopropyl β-d-1-thiogalactopyranoside (IPTG), due to the existence of an inducible promoter.

3.3   I-TASSER

The I-TASSER web tool (Iterative Threading ASSEmbly Refinement) was used to obtain three-dimensional structure predictions of the candidate transporters from the amino acidic sequence (https://zhanglab.ccmb.Med.umich.edu/I-TASSER) (Roy et al., 2010). It is based on a hierarchical approach and it identifies structural templates from the Protein Data Bank (PDB) by multiple threading alignments and iterative structural assembly simulations. The software also proposes the possible protein function by structurally matching the predicted 3D models with other known proteins of known structure. The confidence of quality of the predicted models is expressed as C-score, ranging from -5 to 2, which is based on the threading template alignments. The program performs a structural alignment of the generated models and all structures in the PDB library and reports the top 10 matches.

3.4   Phylogenetic analysis

The phylogenetic analysis of Phat3_J46742 and its close paralogues Phatr3_J46612 and Phatr3_J42874 were done in collaboration with Richard G. Dorrell from Chris Bowler's group

at the Institute de Biologie de l'Ecole Normale Supérieure (IBENS) based in Paris (France) and Pierre Cardol from the Université de Liège in Belgium

To identify homologues of Phat46742 in other taxonomic groups, the complete sequences of the three proteins of the *Phaeodactylum tricornutum* were searched against a composite library of sequences across the tree of life. This library consisted of a complete version of UniProt (accessed 2018), along with decontaminated versions of the MMETSP and 1kp transcriptome projects (Keeling et al., 2014; Dorrell et al., 2019). Possible homologues were extracted by reciprocal BLASTp best hit, with threshold E-value for the initial BLAST search 1×10^{-05}, and best hits identified by reciprocal search against the entire *Phaeodactylum* genome (Rastogi et al., 2018).

Probable localisations of sequences derived from lineages with four membrane plastid structures (cryptomonads, haptophytes and ochrophytes) were inferred using the consensus predictions of SignalP v 3.0, ASAFind, HECTAR, and MitoFates; as previously described (Dorrell et al., 2019; Gschloessl et al., 2008; Gruber et al., 2015; Fukasawa et al., 2015; Bendtsen et al., 2004). A taxonomically representative subset of the sequences obtained were aligned using MAFFT v 5.0 (Katoh et al., 2017), MUSCLE v 8.0 (Edgar, 2004), and GeneIOUS v 4.76 (Kearse et al., 2012) trimmed manually and with trimAl in –gt 0.5 setting (Capella-Gutiérrezet al., 2009). Consensus phylogenies were inferred using MrBayes and RAxML programmes integrated into the CIPRES server, using three substitution matrices (GTR, Jones/JTT, and WAG), as previously described (Dorrell et al., 2019; Miller et al., 2015; Ronquist et al., 2012; Stamatakis, 2014)

3.5 *Phaeodactylum tricornutum* mutant strains generation through CRISPR/Cas9

The CRISPR/Cas9 system derives from a bacterial adaptable immune mechanism (Jinek et al., 2012) and it has been adapted in several different organisms (Sander & Joung, 2014). Two main actors take part to the process: a guide RNA sequence (sgRNA) and the Cas9 DNA endonuclease. The sgRNA is constituted by Cas9 binding sequence and a region complementary to the genomic target, which will be digested by the Cas9 endonuclease. By designing the second component (named CRISPR/Cas9 target sequence hereafter), it is possible to target a specific DNA region into the genome. After the annealing of the sgRNA to the genomic DNA, the Cas9 endonuclease generates double-strand breaks in the nearby region. When trying to fix the damages, the DNA repair system might introduce nucleotide insertion or deletion in the sequence of the genomic DNA. These events modify the amino acid composition of the corresponding protein after translation, eventually leading to the appearance of a premature stop codon. In this case, we apply a protocol developed in our laboratory designed to create a stable targeted gene knockout (KO) mutant strains in *P. tricornutum*, using biolistic transformation (Allorent et al., 2018), as summarised below:

3.5.1 Genomic DNA extraction

P. tricornutum cells were collected from a plated colony and homogeneously resuspended in 20μL of EDTA 50 mM in a 1.5 mL microfuge microtube. After vigorously vortexing for 30", samples were centrifuged at 16,000 g for 5 minutes at 22°C and the supernatant containing the genomic DNA was transferred in a new microfuge tube.

3.5.2 Identification of CRISPR/Cas9 target sequences

CRISPR/Cas9 target sequences in the gene of interest were identified using the PhytoCRISP-Ex web tool (Jinek et al., 2012) (https://www.phytocrispex.Biolo-gie.ens.fr/CRISP-Ex/). For each gene, three target sequences were chosen according to their localisation, as close as possible of the ATG and preferentially in the first exon. This way, we increased the probability to generate a truncated non-functional protein in the mutant strain.

3.5.3 Bioinformatic design of the adapter

The adapter consisted in the annealing of two 20 bp complementary oligonucleotides displaying 5' overhangs (5'-TCGA-3' at the forward adapter, 5'-AAAC-3' at the reverse adapter) with the plasmid's sequence when digested with BasI. Since the Cas9 enzymes recognises a DNA region containing the sequence of 5'-G(19bps)NGG-3', the three NGG nucleotides were removed from the sequences found in the output of the software to avoid digestion of the adapters.

The adapter was generated by annealing the two primers previously described by mixing 1 µg of each primer with 1x of T4 ligase buffer in a total volume of 50 µL in PCR tubes. The mix was incubated in a thermal cycler for 10 min at 85°C and then decrease the temperature of 5 degrees every 5 minutes until 25 °C is reached (Nymark et al., 2016). From this step further, samples were kept on ice. The primers used in this study are indicated in Table 3.3.
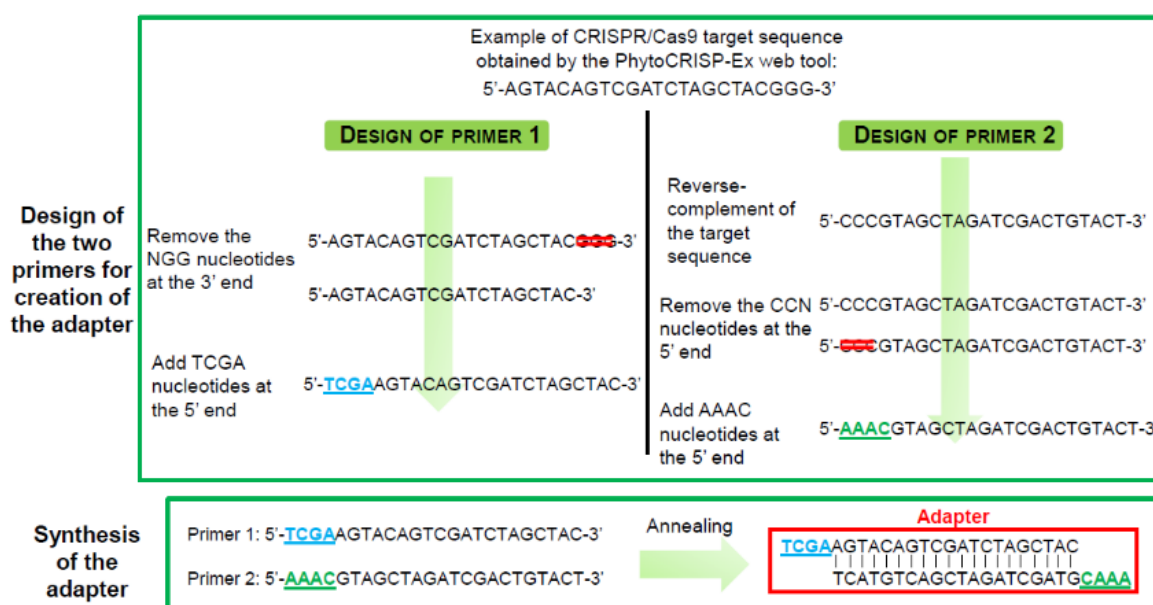
Figure 3.3 | Schematic representation of design and synthesis of the adapter. After selecting the target sequences from the output of PhytoCRISP-Ex web tool, primers for the creation of the adapter were designed by removing the NGG terminal part and by adding TCGA or AAAC overhangs in the CRISPR/Cas9 target sequence. Adapters were synthetized by annealing the two designed primers.

		Forward	**Reverse**
AAC1	**1**	TCGAGTTCCAGTGCGACGACGCGT	AAACACGCGTCGTCGCACTGGAAC
	2	TCGAGGTGTAGCGTGTGACGGCGG	AAACCCGCCGTCACACGCTACACC
	3	TCGAGCCGTTGCGGGAGCCGCGGC	AAACGCCGCGGCTCCCGCAACGGC
AAC2	**1**	TCGAGCCAACCCCAAGATTATCTC	AAACGAGATAATCTTGGGGTTGGC
	2	TCGAGTCGACAATTCCGGTGTAAC	AAACGTTACACCGGAATTGTCGAC
	3	TCGAGACGAGAAACTCGGTAGAAC	AAACGTTCTACCGAGTTTCTCGTC
DTC	**1**	TCGAGCAGGTCTCGGTTTCCTTGA	AAACTCAAGGAAACCGAGACCTGC
	2	TCGAGCAATCGCTTCGTCCTTTGG	AAACCCAAAGGACGAAGCGATTGC
	3	TCGAGCCATGTGTCAATGTTCGAC	AAACGTCGAACATTGACACATGGC
MCF	**1**	TCGAGTTTCCCGCCGTTTTTTTCT	AAACAGAAAAAAACGGCGGGAAAC
	2	TCGAGTCAGCCGAGAAGCCGACGA	AAACTCGTCGGCTTCTCGGCTGAC
	3	TCGAGATGCTGAGCTGCATACCGA	AAACTCGGTATGCAGCTCAGCATC

Table 3.3 | List of oligonucleotides used for synthesis of CRISPR-Cas9 adaptors. Underlined nucleotides represent the overlapping sequences with pKSdiaCas9_sgRNA plasmid when linearized with BsaI and nucleotides NGG were removed from the output sequence from the PhytoCRISP-Ex software.

3.5.4 Modification of the pKSdiaCas9_sgRNA plasmid for transformation

The plasmid used for transformation is pKSdiaCas9_sgRNA (Fig. 3.4), which allowed the expression of a codon-optimized Cas9 nuclease and the sgRNA (Rastogi et al., 2016). The CRISPR/Cas9 target sequence already included in the plasmid had to be replaced by the one identified in the previous step (paragraph 3.5.3) to mutate the gene of interest. Moreover, this plasmid did not harbour a resistance gene for the selection of transformants on plates supplemented with the corresponding antibiotics. Therefore a second plasmid (pAF6) (Falciatore et al., 1999), bearing the zeocin resistance cassette, was required for transformation.
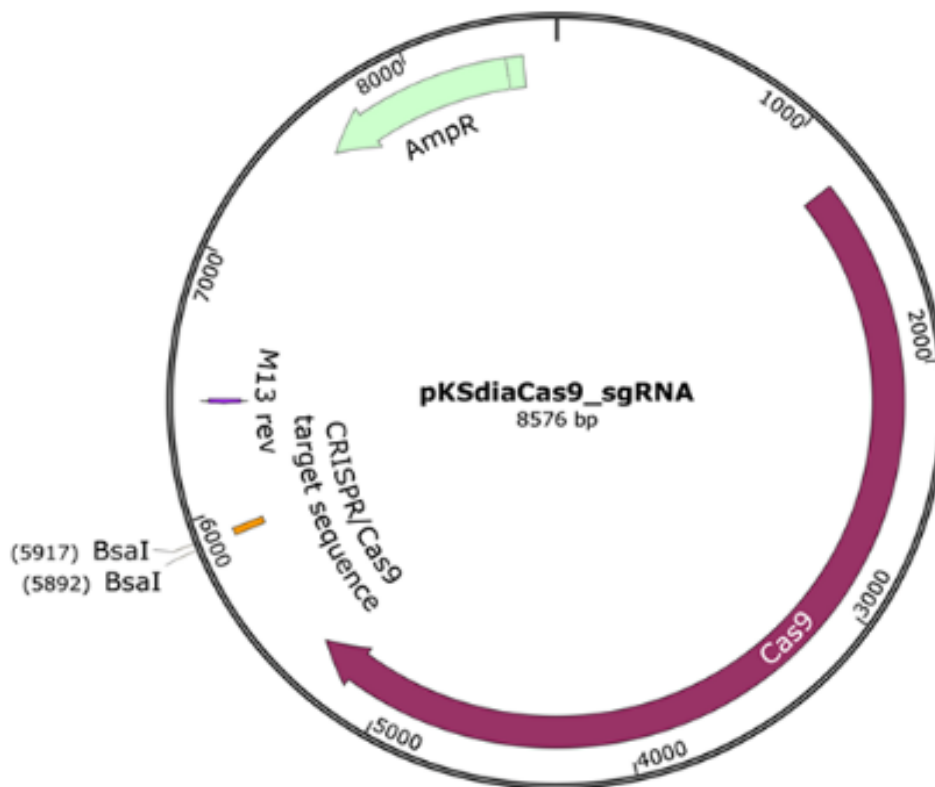

Figure 3.4 | Map of the pKSdiaCas9_sgRNA plasmid. The plasmid allows the expression of a *P. tricornutum* codon-optimized Cas9 protein and the sgRNA containing the CRISPR/Cas9 target sequence between the two BsaI restriction sites. In bacteria, this plasmid confers ampicillin resistance (AmpR).

During my stay at the PCV laboratory, in the team we developed a modified version of the pKSdiaCas9 plasmid that presents the zeocin resistance cassette. It allowed the transformation without the need of the second pAF6 plasmid, reducing the chances to have false positive colonies after the selection with antibiotics. For the first transformation attempt, we used the original pKSdiaCas9_sgRNA plasmid. Since we could not obtain positive transformants carrying the mutation for the AAC2 and DTC genes, we applied the protocol using the custom plasmid carrying the zeocin resistance cassette.

3.5.4.1   Digestion of the pKSdiaCas9_sgRNA plasmid by BsaI

The pKSdiaCas9_sgRNA plasmid was digested with the BsaI restriction enzyme. The reaction was performed by incubation at 37°C for 2 hours of a solution containing 1 µg of the pKSdiaCas9_sgRNA plasmid, 1 µL of BsaI-HF restriction enzyme and 1x of the CutSmart buffer in a total volume of 25 µL. A digested fragment of 20 bp was removed from the plasmid and separated from the linearized plasmid to avoid re-ligation through 1% (w/v) agarose gel electrophoresis (agarose 1% w/v; 100 V; 15'). After migration, the open plasmid was extracted from the corresponding agarose band (expected size: 8500 bp) using a commercial kit and was quantified using Nanodrop 2000 (ThermoFisher, USA) spectrophotometer.

3.5.4.2 Ligation of the adapter into the linearized pKSdiaCas9_sgRNA plasmid

For the ligation step, 5 µL of the adapter were mixed with 100 ng of the linearized pKSdiaCas9-sgRNA plasmid, 2 µL of T4 DNA ligase and 1x of T4 DNA ligase buffer in a total volume of 20 µL. Samples were incubated for 10 minutes at room temperature or 16°C overnight to

generate the pKSdiaCas9_sgRNA plasmid containing the CRISPR/Cas9 target sequence of the gene of interest. *E. coli* competent cells were transformed using 4 µl of the ligation mix following standard heat-shock protocols. Transformed cells were spread on LB agar plates supplemented with 100 µg/mL ampicillin and incubated overnight at 37°C. One colony was selected and transferred in LB liquid medium supplemented with ampicillin (100 µg/mL) under agitation overnight at 37°C. Plasmid was purified using mini-prep extraction kit, quantified at Nanodrop and 2.5 µg of plasmid were used for each bombardment, as explained later in the text (paragraph 3.6.4). Plasmid's sequence was verified by DNA sequencing using the universal M13-rev primer (GTCATAGCTGTTTCCTG) (Fig. 3.4).

3.6   *Phaeodactylum tricornutum* transformation

3.6.1 *P. tricornutum* cells liquid culture and plating before biolistic transformation

P. tricornutum cells were cultivated in ESAW 10NP liquid medium until the culture reaches exponential phase (between $1.5 \cdot 10^6$ and $2 \cdot 10^6$ cells/mL) 24 h before transformation in 12 h light/dark cycles, 40 µmol photons $m^{-2} s^{-1}$, 19°C. From the liquid culture, 10^8 cells were harvested under a sterile hood, collected by centrifugation (3000 g, 10 min, 19°C). The pellet, containing 10^8 cells, was resuspended in 500 µL of fresh medium and spread on ESAW 10NP plate containing 1% (w/v) agar without antibiotics. Once the plate had dried under sterile hood (~20'), it was incubated under dim light (20/30 photons $m^{-2} s^{-1}$), 19°C for 24 hours.

3.6.2 Tungsten beads preparation

The following steps are performed according to the following protocols (adapted from the BIORAD PDS-1000/He system protocol).

1) Weight 30 mg of tungsten beads into a 1.5 mL sterile microfuge tube.

2) Add 1 mL of 70 % (v/v) ethanol.

3) Vortex vigorously for 5 minutes.

4) Let the beads settle for 15 minutes.

5) Pellet the beads by short centrifugation (5 sec, 6000 g, 22°C).

6) Remove and discard the supernatant.

7) Wash the beads: add 1 mL of water, vortex vigorously 1 minute, let the beads settle for 1 minute, pellet beads by short centrifugation (10 sec, 3000 rpm, 22°C), remove and discard the supernatant.

8) Repeat step 7 two times.

9) Finally, resuspend beads in 500 µL sterile 50 % (v/v) glycerol by thoroughly vortexing.

10) Prepare aliquots of 50 µL in 1.5 mL microfuge tubes and store at -20°C. Aliquots can be stored for up to 6 months.

3.6.3 Coating tungsten beads with plasmids

The following steps describe the protocol used to coat the plasmid to the beads before the cell transformation step.

1) Mix in a 1.5 mL microfuge tube 2.5 µg of the pKSdiaCas9_sgRNA plasmid prepared in part 3.2.4 and 2.5 µg of the pAF6 plasmid conferring zeocin resistance (Falciatore et al., 1999).

The total volume of the mix must not exceed 10 µL. When using the custom version of pKSdiaCas9_sgRNA, we used 5 µg.

2) Consider one 50 µL-aliquot of tungsten beads previously prepared.

3) While vortexing, add in order to the beads sample: the mix of both plasmids, 50 µL of 2.5M CaCl$_2$ and 20 µL of 0.1 M spermidine. (Spermidine must be stored in single aliquots at -80°C and thawed on ice just before use).

4) Vortex for 2-3 minutes and let settle for 1 minute at room temperature.

5) Pellet beads by short centrifugation (10 sec, 6000 g, 22°C), remove and discard the supernatant.

6) Add 140 µL of ice-cold 70 % (v/v) ethanol. Do not vortex or mix and directly remove and discard ethanol.

7) Repeat the previous step with ice-cold 100% ethanol.

8) Add 48 µL of 100 % ethanol and proceed immediately to cell bombardment.

3.6.4 Cells bombardment

For cell bombardment we used a PDS-1000/He PDS-1000/He Particle Delivery System (Bio-Rad, USA) under a sterile hood according to the manufacturer's instructions. The device is placed under flow hood thoroughly cleaned with ethanol 70 % (v/v), as well as macrocarrier holders, macrocarrier, stopping screens (except for disposable 1550-psi - pound-force/square inch -rupture disk). The macrocarrier is installed into the macrocarrier holder according to manufacturer's instructions. 10 µL of tungsten beads coated with plasmids (prepared in 3.3.3) are loaded on the macrocarrier. Once the ethanol evaporated (~2'), the system was assembled according to the manufacturer instructions and it consisted (from the top) in the 1550-psi rupture

disk, the microcarrier launch (with the stopping screen, the macrocarrier and macrocarrier holder prepared above) and the solid culture of *P. tricornutum* cells previously plated (see part 3.3.1) on the shelf n°2 (let 6 cm of distance between the microcarrier launch and the plate). Bombardment was performed as described in the manufacturer instructions and it was repeated three times for a given plasmid, each step using a new macrocarrier. After the bombardment, cells were left recovering on plate in an incubator under dim light (30/40 µmol of photons m^{-2} s^{-1}, 19°C) for 24 to 48 hours. They were then harvested by adding of 1mL of fresh sterile ESAW 10NP liquid medium on the plate and gently resuspending the transformant cells using an inoculation loop. Cells were then transferred and spread on a new plate containing 100µg/mL of zeocin for selection in sterile conditions under the flow hood. The first transformants cells appeared as brownish colonies within 2 or 3 weeks after incubation at 19°C under dim light (30/40 µmol phot m^{-2} s^{-1}).

3.6.5 Selection of mutants

Colonies of transformants were spread using an inoculating loop on a new plate of ESAW medium supplemented with zeocin (100µg/mL) in order to increase their size. Genomic DNA was extracted from cells as described in 3.5.1.and the gene of interest is amplified by PCR using appropriate primers (Table 3.4). PCR products are sent for sequencing by a DNA sequencing company (Eurofins), using the primers AAC1rev, AAC2rev, MCFfor, MCFrev.

Since all transformant colonies are resistant to zeocin, conferred by the pAF6 plasmid, after analysis of sequencing chromatograms different profiles were observed:

- WT-like transformants, *i.e.* no modification of the targeted locus, generated in three different cases: when only the pAF6 resistance plasmid has been integrated, if the mutated gene induces lethal phenotype, or when the DNA repair system worked efficiently and did not introduce any sequence modification.

	Foreword Primer	**Reverse Primer**
AAC1	CTTCATGGTCGCTCCTCATGT	TAAAAGATGCCTCCCGCCAG
AAC2	CCCATACGTGTTCTCTGCAGCAGT	GGACACACCACCGGCCATGAAATT
DTC	GGTACGTCCATGTCCCATGTCTCTTT	TCGAATCCTTTGCGACCGCGATTA
MCF	ACGCGCATGTAGTTACAGTTAGCGTATT	CCTGGGTAGCGGGAAGCGTTT

Table 3.4 | List of primers used for PCR for each targeted gene. The PCR product corresponds to the DNA region where the mutation is present after CRISPR-Cas9 mutagenesis. The amplified DNA is sent for sequencing to a private company for molecular characterisation and mutant strains selection.

- Transformant strains: Insertion and/or deletions in the targeted sequence. The type and length of these mutations may vary between different transformants from one modified nucleotide to dozens.

- Mix of modified targeted sequences, highlighted by the superimposition of peaks in the sequencing chromatogram. In this case, cells are isolated by streaking on a new plate to obtain new individual colonies, which will be analysed again through DNA sequencing. It can be necessary to repeat this procedure several times before getting pure isolated mutant.

To limit the possibility of a truncated but functional mutated protein, mutant strains presenting a premature stop codon located as close as possible to the ATG were selected.
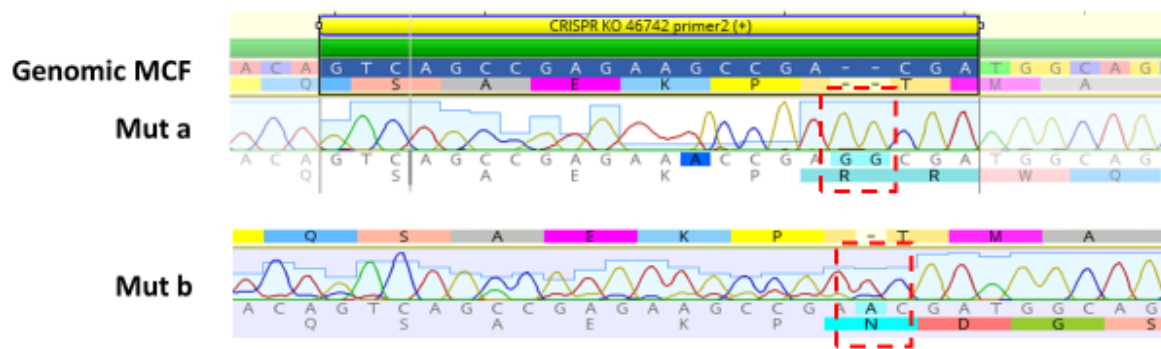
Figure 3.5 | Sequencing chromatograms obtained by sequencing the CRISPR/Cas9 target region, previously amplified by PCR. Red dashed squares in the nucleotides sequence highlight differences in the DNA sequences in the mutant strains compared to the WT.

3.7 Heterologous expression of P. tricornutum proteins of interest to make specific antibodies.

3.7.1 Expression in competent bacterial cells

Rosetta2 *E.coli* competent cells were used for protein expression as they presents advantageous features such as the presence of tRNAs for rare codons and they are capable of high protein expression level. Before transformation, cells (stored at -80°C) were spread on Lysogeny Broth (LB) plates in presence of chloramphenicol (34 µg/ml) and incubated overnight at 37°C. The next day, ~10 colonies were collected and incubated in liquid LB medium for 3 hours (AAC2) or overnight (MCF) at 37°C until they reached a concentration of $OD_{600} = 0.6$. Cells were then collected after 1800g, 10', 4°C centrifugation and resuspended in 2.5 ml $CaCl_2$ (4°C). The centrifugation step was repeated and cells were resuspended in 0.5 ml $CaCl_2$ (4°C). Aliquots of 100µl were transformed by plasmid DNA through heat shock treatment at 42°C for 45" and 2' on ice. After recovering in 1 ml LB for 1 h at 37 °C shacking at 225 rpm, 100 µl cells were spread onto LB plates with addition of chloramphenicol and kanamycine (80 µg/ml) and left at 37°C overnight. The following morning, ~10 colonies were collected and put in 10 ml of LB+chl+kan in 50ml falcon tube, left growing at 37°C until saturation was reached (~3 h) and

subsequently 8 ml of culture were collected and added to 800ml LB+chl+kan fresh medium. When the cell concentration reached an OD_{600} between 0.6 and 0.8 (~3 h), the protein expression is induced by addition of sterile (filtered) IPTG (final concentration 0.4 mM) and incubation at 37°C for 2h:30'. Cells are collected after centrifugation at 1800 g, 10', Room Temperature.

3.7.2 Protein extraction

Cells were resuspended in the Sonication Buffer (50 mM TRIS pH 8; 1 mM EDTA pH 8; 2 mM Dithiothreitol) and sonication (30% amplitude, 5') was performed in order to disrupt the bacterial cell. Samples are kept in ice to avoid excessive heating during the treatment.

3.7.3 Urea solubilisation

After sonication, samples were centrifuged at 13,000 g, 5', 4°C. The pellet corresponding to the insoluble protein fraction was resuspended in 4 mL of Dithiothreitol (DDT) buffer and treated with a sonication step. (From this step further, an aliquot of each sample was conserved for backup analysis). After centrifugation (13,000 g, 20', 4 °C), the supernatant was kept for control analysis while the pellet was washed with 4 ml of Triton buffer (See Table 3.5), centrifuged (13000 g, 10', 4 °C). This step was repeated three times. After the washing steps, the pellet was resuspended in 5 ml of Urea buffer (See Table 3.5). After 1 hour agitation at room temperature, membrane proteins, found in the soluble phase, were harvested from the supernatant after centrifugation (20', 13,000 rpm, 4°C).

DTT Buffer	Final (M)	Triton Buffer	Final (M)	Urea Buffer	Final (M)
TRIS pH 7.5	$25 \cdot 10^{-3}$	TRIS pH 7.5	$25 \cdot 10^{-3}$	TRIS pH 7.5	$25 \cdot 10^{-3}$
NaCl	0.5	NaCl	0.5	NaCl	0.5
DTT	$10 \cdot 10^{-3}$	Triton	1 %	β-mercaptoethanol	$5 \cdot 10^{-3}$
Protease inhibitors cocktail	1x	Urea	2	Urea	8

Table 3.5 | Composition of different buffers used for protein solubilisation in urea.
A sodium dodecyl sulfate-polyacrylamide gel electrophoresis (SDS-PAGE) was performed to verify the presence of the protein of interest in the different samples obtained during the described protocol.

3.7.4 Protein Quantification: BCA Assay

Protein concentration was quantified by colorimetric bicinchoninic acid assay with commercial Pierce™ BCA Protein Assay Kit. This method is based on a two-step reaction including the chelation of copper with proteins in an alkaline environment and the consequent chelation of bicinchoninic acid. After the reaction, an absorption peak at 562 nm that linearly increases with protein concentration is detected. Sample measurements were compared to a protein calibration standard obtained with the Bovine Serum Albumin (BSA).

3.7.5 Purification of His-tagged proteins by gravity-flow chromatography in Ni-NTA Column

Proteins carrying a His-TAG can be purified thanks to their affinity for a Ni-NTA agarose column (Qiagen). To do so, the Ni-NTA column is activated before running the samples by rinsing with 25 mL of Equilibrium buffer (See Table 3.6). Once the sample 8M urea solution is

loaded onto the column, His-tagged proteins will bind to the nickel-charged (Ni-NTA) affinity resin. After washing the column with 20 mL of Washing buffer (See Table 3.6), the protein(s) of interest is (are) eluted by using 16 mL of Elution buffer (See Table 3.6). Aliquots of 1ml were collected and the protein content is estimated by BCA protein assay described above.

Equilibration Buffer	Final (M)	Washing Buffer	Final (M)	Elution Buffer	Final (M)
TRIS pH 8	$25 \cdot 10^{-3}$	TRIS pH 8	$25 \cdot 10^{-3}$	TRIS pH 8	$25 \cdot 10^{-3}$
NaCl	0.5	NaCl	0.5	NaCl	0.5
β-mercapto-ethanol	$5 \cdot 10^{-3}$	β-mercapto-ethanol	$5 \cdot 10^{-3}$	β-mercaptoethanol	$5 \cdot 10^{-3}$
Urea	6	Urea	6	Urea	6
		Imidazole	$50 \cdot 10^{-3}$	Imidazole	$250 \cdot 10^{-3}$

Table 3.6 | Composition of buffers used for His-tagged proteins purification.

2 mg of protein sample were lo loaded on 12% SDS–polyacrylamide gel electrophoresis (PAGE) and migration was carried out over night at 6 mA-10 mA. The band corresponding to the protein of interest was cut at the expected size and protein. The gel band was cut in smaller pieces then placed in a dialysis tube (cut off 3500Da) and the protein was eluted from the gels pieces by electroelution in the dialysis buffer (NH$_4$CO$_3$ 50 mM, SDS 0.1 %) at 50 V intensity for 3 hours. The liquid phase containing the protein of interest was frozen in liquid nitrogen and freeze-dried for at least 8 hours. The purified protein sample (1 mg) was resuspended in 1 mL distilled water and sent to a private company for polyclonal antibody production using guinea pigs.

3.7.6 Algal Protein Extraction

A total of $80 \cdot 10^6$ cells at exponential growth phase (between $1.5 \cdot 10^6$ and 3 cell mL^{-1}) were collected by centrifugation (3,500 g, 10', room temperature) and resuspended in 200 µL of HEPES 50 mM, pH 7.5 with addition of protease inhibition cocktail (cOmplete™, EDTA-free Protease Inhibitor Cocktail) in a 1.5 mL tube. The sample was transferred to a 2 mL screw-on cap tube containing 150 mg Glass Beads. Cell rupture was performed with a Precellys Evolution Homogenizer (Bertin, France) using the following settings: 10000 rpm, 2x 30", Pause 30". From this step on, samples were kept on ice. Cell debris were separated from the glass beads with a Pasteur pipette and centrifuged at 13,000 g, 90", 4°C. The supernatant corresponds to the soluble protein fraction and the pellet to the membrane fraction. The soluble proteins fraction was further treated with 1 mL Acetone 80%, incubated on ice for 20" and centrifuged at 1,3000 g, 20', 4°C. After this step, both soluble and membrane fractions were then solubilised in 75 µL of Lysis Buffer (100 µM TRIS-HCl pH 6.8, 4 % SDS, 20 µM EDTA) and 1x protease inhibitors cocktail solution, incubated for 5' at room temperature. After centrifugation at 13,000 g, 5', 4 °C, the resulting supernatant from both soluble and membrane fractions were collected.

3.8 Western Blot Analysis

3.8.1 SDS-Poly Acrylamide Gel Electrophoresis

An acrylamide gel is composed of a stacking gel on top (0,5 M Tris-HCl pH 6.8; 0.4 % SDS; 5 % acrylamide w/v) and a separating gel at the bottom (1,5 M Tris-HCl pH 8.8; 0.4 % SDS; 12 % acrylamide w/v). Protein migration was performed in a migration Laemli buffer (5 mM Tris; 190 mM Glycine; 0.1 % SDS) first at 10 mA for 15' and then at 20 mA (for a single gel) for ~1

hour. After migration, proteins were transferred onto nitrocellulose membrane for immunodetection.

3.8.2 Protein transfer onto a nitrocellulose membrane and immunodetection

The polyacrylamide gel is placed in contact with a nitrocellulose membrane (0.2-0.45 µm pore size). Protein transfer occurs in a migration system (Bio-rad) at 100 V for 80 minutes in a Transfer buffer (25 mM TRIS pH 8; 190 mM Glycine; 0.04 % SDS; 20 % Ethanol). The system is under constant agitation (magnetic stirrer) and cooled by the presence of an ice block.

After blotting, the nitrocellulose membrane was incubated in TBS-T Solution (20 mM Tris ; 150 mM NaCl ; 0,1 % Tween 20 ; pH 8.3) with addition of 5% (w/v) milk for saturation either overnight at 4°C or for 1 hour at room temperature. After 5 washing steps with TBS-T Solution (5' each), the membrane was incubated with primary antibody solution over night at 4°C with primary antibody. AAC2 primary antibody was used at 1:5000 dilution, Pt_MCF antibody at 1:3000. After washing (5 times for 5'), membranes were incubated 1 hour at room temperature with a commercially available guinea pig secondary antibody coupled with horseradish peroxidase (HRP) at a 1:20000 dilution in TBS-T Solution. The membrane was again washed with TBS-T Solution and it was developed with commercially available Clarity Western ECL Substrates kit and images of the blots were obtained using a CCD (charge-coupled device) imager (Chemidoc MP Imaging, Bio-Rad).

The same protocol was used to test the accumulation of protein of interest in *P. tricornutum* cell extracts by Western Blot.

3.9 Oxygen evolution measurements

3.9.1 Clark type oxygen electrode

Respiratory and photosynthetic rates were measured in living cells using a Clark-type oxygen electrode at 19 °C (Hansatech Instruments, UK). The instrument is composed of a semi-hermetic chamber where a platinum cathode and an Ag/AgCl anode are separated from the sample by a Teflon membrane permeable to O_2. At the cathode level, the O_2 is electrolytically reduced to water, while at the anode Ag releases electrons. Consequently, a current is produced between the two electrodes, which is proportional to the O_2 flux passing across the membrane. The current is quantified as a potential difference, using a fixed resistance. Before performing measurements, the instrument was calibrated first with water in equilibrium with atmospheric oxygen (to obtain the potential corresponding to ambient oxygen concentration). Oxygen was then removed from the solution by purging with argon to obtain the potential corresponding to the zero oxygen level.

During measurements, a magnetic stirring system maintained the sample in homogeneous condition, while a thermostat kept the cell suspension at the desired temperature of 19 °C.

3.9.2 MiMS

This method allows the quantification of the gas fluxes (O_2 and CO_2 in this case) and can be used to quantify in real time the contribution of different pathways of the analysed photosynthetic organism (refer to Beckmann et al., 2009 for a more detailed description of the technique). In this approach, a gas permeable Teflon membrane provides the separation of the gas molecules from the sample (this part of the setup is essentially the same as the one used for O_2 measurements with the Clark electrode, see 3.9.1), which are subsequently driven toward

the mass spectrometer source by a vacuum pump. There, ionisation allows distinguishing them according to their charge density and thus their mass. The stream of ionized gas molecules passes through an electromagnetic field, which modifies the ions' trajectories, before they hit the detector. It is possible to decide which flux of molecules to record by changing the intensity of the electromagnetic field. During the measurement, the intensity of the magnetic field is changed rapidly to analyse the different molecular species almost simultaneously and in real time. In our measurements, the recording for each molecule lasted for 5 minutes. All components of the mass spectrometer are all maintained under high vacuum for accurate propagation of ion trajectories. By recording changes of concentration of different gas molecules, including stable isotopes of Oxygen ($^{18}O_2$) and Carbon ($^{13}CO_2$), it is possible to measure fluxes corresponding to PSII water splitting, Rubisco CO_2 fixation, respiration and any regulatory or protective O_2 uptake.
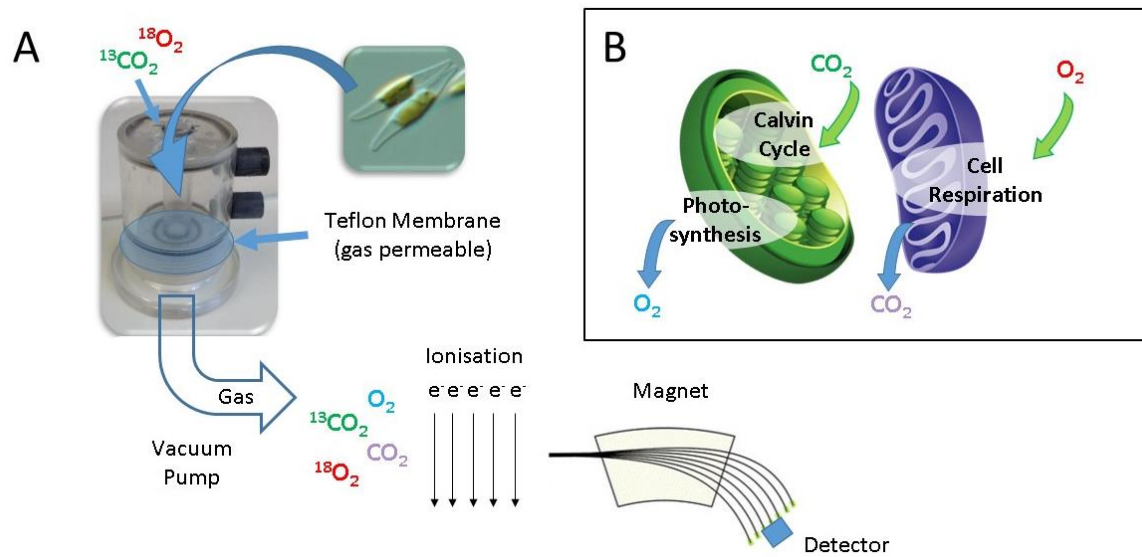
Figure 3.6 | Schematic representation of a MiMS setup (modified from Beckmann et al 2009). A, Diatoms are placed in an appropriate chamber and maintained in suspension by a magnetic stirrer. Gas molecules cross the selective Teflon membrane thanks to the activity of a vacuum pump and undergo the ionization process. The trajectory of the newly produced ions is modified under the influence of an external magnetic field according to their charge densities and selectively hit the detector. **B**, Schematic representation of uptake and production of CO_2 and O_2 by the chloroplast and the mitochondrion

Measurements were performed as follows:

- Wild-type and mutant strains of *P. tricornutum* Pt1 8.6 (CCMP 2561) were grown as described above. Cell cultures concentration was determined by measuring the optical at 750 nm in order to keep them in the exponential phase, at a corresponding concentration between $1.5 \cdot 10^6$ cell/ml and $3 \cdot 10^6$ cell/ml.

- Cells were concentrated by centrifugation and resuspended in their growth medium and 1.5 ml samples was loaded equivalent to approximately 10 µg/mL of chlorophyll. When performing measurements, the sample in the thermostated cuvette was kept at 19°C. A magnetic stirrer provided homogenous sampling of the gases and culture suspensions in a homogenous light.

- Before starting measurements, samples were bubbled with N_2 in darkness in order to remove all traces of gas from the sample and instrument was calibrated for background signals.

- The gas $^{18}O_2$ isotope was introduced in the sample as a bubble while a HCO_3^- solution was injected at a final concentration of 500 µM. The conversion to $^{13}CO_2$ is enhanced by adding a small volume of Carbonic Anhydrase (Sigma, USA) at 1 mg mL^{-1}.

- Once the system had reached equilibrium, data were first recorded in darkness and later at 25 and 250 µmol photons m^{-2}s^{-1}. Measurements were performed for 5 minutes at each light condition.

- At the end of the protocol, sample aliquots were taken for chlorophyll concentrations analysis for data normalisation.

After applying calibration offsets, gas fluxes are expressed as µmol of gas mg Chl^{-1} hr^{-1}.

3.10   Fluorescence and ECS measurements

The analysis of photosynthetic parameters based on imaging of Chlorophyll fluorescence by pulse-amplitude modulation (PAM) approach is based on the possible fate that the light can encounter once it is absorbed by the photosynthetic apparatus, mainly PSII. It can in fact be directed toward three different processes (Maxwell & Johnson, 2000):

- Fluorescence: energy is re-emitted as radiation with a lower wave length compared to the absorbed one;

- Non Photochemical Quenching (NPQ): energy is dissipated as heat. Photosynthetic organisms use this process to protect themselves from excessive light intensity, able to generate dangerous molecular species such as Reactive Oxygen Species (ROS).

- Photochemistry: light energy used by photosynthesis and converted in chemical energy.

The total amount of absorbed energy is constant, therefore when one of these three even increases, the other two decrease: by monitoring the changes of fluorescence, it is possible to measure indirectly the evolution of photochemistry and NPQ.

The instrument provides three types of light, all three belonging to the PAR (Photosynthetically Active Radiation) region of the electromagnetic spectrum. Hence, they can all interact with the photosynthetic apparatus:

- a Measuring Fluorescence Light (MFL) of low intensity light, which does not alter substantially PSII photochemistry. It is provided as an impulse and the fluorescence signal deriving from this light is recorded from the instrument;
- a Saturating Pulse of high intensity flash ($3 \cdot 10^3$ μmol photons m^{-2} s^{-1} ca) allowing the saturation of the reaction centres. The pulse is short enough (0.25 s) in order not to induce photochemistry or photodamage.
- Actinic Light of variable intensity that induces photosynthetic activity.

When performing measurements, the measuring beam is switched on to measure the minimum fluorescence emission (F_0) that corresponds to a maximum photochemical capacity of PSII. The actinic light and the saturating pulse can be switched on independently, to modulate the fraction of photochemically competent PSII, and therefore to increase the fluorescence level from F_0 to F_{ss} (when the actinic light is on) or F_m (when the saturating pulse is on, and no photochemically competent PSII is left). In all cases, the emitted light derived from the fluorescence signal has a greater wavelength (near infrared) compared to the absorbed radiation (PAR). Thus, light emitted by the measuring beam, the actinic and saturating pulse sources can be filtered out using an infrared filter that eliminates all the PAR photons from the camera.

In the dark conditions, plastoquinones Q_A are in the oxidized state and the PSII reaction centres are available to exploit light energy for photosynthesis (called "opened" conformation).

What are the origin of the F_0, F_{ss} and F_m? As mentioned above dark-adapted photosynthetic organisms show a basal level of fluorescence, F_0, when exposed to the measuring beam, because absorbed light is mostly used photochemically. A first short pulse of saturating light leads to the reduction of Q_A (*i.e.* reaction centres are "closed") and all absorbed light is re-emitted, giving the maximum fluorescence signal, F_m. F_v is defined as the difference between F_m and F_0 and the F_v/F_m ratio determines the maximum efficiency of PSII photochemistry (if all the reaction centres were opened). F_v/F_m optimal values are specific for each species and can be used as a non-invasive probe to monitor the physiological condition of the analysed photosynthetic organism, as it decreases under stress conditions. By following the fluorescence signal response to different actinic light intensities and exposure times, several photosynthetic parameters can be measured.

3.10.1 Electron Transfer Rate (ETR)

ETR is proportional to the contribution of PSII to the linear electron transport chain. It is calculated as $(F_m'-F)/F_m'$ x PAR x 0.5 where F_m' and F represent the maximum and the minimum fluorescence upon saturating light during illumination with actinic light; PAR is the intensity of actinic light used to stimulate the photosynthesis and the term 0.5 represents the 50% of probability that one electron goes to the PSII (instead of to the PSI). $(F_m'-F)/F_m'$ is similar to the F_v/F_m value but in this case is an indicator of the real amount of energy that can be used by PSII during the photosynthesis.

3.10.2 Non-photochemical quenching (NPQ)

It is calculated as $(F_m-F_m')/F_m'$ and it corresponds to the light energy which is absorbed by the photosynthetic apparatus but that is not used for photochemistry. Instead, this fraction of absorbed light is dissipated as heat through photoprotection mechanisms.

3.10.3 Electrochromic shift measurements (ECS)

This method allows a non-invasive analysis of the main components of the photosynthetic apparatus (Bailleul et al., 2010). The shifting of the absorption spectrum of a given molecule in the presence of an electric field is defined as Stark effect and it can also be observed in thylakoid's membranes. During photosynthesis, light absorption induces the formation of an electric field across the thylakoid's membrane, which is experienced by membranes embedded pigments (chlorophyll and carotenoids). This translates in a shift in their absorption spectra, which can be measured and used to characterise several photosynthetic parameters (Fig. 3.7).

The electric field induced by light absorption, called electrochemical proton gradient ($\Delta\mu H^+$) provides the energy source for ATP synthesis through the activity of the ATP-synthase and consists of two different components: the proton concentration gradient (ΔpH) and the electric potential ($\Delta\Psi$). The existence of the $\Delta\Psi$ derives from peculiar topology of the electron transfer complexes (PSII, PSI and cytochrome b_6f), where all the electron donors are localised toward the luminal side while acceptors are located at the stromal side of the membranes.
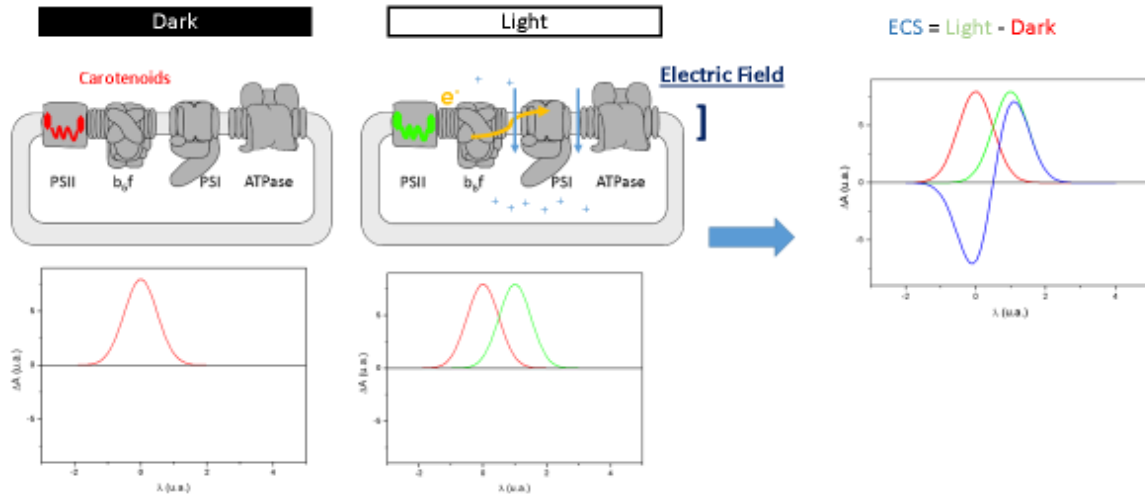
Figure 3.7 | Electrochromic Shift of photosynthetic membrane embedded pigments. In the dark, carotenoids display a characteristic absorption spectrum (red). In presence of light, the import of protons in the thylakoid's lumen (ΔpH, blue arrows) and the electron transfer chain ($\Delta\Psi$, yellow line) establish an electric field across the membranes. The latter component is responsible for the shift of the carotenoids' absorption spectrum (green) toward longer wavelengths. The ECS spectrum is finally obtained by subtracting the spectrum in the dark from the one in the light.

It is possible to follow the kinetics of different components of the ECS signal along time at appropriate wavelengths. The ECS signal kinetics is made up of different phases, corresponding to the activity of different components of the photosynthetic apparatus. After dark to light transition, the photon absorption, energy transfer to the reaction centre and primary photochemistry (10^{-15}-10^{-9} s) constitute the first fast phase (phase "a" according to Joliot and Delosme 1974), reflects the rapid onset of the electric field due to charge separation by the PSs. The subsequent oxidation of plastoquinols by cytochrome b_6f establishes the slower "b" phase (10^{-3} s) (Joliot and Delosme 1974). Finally, the H^+ flux through the ATP-synthase complex is responsible for the relaxation of the light induced pmf and thus to the decreased ECS signal (phase "c" phase, Joliot and Delosme 1974).

Different components of the ECS signal present a peak in different region of the spectrum according to the pigment composition of the photosynthetic membranes. Thus the ECS can provide information about the nature of these molecules of a given organism (see Bailleul et

al., 2010 for a review). The shift of the absorption maxima derives from the different dipole moments or polarizabilities of the pigments between their ground state, in the dark, and excited state, after the absorption of a photon. These properties change in a linear and quadratic fashion respectively in relation to the intensity of the $\Delta\Psi$. In most species (i.e. *Arabidopsis thaliana*), the ECS mainly consists on the first linear component (ECS_{lin}), which usually presents a peak at 520 nm in the ECS spectrum and it corresponds to the presence of polar pigments (*i.e.* chlorophylls) embedded in the thylakoid's membranes. Although this signal can be exploited as an internal voltmeter to monitor changes in the membrane potential, it is independent on the absolute value of the $\Delta\Psi$ before illumination (Witt, 1979). In contrast, the amplitude of the quadratic component (ECS_{quad}) depends on the intensity of the pre-existing field (*i.e.* in darkness). This is observed in *C. reinhardtii* and *C. sorokiniana* mutant strains lacking the light harvesting complexes, thus presenting a lower ECS_{lin} (Witt, 1979; Joliot & Joliot, 1989). In this case, it is possible to measure the absolute value of the $\Delta\Psi$ before light induction, since the ECS_{quad} is now measurable. In some species, both components of the ECS are detectable. This is the case of diatoms, where a second peak also appears in the ECS spectrum at 566 nm, corresponding to the ECS_{quand} (Fig3.8). Therefore, the amplitude of the flash-induced quadratic ECS can be used to probe the absolute value of the electric field already present in dark conditions.

To measure the ECS *in vivo*, we employed a Joliot-type spectrophotometer (JTS-10, Biologic, France) (Fig 3.9). Dark adapted cells were exposed to a 10 ms pulse of saturating (4 500 µmol photons m^2 s^{-1}) of red light. As $\Delta\Psi$ increased, kinetics at the two corresponding wavelengths were recorded with appropriate interference filters (3-8 nm bandwidth).
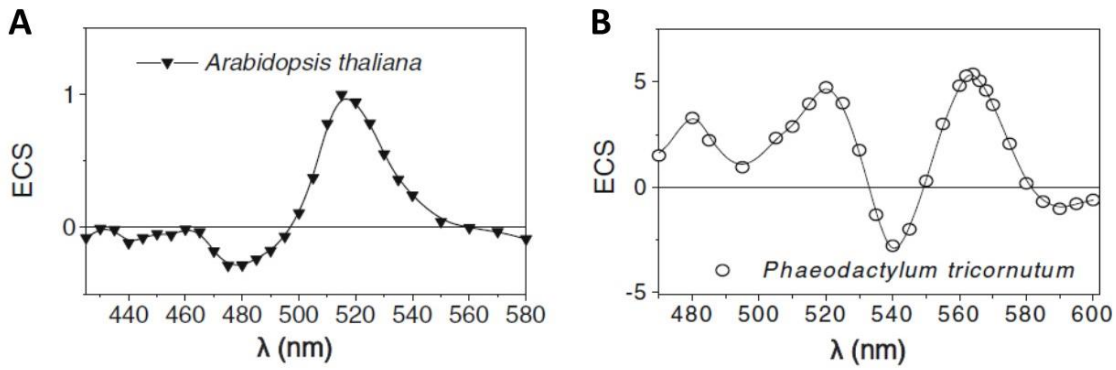
Figure 3.8 | ECS spectrum of *Arabidopsis thaliana* (A) and *Phaeodactylum tricornutum* (B). The spectrum of Arabidopsis presents a main peak at 520 nm, corresponding to the linear component of the ECS, whilst in *P. tricornutum* it also shows a peak (the quadratic component) at 565 nm.

The linear and quadratic components display a peak in the ECS spectrum at 520 nm and 566 nm respectively. A third filter is used to evaluate the contribution of the cytochrome c signal, showing a peak at 554 nm: this soluble PSI donor shows a partially overlapping absorption spectrum with both components of the ECS and thus needs to be considered during the measurements.

The kinetics of the linear and quadratic components of the PMF are calculated as follows:

- $ECS_{lin} = [520] - 0.25cyt\ c$

- $ECS_{quad} = [566] - 0.15cyt\ c$

where the spectral contribution of cytochrome c (cyt c) is convoluted as

- $cyt\ c = [554] - 0.4[520] - 0.4[566]$

The correlation between the two signals allows us to quantify the absolute value of the PMF in the dark ($\Delta\Psi_d$). This relationship if fitted with the parabolic function:
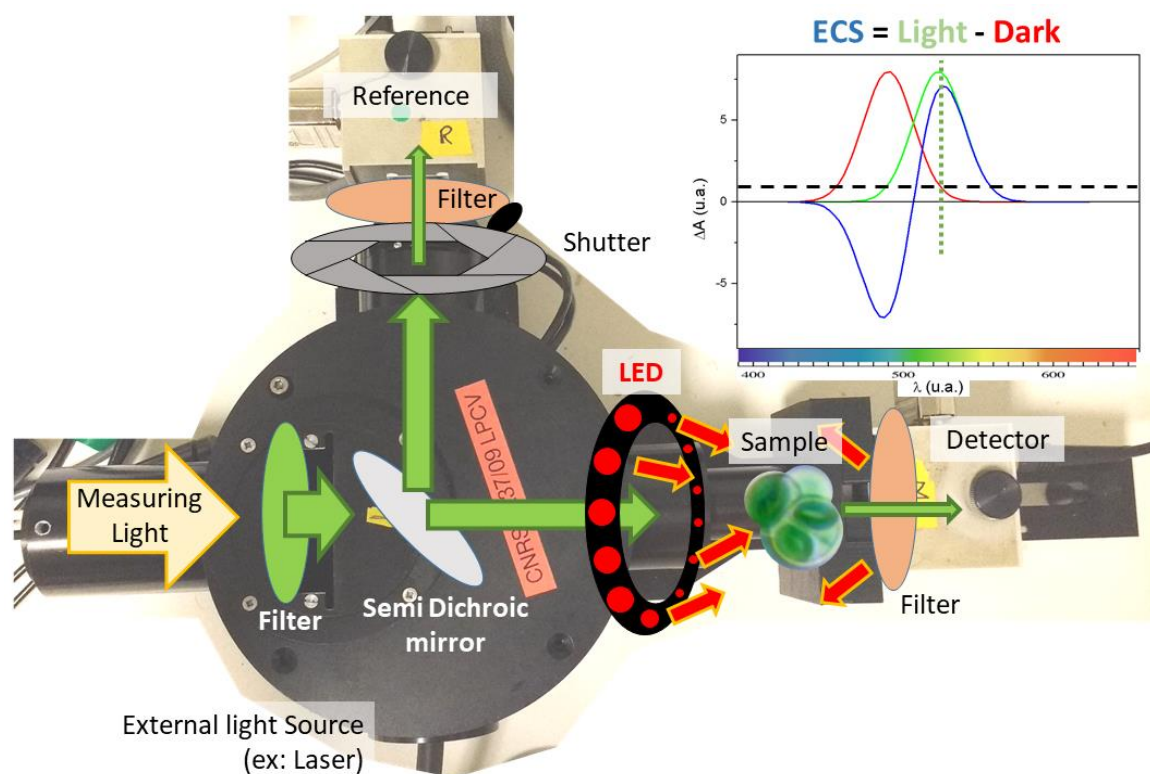
- $ECS_{quad} + a\Delta\Psi_d^2 = a(ECS_{lin} + \Delta\Psi_d)^2$

where 'a' is constant for all the conditions and $\Delta\Psi_d$ is the electrical component of the PMF in the dark. This leads to the evaluation of $\Delta\Psi_d$ as the minimal ECS_{lin} value of the experimental data. The correlation between the two signals allow us to quantify the absolute value if the PMF in the dark.


Figure 3.9 | Kinetic measurements are performed with a Joliot Type Spectrophotometer. During ECS kinetics measurements, the absorbance of a measuring non actinic light is recorded. Different wavelengths of the measuring light are selected through a specific bandpass interference filter (green ellipse, green dotted vertical line in the graph). Before reaching the sample, the light is splitted through a semi-dichroic filter into two perpendicular beams, one toward a reference detector and the other toward sample. Before the measurement, the zero is set by adjusting the reference signal by opening or closing a shutter, in order to match the absorbance in the dark signal reaching the detector (black dashed horizontal line in the graph). The kinetics of the ECS signal is recorded in darkness and in presence of actinic red light (red arrows), provided by LEDs ring. To prevent the actinic light to be mistakenly recorded, specific high pass filters are placed before the detectors. An external light source (laser or xenon lamp) can also be used for specific analysis. The ECS spectrum (blue line in the graph) is obtained by using different filters for the measuring light and by recording the ECS signal after a saturating light pulse (graph on the up-right).

3.11 Inhibitors

DCMU (3-(3,4-dichlorophenyl)-1,1-dimethyl-urea), DBMIB, (2,5-dibromo-3-methyl-6-isopropyl-p-benzoquinone), FCCP (Carbonyl cyanide-4-(trifluoromethoxy)phenylhydrazone), Antimycin A (AA), myxothiazol and Salicylhydroxamic acid (SHAM), (Sigma-Aldrich) were dissolved in ethanol, whereas hydroxylamine in deionized water. FCCP was used at 8 mM solution to allow the depletion of the dark PMF without preventing the light-induced generation of PMF needed to quantify $\Delta\Psi_d$. AA and myxothiazol were used at 5 mM, DCMU at 15 µM, unless otherwise stated. When using hydroxylamine or SHAM, the lowest inhibitor concentration to induce a full inhibition of PS II activity or maximum inhibition of respiration, respectively, was considered. Concerning hydroxylamine and SHAM, the range of concentrations used was 30–100 mM and 0.5–1 mM, respectively. AA and myxothiazol were preferred to potassium cyanide to block the cyanide sensitive pathway of respiration because potassium cyanide also affects Rubisco activity (Wishnick & Lane, 1969), ascorbate peroxidase (Nakano & Asada, 1987) and Cu/ Zn superoxide dismutase (Asada et al., 1974). Bongkrekic acid (BKA) and carboxyatractyloside (CATR) (Sigma) were stored at -80°C in aliquots.

Chapter 4: Discussion

Photosynthetic organisms are able to exploit light energy to drive the production of ATP, the energetic currency of the cell, and NADPH, the reducing equivalent, which are both necessary for carbon assimilation during the Calvin cycle in the chloroplast. While the main components of the photosynthetic apparatus are conserved (Photosystems, cytochrome, ATP synthase), different regulation mechanisms can exist in different species across the tree of life, either occurring in the chloroplast or depending from other cell mechanisms occurring in different cellular compartments. Together with the plastid, the mitochondrion is also present in the photosynthetic eukaryotic cells and since it also contributes to the energy metabolism, the activities of both organelles need to be regulated, possibly through mutual interactions. In diatoms an essential control mechanism exists in form of direct exchange of ATP and reducing equivalents between the organelles, which appear to play a vital role in the cell's metabolism. The objective of this PhD research work was to better understand the chloroplast and mitochondrion cross talk in the marine diatom *Phaeodactylum tricornutum* through the identification and characterization of proteins possibly involved in the ATP and NADPH exchange mechanism between the two organelles.

4.1   The selected genes are putative membrane transporters

We adopted two strategies to select the candidate proteins. Two first candidates arose from the analysis of transcriptomic data and two more through a pharmacological approach. Moreover, since we looked for proteins likely involved in the transport of solutes across organelles' membranes we selected genes displaying specific properties. Membrane localisation was addressed using prediction tools of both secondary and tertiary protein structures to identify

transmembrane domains, while solute specificity was deduced by looking for homologs annotated proteins in other organisms, possibly closely related to diatoms.

4.1.1 Transcriptomic data analysis

Photosynthetic organisms can thrive in different growth conditions according to the different energy sources that are available in the environment. Moreover, in presence of both light and reduced carbon, an organism can behave in three ways: it can exploit the activity of either one of the two energetic organelles or have them working at the same time. In the former case, we say that the cells grow in a phototrophic or heterotrophic manner, *i.e.* when they rely on either the photosynthetic or the mitochondrial activity respectively. In the latter case, the chloroplast and the mitochondrion are both active at the same time and thus the photosynthetic organism is defined as a mixotroph.

In the laboratory, *P. tricornutum* cells usually grow phototrophically, since they are kept in ESAW 10NP minimum medium and light is the only available energy source. Thanks to my contribution, in a previous study conducted in the laboratory we showed that this algal species is able to grow at a faster rate when glycerol is added to the medium (Villanova et al., 2017). This means that *P. tricornutum* is indeed a mixotroph, as it is able to uptake and exploit the external carbon source present in the medium in addition to light through photosynthesis.

Since we know that the exchange of ATP and reducing equivalent between chloroplast and the mitochondrion plays an important role in diatoms, we reasoned that transporters responsible for this crosstalk may be differentially expressed in different growth conditions. Therefore, we decided to analyse the transcription profile of this marine diatom when grown in light and in presence or absence of glycerol and look for potential transporters for ATP or reducing

equivalent. After this first selection process, the proteins encoded by Phatr3_J46742 and Phatr3_J35625 genes, named Pt_MCF (Mitochondrial Carrier Family gene) and DTC (Dicarboxylate-Tricarboxylate Carrier), were chosen for further analysis.

4.1.2 Putative ADP/ATP transporters

Two more candidate transporters were selected after a pharmacological approach. In the eukaryotic cell, the ATP produced by oxidative phosphorylation in mitochondria is exported across the inner membrane thanks to the presence of specific ATP/ADP carriers (AAC). Furthermore, these transporters allow the import of ADP into the mitochondrial matrix, which will be used as substrate of the ATP synthase for the production of new ATP. AACs have been characterized from both structural and functional point of views (Pebay-Peyroula et al., 2003) (Zeman et al., 2003) also using specific inhibitors, such as bongkrekic acid (BKA) and carboxyatractyloside (CATR). After testing the effect of these inhibitors with a spectroscopic approach, we realised that BKA did in fact altered the proton motive force in the dark ($\Delta\Psi_d$) of the thylakoids of *P. tricornutum.* A lower $\Delta\Psi_d$ is also observed when using inhibitors of complexes involved in the electron transport chain in the mitochondrion, *i.e*. SHAM and Antimicin A (AA), which are specific for AOX and complex III respectively. Our measurements of the $\Delta\Psi_d$ made us conclude that homologs of AACs proteins must be present in *P. tricornutum*. When looking for such candidates in the abovementioned transcriptomic data, we identified the gene Phatr3_J15797, which was then named AAC1. As the AAC group present multiple members, we searched for additional homologous transporters in *P. tricornutum* by BLAST analysis. When using the amino acidic sequence of AAC1 as query, we found that Phatr3_J22873 (AAC2) was the best hit. This protein was lacking the secondary plastid target sequence, making it a possible mitochondrial transporter.

4.2   The selected genes belong to the Mitochondrial Carrier Family

After further sequence alignment analyses, the four selected genes appeared to share common traits with proteins belonging the "Mitochondrial Carrier Family" (MCF, also known as SLC25) (Palmieri, 2013). This group is the most represented in the eukaryotic cell and it comprises carriers and transporters of a broad spectrum of substrates. Moreover, the four candidates were all predicted to have between 6 and 8 transmembrane α-helices and putative transporter three-dimensional conformations. Finally, a secondary plasmid target sequence was identified by the ASAFind software at the N-terminus of the amino acid sequence of Pt_MCF and DTC, with high and low level of confidence, respectively. The chloroplastic localisation of the first candidate was also strongly suggested by the phylogenetic analysis performed in collaboration with Pierre Cardol and Richard Durrel, which showed that homologous proteins are present in secondary endosymbionts closely related to diatoms. The phylogenetic analysis revealed that Phatr3_J49742 (Pt_MCF) gene is shared between secondary endosymbiotic species, especially in diatoms and in closely related organisms. This suggests that this protein might play a relevant role in metabolic processes that are specific or at least more important in these species, including *P. tricornutum*.

To understand the physiological role of the candidate transporters, we used CRISPR-Cas9 technology to generate knock-out mutant lines and, when no mutant was obtained, antisense strains of the putative transporters and analysed their growth, photosynthetic and respiratory properties. We reasoned that a phenotype of either organelle's energetic activity would reflect the implication of the lacking gene in the cross-talk mechanisms.

4.3 Pt_MCF is likely to be involved in the chloroplast-mitochondrion crosstalk mechanisms

After the application of the transformation protocol, described in Chapter 3, Pt_MCF knock out mutant strains were obtained. To understand the effect derived from the mutation, we analysed different parameters linked to the photosynthetic and the respiratory activities of the cells. Since this transporter is not part of the photosynthetic apparatus nor directly involved in the cell respiration processes, we inferred that the effects observed in the *mcf* mutant algae lacking the Pt_MCF coding gene on the activity of the chloroplast or the mitochondrion underline a possible role of this protein in the interaction between the two organelles.

Accordingly, spectroscopic analysis revealed a lower proton motive force in the dark ($\Delta\Psi_d$) in the *mcf* mutant strains compared to the wild type. As showed from previous studies (Bailleul et al., 2015), the existence of such $\Delta\Psi_d$ is derived from the hydrolysis of the ATP derived from the mitochondrion. Since Pt_MCF does not take part in the respiration process but rather it is predicted to be a transporter, we speculate that the transport mechanisms might be compromised in the mutant strain.

Moreover, chlorophyll fluorescence measurements indicated lower mutant photosynthetic performances at high light intensities compared to the wild-type cells.

This trend was also observed when investigating the relationship between the photosynthetic and respiration activity by measuring oxygen evolution and consumption rate respectively. As demonstrated by Bailleul and colleagues (Bailleul et al., 2015), these two processes have a linear relationship with one another due to the importance of the ATP and NADPH exchanges between the organelles in diatoms. The actual model indicates that in this organisms the chloroplast is not able to adjust the ATP/NADPH ratio during the photosynthesis to fuel the CO_2 assimilation (*i.e.* cyclic electron flow), thus importing the extra ATP needed from the

mitochondrion. Consequently, the photosynthetic activity is optimized when the mitochondrion is fully functional. This is a mutual relationship, since the mitochondrion needs reducing equivalents to produce ATP through oxidative phosphorylation. Following this model, we speculated that Pt_MCF might be responsible either for the import of ATP or for the export of reducing power from the chloroplast toward the mitochondrion, since is predicted to be localised in the chloroplastic envelope.

O_2 evolution and uptake rates were measured at the Clark electrode, with a titration of inhibitors of the mitochondrion, and with MiMS, at different light intensities. In the first case, despite still maintaining a linear relation with the photosynthesis, the respiration rate of the mutant strain appeared to be more sensitive to the presence of the inhibitors compared to the wildtype. When measuring the O_2 consumption rate with MiMS, a spike was observed when cells passed from low to high light conditions before setting at a lower steady state. We explain this effect as a transient boost of the mitochondrial activity in order to help the chloroplast to cope with the high light. In these situation in fact, photosynthesis saturates and Calvin cycle is fully active. In the *mcf* mutant the contribution of the mitochondrion is affected due to the lower capability of the plastid to either import ATP or export NADPH, therefore the cell respiration is transiently enhanced to increase the probability for the ATP to reach the chloroplast.

Overall, the characterisation of the *mcf* mutant strains contributed to a better understanding the role of the Pt_MCF protein in the energetic crosstalk between the organelles: thanks to these studies, we were able to conclude that this transporter plays at least a partial role in photosynthesis regulation. The mild effect might be due to the presence of other systems able to carry ATP or reducing equivalents present in the chloroplastic envelope that have not yet been studied.

The second selected gene was a putative transporter of reducing equivalent Phatr3_J35625 (DTC), predicted to be localised in the chloroplastic envelope. Despite several efforts, we could

120

not obtain any knock-out mutant strain. This made us speculate that the lack of this protein might be a lethal condition for the cell. This hypothesis is supported by the fact that when looking for homologs of DTC in *P. tricornutum*, only one protein with low identity was found, suggesting that this candidate might be the only specific transporter for its still unknown substrate.

4.4 The role of AAC proteins in diatoms

Two final candidates were selected after observing the effects of bongkrekic acid (BKA) on the $\Delta\Psi_d$ in wild-type cells of *P. tricornutum*. This motivated us to look for homologs in diatoms of mitochondrial ADP/ATP carriers, the specific target of BKA. Thus, we chose Phatr3_J15797 (AAC1) and Phatr3_J22873 (AAC2) genes as putative mitochondrial ATP transporters. When analysing the KO mutant strain for the former candidate, no effect on the growth rate nor photosynthetic parameters were observed during fluorescence measurements. We deduced that AAC1 is either not involved in ATP or reducing equivalents exchange or its function is redundant in the cell and can be accomplished by other transporters. On the other hand, we could not obtain any KO mutant strain for the latter AAC candidate, called AAC2, therefore we made the hypothesis that the activity of this protein is vital for the cell. Moreover, as no significant phenotype was observed on the photosynthetic or respiratory activity in the knock down lines, it is possible that even a low protein concentration is sufficient to guarantee the ATP export from the mitochondrion.

4.5 Future perspectives

To obtain a more complete picture of the influence that these membrane proteins have in the crosstalk between the chloroplast and the mitochondrion in *P. tricornutum*, additional analyses need to be done in order to understand the substrate selectivity of the transporters. These are ongoing studies, thanks to the collaboration with Ferdinando Palmieri and his research team,

based in Bari, Italy. The expression of the candidate proteins in lipid micelles and the further test with radioactive compounds will allow us to investigate their substrate specificity.

Another important piece of information will be the intracellular localisation of the proteins of interest. Besides understanding whether they are localised in the plastid envelope, as suggested from the presence of the target sequence present in the Pt_MCF, we speculate that this transporter might in fact be localised at the interface of the chloroplast and the mitochondrion. It has been hypothesised that the contact points present in these regions might contribute to the optimisation of the crosstalk between the organelles (Bailleul et al., 2015; Flori et al., 2017). This part of the project will be performed in collaboration with Richard Durrel, from Institute de Biologie de l'Ecole Normale Supérieure (IBENS) in Paris, France, who will contribute to the generation of *P.tricornutum* lines presenting the Pt_MCF protein coupled with GFP. Overall, the complete characterisation of these genes, especially Pt_MCF and AAC2 will shed light on their possible role in the energetic crosstalk between the organelles in diatoms, hopefully to better comprehend this process and the possible reasons of the ecological success of this group of microalgae in the oceans.

4.6   List of Acronyms

aa Amino acid

AA Antimycin A

AAC ADP/ATP carrier

ADP Adenosine di-phosphate

ANR1 Anaerobic response 1 protein

AOX Alternative oxidase

APX Chloroplast-associated ascorbate peroxidase

AS Antisense

ATP Adenosine tri-phosphate

BKA Bongkrekic acid

CATR Carboxyatractyloside

CBB Calvin-Benson-Bassham cycle

CCM CO_2-concentrating mechanism

CEF Cyclic electron flow

cERM Chloroplast endoplasmic reticulum

Chl Chlorophyll

Cyt Cytochrome

DCMU 3-(3,4-dichlorophenyl)-1,1-dimethylurea

DTC Dicarboxylate/tricarboxylate carrier

ECS Electrochromic shift

Em Redox Potential

ER Endoplasmic reticulum

ERAD ER-associated degradation

ESAW Enriched Seawater medium

ETR Electron transport rate

FCCP (Trifluoromethoxy) phenylhydrazone

FCP Fucoxanthin chlorophyll-*a/c* binding proteins

FLV Flavodiiron proteins

FNR Fd-NADP$^+$-oxidoreductase

Fm Maximal fluorescence after dark acclimation

Fm′ Maximal fluorescence in the light acclimated state

Fv Variable Fluorescence after dark acclimation

GA Gibson Assembly

Gly Glycerol

IPTG Isopropyl-β-thiogalactopyranoside

iEM Inner envelope membrane

KD Knock-down

KO Knock-out

LEF Linear electron flow

MC Mitochondrial carrier

MCF Mitochondrial carrier family

MDA Monodehydroascorbate radical

MGDG Monogalactosyl-diacyl- glycerol

MiMS Membrane inlet Mass Spectroscopy

NADH Nicotinamide adenine dinucleotide

NADPH Nicotinamide adenine dinucleotide phosphate

Ndh NADPH dehydrogenase

NPQ Non-photochemical quenching

OE Over expression

oEM Outer envelope membrane

PMF Proton motive force

PPC Periplastidial compartment

PPM Periplastidial membrane

PQ Plastoquinone

PS Photosystem

PSI Photosystem I

PSII Photosystem II

Pt *Phaeodactylum tricornutum*

PTOX Plastoquinone terminal oxidase

ROS Reactive oxygen species

Rubisco Ribulose-1,5-bisphosphate carboxylase/oxygenase

SDS-PAGE Sodium dodecyl sulphate - polyacrylamide gel electrophoresis

SELMA symbiont specific ERAD-like machinery

SEM Scan electron microscopy

sgRNA Guide RNA sequence

SHAM Salicylhydroxamic acid

SOD Superoxide dismutase

SQDG Sulfoquinovosyl diacylglycerols

TIC Translocase of the inner chloroplastic mambrane

TOC Translocase of the outer chloroplastic mambrane

TIM Translocase of the inner mitochondrial mambrane

TOM Translocase of the outer mitochondrial mambrane

VDAC Voltage-dependent anion channel

WB Western blot

WT Wild-type

WWC Water to water cycles

ΔΨ Electric field

ΔΨ$_d$ Electric field in the dark

ΔμH$^+$ Proton motive force

ΔpH Proton gradient

4.7   List of figures and tables

Chapter 1

Figure 1.1 | Electrochromic shift measurements allow visualising the different time frames of photosynthetic linear electron flow. The kinetics of the electrochromic shift measured in dark adapted Chlamydomonas cells (top) display different phases. After exposure to a single turnover saturating laser flash (intensity 2 mJ, duration 5 ns), a rapid increase of the ECS signal (< 100 µs) is observed (red), which is related to the turnover of the two photosystems working in series: PSII and PSI (also in red in lower panel). The following slower phase (in the millisecond time range, blue) reflects electron transfer within the cytochrome b_6f complex (in blue in the lower panel). The kinetics of the ECS signal also allows visualising proton fluxes across the photosynthetic membranes. This is shown by the slow signal decay (in the tens of ms time range, green), which is associated with proton flux through the ATP synthase CF_O-F_1.

Figure 1.2| Schematic representation of different kinetics of electron transfer chain in the photosynthetic apparatus. Electron flow is progressively slowed down from light driven photochemistry to $NADP^+$ reduction. Electron flow rates from 10 to 250 $e^- s^{-1}$ are represented by different colours. Linear electron flow: solid line; Cyclic electron flow: dashed line; Mehler reaction and chlororespiration: dotted line. Protein complexes involved in different electron transfer reaction are indicated with different colours: LEF in blue; CEF orange; Mehler and WWC in green.

Table 1.1 | Partition of photosynthetic electron flow between alternative electrons sink in vascular plans, and different microalgae. Data are referred as electrons per second unless specified. LEF, linear electron flow; FLVs, flavodiiron proteins, Photoresp, photorespiration; Cyt b_6f, cytochrome b_6f; Photoresp, photorespiration; CEF, cyclic electron flow.

Chapter 2

Figure 2.1 | Schematic representation of the phylogenetic tree of the main algal groups (adapted from Marchand et al., 2018). The primary endosymbiosis event (grey line) gave rise to Glaucophyta. Two subsequent events of endosymbiosis allowed the formation of the Chlorophytes (green line), which includes Chlamydamonas rehinardtii, when a host eukaryotic cell engulfed a green alga. Diatoms *arose* after an endosymbiotic event where the guest cell was a red alga (red line).

Figure 2.2 | Scan Electron Microscopy (SEM) images of the three morphotypes of *Phaeodactylum tricornutum* (from De Martino et al., 2007). This alga can exist in three different morphotypes: Fusiform cell (a), two oval cells (b), and triradiate cell (c). Scale bar, 1 µm.

Figure 2.3 | Representation of the plant chloroplast transporters (Facchinelli and Weber, 2011). The presence of transporters in the chloroplast's envelope allow the exchanges of a wide range of metabolites, including carbon and nitrogen compound, thus regulating different metabolic pathways of both the plastid and the whole cell.

Figure 2.4 | Schematic representation of energetic interaction between the mitochondrion and the chloroplast. According to the model, the optimum ATP/NADPH needed for carbon fixation is achieved through the import of ATP produced by the mitochondrion. Light blue lines: photosynthetic linear electron transport chain; red lines: respiratory electron flow; dark blue dashed lines: putative ATP/ADP exchange pathway between the organelles.

Figure 2.5 | Electron micrographs of *Phaeodactylum tricornutum* (from Bailleul et al., 2015). The arrows indicate the physical contacts between the chloroplast (upper structure in green) and mitochondrion (in violet).

Figure 2.6 | Structural organisation of organelles' membrane in *Phaeodactylum tricornutum* (adapted from Flori et al., 2016). Scheme of the four membranes surrounding the Chloroplast of secondary endosymbionts; from the outside, Chloroplastic ER (cERM) also surrounding the nucleus, Periplastidial Membrane (PPM), outer Envelope Membrane (oEM), inner Envelope Membrane (iEM). The Periplastidial space (PPC) is the region comprised between the PPM and oEM. M: Mitochondrion N: Nucleus.

Figure 2.7 | Schematic representation of Mitochondrial Carriers (MCs) localised across the mitochondrial inner membrane (from Palmieri, 2013). So far, 16 MCs have been functionally identified (in green) and their roles in transporting catalyzing metabolites, nucleotides or coenzymes transport regulate multiple pathways of the mitochondrial metabolism. AAC, ADP/ATP carrier; AGC, aspartate glutamate carrier; APC, ATP-Mg/Pi carrier; CAC, carnitine-acylcarnitine carrier; CIC, citrate (tricarboxylate) carrier; CoA, coenzyme A carrier; DIC, dicarboxylate carrier; GC, glutamate carrier; ODC, oxoadipate carrier; OGC, oxoglutarate carrier; ORC, ornithine carrier; PiC, phosphate carrier; PNC, pyrimidine nucleotide carrier; SAMC, S-adenosylmethionine carrier; TPC, thiamine pyrophosphate carrier; UCP, uncoupling protein.

Figure 2.8 | Protein structure prediction derived from the amino acid sequence of the Phatr3_J46742 gene product with I-TASSER. The best model of MCF (in green) and the most similar crystal structure present in the PDB, corresponding to the mitochondrial ADP/ATP carrier (purple) (Pebay-Peyroula et al., 2003). **A**, side view of the carriers, top corresponds to the intermembrane space, bottom to mitochondrial lumen, according to the topology of the ADP/ATP carrier (Pebay-Peyroula et al., 2003). **B**, Top view of the channel, from the intermembrane space.

Figure 2.9 | Phylogenetic tree of Phat 46274 and its closest relatives. The tree topology shown is the consensus inferred using MrBayes with three substitution matrices (GTR, Jones, WAG) and RAxML with three matrices (GTR, JTT, WAG). Branches are coloured by taxonomic affiliation. Taxon names are coloured by the inferred subcellular localisation of the protein (for lineages containing four-membrane bound plastids), or in grey (for lineages that do not contain four membrane-bound plastids). Circles at each node are shaded by consensus support for the topology shown. Three evolutionarily distinct families of homologues identifiable in the *Phaeodactylum* genome are labelled with circular brackets.

Figure 2.10 | Molecular characterisation of the Pt_MCF KO mutants. A, Sequencing of the Phatr3_J46742 gene in *mcf-a* and *mcf-b* indicates that both clones bear a stop codon after 90 aa due to the insertion of 2 and 1 base pair, respectively. Western blot analysis (**B**) confirm the successful knocking out of the Pt-MCF gene by revealing the absence of a specific protein at around 40 KDa in the two mutant lines. Note that mutant complementation did not proved successful, as the MCF protein was still missing in putative complemented lines (data not shown).

Figure 2.11 | Photosyntetic phenotype of two PT_MCF knockout mutant strains. Measurements were performe on *P. tricornutum* cells in exponential growth phase (between 1 and $3 \cdot 10^6$ cell ml^{-1}). After centrifugation (3500g, 5',19°C) cells were distributed on a 96-well plate at $20 \cdot 10^6$ cell ml^{-1} concentration in 150 µL volume. For both ETR (**A**) and NPQ (**B**) data correspond to average +SD of 3 replicate independent experiments, each comprising 3 technical replicates. ETR and NPQ were calculated according to (Maxwell & Johnson, 2000) (see Materials and Methods).

Figure 2.12 | ECS signal observed in *Phaeodactylum tricornutum*. A, The ECS spectrum (black) is constituted by two different components and their association to polar and polarizable

pigments embedded in the thylakoid membranes (**B**) exhibiting a linear (blue) and quadratic (red) growth relationship to the $\Delta\Psi$ (r.u., relative units). The relationship between quadratic and linear ECS fitting a parabolic function in control conditions (**C**), with addition of the uncoupler (FCCP, black squares), anaerobiosis (red circles) and respiratory inhibitors (AA and SHAM; blue circles) (**D**). The green arrow indicates the proton motive force in the dark ($\Delta\Psi_d$). **E**, Putative model of the energetic crosstalk between chloroplasts (left) and mitochondria (right) in the dark. Red arrows: oxidative phosphorylation electron flows. Green dashed line: possible ADP/ATP transfer mechanism between the organelles. ATPase, ATPase/ synthase; b6f, cytochrome b6f; I/III/IV, respiratory complexes I, III and IV. Adapted from (Bailleul et al., 2015).

Figure 2.13 | Effect of the lack of the Pt-MCF gene on the proton motive force in the dark ($\Delta\Psi_d$) in *P. tricornutum* cells. Measurements were performed on *P. tricornutum* cells in exponential growth phase (between 1 and $3 \cdot 10^6$ cell ml^{-1}). After centrifugation (3500g, 5', 19°C) cells were placed in a 2 ml plastic cuvette at $20 \cdot 10^6$ cell ml^{-1} concentration in 1.5 ml volume. ECS measurements were conducted using a Joliot Type Spectrophotometer (JTS). Data ± SE form 3 independent experiments, the $\Delta\Psi_d$ in the control sample was set to 100%. ECS Linear and quadratic components of P. tricornutum cells were deconvoluted and $\Delta\Psi_d$ calculated as described in Chapter 3: Materials and Methods.

Figure 2.14 | Photosynthesis/respiration relationship. A, Linear relationship between the photosynthetic and the mitochondrial respiration activities (adapted from Bailleul et al. 2015). **B**, Schematic representation of the energetic exchanges model connecting the mitochondrial and chloroplastic activities.

Figure 2.15 | Analysis of photosynthesis/respiration relationship. *P. tricornutum* cells in exponential growth phase (between 1 and $3 \cdot 10^6$ cell ml^{-1}) were centrifuged (3500g, 5',19°C)

and placed in a specific 2 ml cuvette at $20 \cdot 10^6$ cell ml^{-1} concentration in 1 ml volume. Photosynthetic activity was measured as O_2 evolution in light and cellular respiration rate as O_2 uptake in the dark. The mitochondrial activity was titrated with increasing amount of the respiratory inhibitors SHAM and Antimycin A (SHAM+AA: 0; 0,4mM+2µM; 0,66mM+3,33µM; 1mM+5µM; 2mM+10µM; 4mM+20µM). Data ± SD from 3 independent experiments.

Figure 2.16 | O_2 uptake rates of *P. tricornutum* cells at different light intensities (dark, 25µEm^{-2}s^{-1}, 250 µEm^{-2}s^{-1}, dark). **A,** After dark adaptation, cells were kept for four minutes in each condition. Data correspond to the average + SD of 4 independent replicates. **B,** Ratio between O_2 uptake peak from low (25 µEm^{-2}s^{-1}) to high (250µEm^{-2}s^{-1}) light transition and the Steady State (see Fig. A). Net values of both Peak and Steady State were obtained by subtracting the average value of O_2 consumption in the dark.

Figure 2.17 | Comparison of the measured O_2 evolution and $^{18}O_2$ uptake rates with previously published data (Bailleul et al., 2015). Respiration values correspond to the peak phase after low (25 µEm^{-2}s^{-1}) to high light transition (250 µEm^{-2}s^{-1}). Data correspond to the average + SD of four independent replicates.

Figure 2.18 | SDS-PAGE confirming the expression of Pt-MCF protein in Rosetta2 *E.coli* competent cells. The two lines correspond to protein extractions performed on samples before and after induction of protein expression, which was carried out by incubation with 0,4mM IPTG over night at 37 °C. The red arrow indicates the band at 40 KDa corresponding to the predicted molecular weight of Pt-MCF.

Figure 2.19 | Growth curve of *Phaeodactylum tricornutum* knock-out mutant strains lacking the gene Phatr3_J46742 coding for Pt-MCF. Cells cultures of $0.5 \cdot 10^6$ cells ml^{-1} were

cultivated in ESAW10NP medium and growth was followed for 27 days during week days. Data ± SD form 3 biological replicates.

Figure 2.20 | ADP/ATP Carrier transport mechanism (from Ruprecht and Kunji, 2019). The "cytosolic open" state (c-state) allow either the binding of ADP or the release of mitochondrial ATP. The transition to the "matrix open" state (m-state) conformation consists on the rotation of six mobile transmembrane helices around a central substrate binding site, allowing the release of ADP and the binding of ATP.

Figure 2.21 | Effect of bongkrekic acid (BKA) and Carboxyatractyloside (CATR) on the $\Delta\Psi_d$ in *P. tricornutum*. Cells were incubated with either 20µM BKA, 100µM CATR or 1 mM SHAM and 5µM Antimycin A for at least 15 minutes before performing the measurements. Note that to provide efficient inhibition of $\Delta\Psi_d$ BKA has to be employed at acid pH (pH 5). The potential negative effects of the non-physiological pH were investigated and resulted negligible in the dark. The $\Delta\Psi_d$ in the control sample was set to 100%; Data ± SD from 5 independent experiments for measurements with BKA, 3 replicates with CATR.

Figure 2.22 | Molecular and photosynthetic characterisation of *aac1* knock out mutant strain. A, After CRISPR-Cas9 mutagenesis and biolistic transformation, gene sequencing revealed a 2 bp deletion in one colony, which was selected for further analysis. **B**, Measurement of growth rates (starting concentration: $0.5 \cdot 10^6$ cell ml^{-1}). **C**, Analysis of chlorophyll fluorescence parameters, ETR and NPQ (D). *P. tricornutum* cells at exponential growth phase were distributed on a 96-well plate at $20 \cdot 10^6$ cell ml^{-1} concentration in 150 µL volume and measurements were performed with a imaging system.

Figure 2.23 | Western blot analysis of AAC2 knock down (AS1 and AS2) and overexpressor (OE) mutant strains. Total cell extracts were blotted with a specific antibody. ATPb was used as a loading control.

Figure 2.24 | Electron Transfer Rate phenotype of AAC2 Antisense and Over Expression lines. Measurements were performed on *P. tricornutum* cells in exponential growth phase (between 1 and 3·10^6 cell ml^{-1}). After centrifugation (3500g, 5', 19 °C) cells were distributed on a 96-well plate at 20·10^6 cell ml^{-1} concentration in 150 µL volume. Data correspond to average + SD of 3 independent experiments, each comprising 3 technical replicates.

Figure 2.25 | ETR measurements of AAC2-AS and OE lines in presence of BKA. Measurements were performed on *P. tricornutum* cells in exponential growth phase (between 1 and 3·10^6 cell ml^{-1}). After centrifugation (3500g, 5', 19 °C) cells were distributed on a 96-well plate at 20·10^6 cell ml^{-1} concentration in 150 µL volume. Since BKA is effective only at acidic pH (pH 5). The potential negative effects of the non-physiological pH were also investigated. Data ± SE form 3 independent experiments.

Table 2.1 | List of selected transporters, putatively involved in the energetic crosstalk between the chloroplast and the mitochondrion in *Phaeodactylum tricornutum*. Gene names are indicated as reported in the Ensemble Protists Gene Browser (protists.ensembl.org). The first two genes have been selected from previous transcriptome analysis (light blue background), comparing algal gene expression profile in presence or absence of glycerol. Additional transporters (orange background) was chosen since it was considered to be a possible target of bongkrekic acid. Differential gene expression is reported as the logarithm of the ratio of the two growth conditions (+/- gly). The webtool ASAFind (Gruber et al., 2015) was used for subcellular localisation prediction in secondary endosymbionts; TMHMM for the number of transmembrane domain (Krogh et al., 2001). Online service I-TASSER provided a 3D model prediction (Roy et al., 2010) (https://zhanglab.ccmb.med.umich.edu/I-TASSER/).

Table 2.2 | Homologs proteins of the Phatr3_J46742 corresponding amino acid sequence (BLAST output). The first hits appear to be proteins belonging to other species of diatoms

(*Fistulifera solaris, Pseudo-nitzschia multistriata, Thalassiosira oceanica, Fragilariopsis cylindrus*), suggesting the possible specific physiological role of this protein in this group of organisms.

Table 2.3 | Homologs proteins of Phatr3_J46742 in *P. tricornutum*. The closest related proteins, encoded by Phatr3_J46612 and Phatr3_J42874 genes, were selected for further phylogenetic studies. The results of the ASAFind software indicates whether the gene product is likely to be targeted to the secondary plastid, which was predicted only in Phatr3_J46742.

Table 2.4 | Homologs proteins of the Phatr3_J15797 corresponding amino acid sequence. First hits BLAST output with E-value lower than 10^{-10} are listed. The presence of other AAC protein from different species suggest the AAC nature of the selected protein in *P. tricornutum*.

Table 2.5 | Homologs proteins of Phatr3_J15797 in *P. tricornutum*. First hits from BLAST output with E-value lower than 10^{-10} are listed. The best hit was selected for further physiological analysis.

Table 2.6 | Homologs proteins of the bovine AAC (PDB: 1OKC) in *P. tricornutum*. First five hits from BLAST output are listed. A total of 17 proteins with E-value lower than 10^{-10} were found. The best hit corresponds to the already selected AAC2 gene (Phatr3_J22873), making it a the best candidate to be the target for the BKA in *P. tricornutum*.

Table 2.7 | Homologs proteins of AAC2 (Phatr3_J22873). First five hits from BLAST output appear to belong to other ADP/ATP transporter present in other species of diatoms.

Table 2.8 | Homologs proteins of the Phatr3_J35626 corresponding amino acid sequence. First six hits BLAST output are listed.

Table 2.9 | Homologs proteins of Phatr3_J35625 (DTC) in *P. tricornutum*. The closest related protein shares only 44% of coverage and 27% of homology, possibly making the DTC protein a unique transporter for its substrate.

Chapter 3

Figure 3.1 | Schematic representation of Gibson Assembly steps. The simultaneous presence of the exonuclease, the DNA polymerase and the DNA ligase allows the fusion of multiple fragment of DNA.

Figure 3.2 | pET-28a(+) presenting a sequence coding for an His-Tag either at the C-terminal or at the N-terminal of the insert. Unique restriction sites are reported and the black arrow indicates the Multicloning site. The plasmid presents a gene conferring the resistance to the antibiotic kanamycin to transformed cells. The T7 terminator can be used for sequencing.

Figure 3.3 | Schematic representation of design and synthesis of the adapter. After selecting the target sequences from the output of PhytoCRISP-Ex web tool, primers for the creation of the adapter were designed by removing the NGG terminal part and by adding TCGA or AAAC overhangs in the CRISPR/Cas9 target sequence. Adapters were synthetized by annealing the two designed primers.

Figure 3.4 | Map of the pKSdiaCas9_sgRNA plasmid. The plasmid allows the expression of a *P. tricornutum* codon-optimized Cas9 protein and the sgRNA containing the CRISPR/Cas9 target sequence between the two BsaI restriction sites. In bacteria, this plasmid confers ampicillin resistance (AmpR).

Figure 3.5 | Sequencing chromatograms obtained by sequencing the CRISPR/Cas9 target region, previously amplified by PCR. Red dashed squares in the nucleotides sequence highlight differences in the DNA sequences in the mutant strains compared to the WT.

Figure 3.6 | Schematic representation of a MiMS setup (modified from Beckmann et al 2009). A, Diatoms are placed in an appropriate chamber and maintained in suspension by a magnetic stirrer. Gas molecules cross the selective Teflon membrane thanks to the activity of a vacuum pump and undergo the ionization process. The trajectory of the newly produced ions are modified under the influence of an external magnetic field according to their charge densities and selectively hit the detector. **B**, Schematic representation of uptake and production of CO_2 and O_2 by the chloroplast and the mitochondrion.

Figure 3.7 | Electrochromic Shift of photosynthetic membrane embedded pigments. In the dark, carotenoids display a characteristic absorption spectrum (red). In presence of light, the import of protons in the thylakoid's lumen (ΔpH, blue arrows) and the electron transfer chain ($\Delta\Psi$, yellow line) establishes an electric field across the membranes. The latter component is responsible for the shift of the carotenoids' absorption spectrum (green) toward longer wavelengths. The ECS spectrum is finally obtained by subtracting the spectrum in the dark from the one in the dark.

Figure 3.8 | ECS spectrum of *Arabidopsis thaliana* (A) and Phaeodactylum tricornutum (B). The spectrum of Arabidopsis present a main peak at 520 nm, corresponding to the linear component of the ECS, whilst in *P. tricornutum* it also shows a peak (the quadratic component) at 565 nm.

Figure 3.9 | Kinetic measurements are performed with a Joliot Type Spectrophotometer.
During ECS kinetics measurements, the absorbance of a measuring non actinic light is recorded. Different wavelengths of the measuring light are selected through a specific bandpass

interference filter (green ellipse, green dotted vertical line in the graph). Before reaching the sample, the light is split through a semi-dichroic filter into two perpendicular beams, one toward a reference detector and the other toward sample. Before the measurement, the zero is set by adjusting the reference signal by opening or closing a shutter, in order to match the absorbance in the dark signal reaching the detector (black dashed horizontal line in the graph). The kinetics of the ECS signal is recorded in darkness and in presence of actinic red light (red arrows), provided by LEDs ring. To prevent the actinic light to be mistakenly recorded, specific high pass filters are placed before the detectors. An external light source (laser or xenon lamp) can also be used for specific analysis. The ECS spectrum (blue line in the graph) is obtained by using different filters for the measuring light and by recording the ECS signal after a saturating light pulse (graph on the up-right).

Table 3.1 | ESAW 10NP components and their concentration in the final medium. Salts solutions were made as 10x stock solutions; vitamins, trace metal and Fe EDTA at 1000x, nitrate and phosphate as 100x stock solutions. Individual stock solutions were sterilised either by autoclave treatment or through 2 μm filters under flow hood before use.

Table 3.2 | List of components of for the Gibson Assembly reaction and their concentrations in the final mix.

Table 3.3 | List of oligonucleotides used for synthesis of CRISPR-Cas9 adaptors. Underlined nucleotides represent the overlapping sequences with pKSdiaCas9_sgRNA plasmid when linearized with BsaI and nucleotides NGG were removed from the output sequence from the PhytoCRISP-Ex software.

Table 3.4 | List of primers used for PCR for each targeted gene. The PCR product corresponds to the DNA region where the mutation is present after CRISPR-Cas9 mutagenesis.

The amplified DNA is sent for sequencing to a private company for molecular characterisation and mutant strains selection.

Table 3.5 | Composition of different buffers used for protein solubilisation in urea.

A sodium dodecyl sulfate-polyacrylamide gel electrophoresis (SDS-PAGE) was performed to verify the presence of the protein of interest in the different samples obtained during the described protocol.

Table 3.6 | Composition of buffers used for His-tagged proteins purification.

4.8 References

Abida, H., Dolch, L.-J., Meï, C., Villanova, V., Conte, M., Block, M. A., … Maréchal, E. (2015). Membrane glycerolipid remodeling triggered by nitrogen and phosphorus starvation in Phaeodactylum tricornutum. *Plant Physiology*, *167*(1), 118–136. https://doi.org/10.1104/pp.114.252395

Alboresi, A., Storti, M., & Morosinotto, T. (2019). Balancing protection and efficiency in the regulation of photosynthetic electron transport across plant evolution. *New Phytologist*, *221*(1), 105–109. https://doi.org/10.1111/nph.15372

Allahverdiyeva, Y., Isojärvi, J., Zhang, P., & Aro, E.-M. (2015). Cyanobacterial Oxygenic Photosynthesis is Protected by Flavodiiron Proteins. *Life (Basel, Switzerland)*, *5*(1), 716–743. https://doi.org/10.3390/life5010716

Allahverdiyeva, Y., Suorsa, M., Tikkanen, M., & Aro, E.-M. (2014). Photoprotection of photosystems in fluctuating light intensities. *Journal of Experimental Botany*, *66*(9), 2427–2436. https://doi.org/10.1093/jxb/eru463

Allen, A. E., Dupont, C. L., Oborník, M., Horák, A., Nunes-Nesi, A., McCrow, J. P., … Bowler, C. (2011). Evolution and metabolic significance of the urea cycle in photosynthetic diatoms. *Nature*, *473*(7346), 203–207. https://doi.org/10.1038/nature10074

Allen, A. E., Laroche, J., Maheswari, U., Lommer, M., Schauer, N., Lopez, P. J., … Bowler, C. (2008). Whole-cell response of the pennate diatom Phaeodactylum tricornutum to iron starvation. *Proceedings of the National Academy of Sciences of the United States of America*, *105*(30), 10438–10443. https://doi.org/10.1073/pnas.0711370105

Allen, J. F. (1975). Oxygen reduction and optimum production of ATP in photosynthesis. *Science*, *256*, 599–600.

Allen, J. F. (2002). Photosynthesis of ATP-Electrons, Proton Pumps, Rotors, and Poise. *Cell*, *110*(3), 273–276. https://doi.org/10.1016/S0092-8674(02)00870-X

Allorent, G., Guglielmino, E., Giustini, C., & Courtois, F. (2018). Generation of Mutants of Nuclear-Encoded Plastid Proteins Using CRISPR/Cas9 in the Diatom Phaeodactylum tricornutum BT - Plastids: Methods and Protocols. In E. Maréchal (Ed.) (pp. 367–378). New York, NY: Springer US. https://doi.org/10.1007/978-1-4939-8654-5_24

Allorent, G., Osorio, S., Ly Vu, J., Falconet, D., Jouhet, J., Kuntz, M., … Finazzi, G. (2015). Adjustments of embryonic photosynthetic activity modulate seed fitness in Arabidopsis thaliana. *New Phytologist*, *205*(2), 707–719. https://doi.org/10.1111/nph.13044

Alric, J. (2010). Cyclic electron flow around photosystem I in unicellular green algae, 47–56. https://doi.org/10.1007/s11120-010-9566-4

Altschul, S. F., Gish, W., Miller, W., Myers, E. W., & Lipman, D. J. (1990). Basic local alignment search tool. *Journal of Molecular Biology*, *215*(3), 403–410. https://doi.org/https://doi.org/10.1016/S0022-2836(05)80360-2

Annunziata, R., Ritter, A., Fortunato, A. E., Cheminant-Navarro, S., Agier, N., Huysman, M. J. J., … Falciatore, A. (2018). A bHLH-PAS protein regulates light-dependent diurnal rhythmic processes in the marine diatom Phaeodactylum tricornutum. *BioRxiv*, 271445. https://doi.org/10.1101/271445

Apt, K. E., Grossman, A. R., & Kroth-Pancic, P. G. (1996). Stable nuclear transformation of the diatom Phaeodactylum tricornutum. *Molecular and General Genetics MGG*, *252*(5), 572–579. https://doi.org/10.1007/BF02172403

Archibald, J. M. (2009). The Puzzle of Plastid Evolution. *Current Biology*, *19*(2), R81–R88. https://doi.org/https://doi.org/10.1016/j.cub.2008.11.067

Asada, K. (2000). The water-water cycle as alternative photon and electron sinks. *Philosophical Transactions of the Royal Society of London. Series B, Biological Sciences*, *355*(1402), 1419–1431. https://doi.org/10.1098/rstb.2000.0703

Asada, K., Takahashi, M., & Nagate, M. (1974). Assay and Inhibitors of Spinach Superoxide Dismutase. *Agricultural and Biological Chemistry*, *38*(2), 471–473. https://doi.org/10.1080/00021369.1974.10861178

Badger, M. R., von Caemmerer, S., Ruuska, S., & Nakano, H. (2000). Electron flow to oxygen in higher plants and algae: rates and control of direct photoreduction (Mehler reaction) and rubisco oxygenase. *Philosophical Transactions of the Royal Society of London. Series B, Biological Sciences*, *355*(1402), 1433–1446. https://doi.org/10.1098/rstb.2000.0704

Bailleul, B., Berne, N., Murik, O., Petroutsos, D., Prihoda, J., Tanaka, A., … Finazzi, G. (2015). Energetic coupling between plastids and mitochondria drives CO2 assimilation in diatoms. *Nature*, *524*(7565), 366–369. https://doi.org/10.1038/nature14599

Bailleul, B., Cardol, P., Breyton, C., & Finazzi, G. (2010). Electrochromism: a useful probe to study algal photosynthesis. *Photosynthesis Research*, *106*(1), 179. https://doi.org/10.1007/s11120-010-9579-z

Bamber, L., Harding, M., Monne, M., Slotboom, D., & Kunji, E. R. S. (2007). The yeast mitochondrial ADP/ATP carrier functions as a monomer in mitochondrial membranes.

Bar-Even, A., Noor, E., Savir, Y., Liebermeister, W., Davidi, D., Tawfik, D. S., & Milo, R. (2011). The moderately efficient enzyme: Evolutionary and physicochemical trends shaping enzyme parameters. *Biochemistry*, *50*(21), 4402–4410. https://doi.org/10.1021/bi2002289

Baurain, D., Brinkmann, H., Petersen, J., Rodriguez-Ezpeleta, N., Stechmann, a., Demoulin, V., … Philippe, H. (2010). Phylogenomic Evidence for Separate Acquisition of Plastids in Cryptophytes, Haptophytes, and Stramenopiles. *Molecular Biology and Evolution*, *27*(7), 1698–1709. https://doi.org/10.1093/molbev/msq059

Beckmann, K., Messinger, J., Badger, M. R., Wydrzynski, T., & Hillier, W. (2009). On-line mass spectrometry: membrane inlet sampling. *Photosynthesis Research*, *102*(2–3), 511–522. https://doi.org/10.1007/s11120-009-9474-7

Benz, R., Kottke, M., & Brdiczka, D. (1990). The cationically selective state of the mitochondrial outer membrane pore: a study with intact mitochondria and reconstituted mitochondrial porin. *Biochimica et Biophysica Acta (BBA) - Biomembranes*, *1022*(3), 311–318. https://doi.org/https://doi.org/10.1016/0005-2736(90)90279-W

Berges, J. A., Franklin, D. J., & Harrison, P. J. (2001). Evolution of an artificial seawater medium: improvements in enriched seawater, artificial water over the last two decades. *Journal of Phycology*, *37*(6), 1138–1145. https://doi.org/10.1046/j.1529-8817.2001.01052.x

Blachly-Dyson, E., & Forte, M. (2001). VDAC Channels. *IUBMB Life*, *52*(3-5), 113–118. https://doi.org/10.1080/15216540152845902

Borowitzka, M. A., & Volcani, B. E. (1978). The polymorphic diatom Phaeodactylum tricornutum: Ultrastructure of its morphotypes. *Journal of Phycology*, *14*(1), 10–21. https://doi.org/10.1111/j.1529-8817.1978.tb00625.x

Bowler, C., Allen, A. E., Badger, J. H., Grimwood, J., Jabbari, K., Kuo, A., … Grigoriev, I. V. (2008). The Phaeodactylum genome reveals the evolutionary history of diatom genomes. *Nature*, *456*(7219), 239–244. https://doi.org/10.1038/nature07410

Broddrick, J. T., Du, N., Smith, S. R., Tsuji, Y., Jallet, D., Ware, M. A., … Allen, A. E. (2019). Cross-compartment metabolic coupling enables flexible photoprotective mechanisms in the diatom Phaeodactylum tricornutum, 1364–1379. https://doi.org/10.1111/nph.15685

Burey, S. C., Poroyko, V., Ergen, Z. N., Fathi-Nejad, S., Schüller, C., Ohnishi, N., … Löffelhardt, W. (2007). Acclimation to low [CO2] by an inorganic carbon-concentrating mechanism in Cyanophora paradoxa. *Plant, Cell & Environment*, *30*(11), 1422–1435. https://doi.org/10.1111/j.1365-3040.2007.01715.x

Burnap, R., Hagemann, M., & Kaplan, A. (2015). Regulation of CO2 Concentrating Mechanism in Cyanobacteria. *Life*, *5*, 348–371. https://doi.org/10.3390/life5010348

Busch, F. (2012). Current methods for estimating the rate of photorespiration in leaves. *Plant Biology (Stuttgart, Germany)*, *15*. https://doi.org/10.1111/j.1438-8677.2012.00694.x

Busch, F. A., Sage, T. L., Cousins, A. B., & Sage, R. F. (2013). C3 plants enhance rates of photosynthesis by reassimilating photorespired and respired CO 2, 200–212. https://doi.org/10.1111/j.1365-3040.2012.02567.x

Capella-Gutiérrez, S., Silla-Martínez, J. M., & Gabaldón, T. (2009). trimAl: a tool for automated alignment trimming in large-scale phylogenetic analyses. *Bioinformatics (Oxford, England)*, *25*(15), 1972–1973. https://doi.org/10.1093/bioinformatics/btp348

Cardol, P., Alric, J., Girard-Bascou, J., Franck, F., Wollman, F.-A., & Finazzi, G. (2009). Impaired respiration discloses the physiological significance of state transitions in Chlamydomonas. *Proceedings of the National Academy of Sciences of the United States of America*, *106*(37), 15979–15984. https://doi.org/10.1073/pnas.0908111106

Cardol, P., Bailleul, B., Rappaport, F., Derelle, E., Béal, D., Breyton, C., … Finazzi, G. (2008). An original adaptation of photosynthesis in the marine green alga Ostreococcus. *Proceedings of the National Academy of Sciences of the United States of America*, *105*(22), 7881–7886. https://doi.org/10.1073/pnas.0802762105

Cavalier-Smith, T. (2003). Genomic reduction and evolution of novel genetic membranes and protein-targeting machinery in eukaryote-eukaryote chimaeras (meta-algae). *Philosophical Transactions of the Royal Society of London. Series B, Biological Sciences*, *358*(1429), 109–134. https://doi.org/10.1098/rstb.2002.1194

Chaux, F., Burlacot, A., Mekhalfi, M., Auroy, P., Blangy, S., Richaud, P., & Peltier, G. (2017). Flavodiiron Proteins Promote Fast and Transient O2 Photoreduction in Chlamydomonas. *Plant Physiology*, *174*(3), 1825 LP – 1836. https://doi.org/10.1104/pp.17.00421

Chisti, Y. (2007). Biodiesel from microalgae. *Biotechnology Advances*, *25*(3), 294–306. https://doi.org/https://doi.org/10.1016/j.biotechadv.2007.02.001

Curien, G., Flori, S., Villanova, V., Magneschi, L., Giustini, C., Forti, G., … Finazzi, G. (2016). The water to water cycles in microalgae. *Plant & Cell Physiology*, *57*(March), 1–39. https://doi.org/10.1093/pcp/pcw048

Curien, G., Flori, S., Villanova, V., Magneschi, L., Matringe, M., Forti, G., … Finazzi, G. (2016). The Water to Water Cycles in Microalgae Special Focus Issue – Invited Review, *57*(March), 1354–1363. https://doi.org/10.1093/pcp/pcw048

Daboussi, F., Leduc, S., Maréchal, A., Dubois, G., Guyot, V., Perez-Michaut, C., … Duchateau, P. (2014). Genome engineering empowers the diatom Phaeodactylum tricornutum for biotechnology. *Nature Communications*, *5*, 3831.

Dal Corso, G., Pesaresi, P., Masiero, S., Aseeva, E., Schu, D., Finazzi, G., … Leister, D. (2008). A Complex Containing PGRL1 and PGR5 Is Involved in the Switch between Linear and Cyclic Electron Flow in Arabidopsis, 273–285. https://doi.org/10.1016/j.cell.2007.12.028

Davis, M. C., Fiehn, O., & Durnford, D. G. (2013). Metabolic acclimation to excess light intensity in Chlamydomonas reinhardtii, 1391–1405. https://doi.org/10.1111/pce.12071

de Bruijn, J., Frost, D. J., Nugteren, D. H., Gaudemer, A., Lijmbach, G. W. M., Cox, H. C., & Berends, W. (1973). The structure of bongkrekic acid. *Tetrahedron*, *29*(11), 1541–1547. https://doi.org/https://doi.org/10.1016/S0040-4020(01)83395-0

De Martino, A., Bartual, A., Willis, A., Meichenin, A., Villazán, B., Maheswari, U., & Bowler, C. (2011). Physiological and Molecular Evidence that Environmental Changes Elicit Morphological Interconversion in the Model Diatom Phaeodactylum tricornutum. *Protist*, *162*(3), 462–481. https://doi.org/https://doi.org/10.1016/j.protis.2011.02.002

De Martino, A., Meichenin, A., Shi, J., Pan, K., & Bowler, C. (2007). De Martino A, Meichenin A, Shi J, Pan KH, Bowler C.. Genetic and phenotypic characterization of Phaeodactylum tricornutum (Bacillariophyceae) accessions. J Phycol 43: 992-1009. *Journal of Phycology*, *43*, 992–1009. https://doi.org/10.1111/j.1529-8817.2007.00384.x

Decelle, J., Romac, S., Stern, R. F., Bendif, E. M., Zingone, A., Audic, S., … Christen, R. (2015). PhytoREF: a reference database of the plastidial 16S rRNA gene of photosynthetic eukaryotes with curated taxonomy. *Molecular Ecology Resources*, *15*(6), 1435–1445. https://doi.org/10.1111/1755-0998.12401

Dorrell, R. G., Azuma, T., Nomura, M., Audren de Kerdrel, G., Paoli, L., Yang, S., … Kamikawa, R. (2019). Principles of plastid reductive evolution illuminated by nonphotosynthetic chrysophytes. *Proceedings of the National Academy of Sciences*, *116*(14), 6914 LP – 6923. https://doi.org/10.1073/pnas.1819976116

Dorrell, R. G., Nisbet, R. E. R., Barbrook, A. C., Rowden, S. J. L., & Howe, C. J. (2019). Integrated Genomic and Transcriptomic Analysis of the Peridinin Dinoflagellate Amphidinium carterae Plastid. *Protist*, *170*(4), 358–373. https://doi.org/https://doi.org/10.1016/j.protis.2019.06.001

Duy, D., Jürgen, S., & Katrin, P. (2007). Solute channels of the outer membrane: from bacteria to chloroplasts. *Biological Chemistry*. https://doi.org/10.1515/BC.2007.120

Dyrløv Bendtsen, J., Nielsen, H., von Heijne, G., & Brunak, S. (2004). Improved Prediction of Signal Peptides: SignalP 3.0. *Journal of Molecular Biology*, *340*(4), 783–795. https://doi.org/https://doi.org/10.1016/j.jmb.2004.05.028

Eberhard, S., Finazzi, G., & Wollman, F.-A. (2008). The Dynamics of Photosynthesis. *Annual Review of Genetics*, *42*(1), 463–515. https://doi.org/10.1146/annurev.genet.42.110807.091452

Edgar, R. C. (2004). MUSCLE: multiple sequence alignment with high accuracy and high throughput. *Nucleic Acids Research*, *32*(5), 1792–1797. https://doi.org/10.1093/nar/gkh340

Ellis, R. J. (2009). Tackling unintelligent design R. *Geophysical Research Letters*, *36*(1). https://doi.org/10.1029/2008GL036500

Embley, T. M., & Martin, W. (2006). Eukaryotic evolution, changes and challenges. *Nature*, *440*(7084), 623–630. https://doi.org/10.1038/nature04546

Falciatore, A., Casotti, R., Leblanc, C., Abrescia, C., & Bowler, C. (1999). Transformation of Nonselectable Reporter Genes in Marine Diatoms. *Marine Biotechnology*, *1*(3), 239–251. https://doi.org/10.1007/PL00011773

Feilke, K., Streb, P., & Cornic, G. (2016). Effect of Chlamydomonas plastid terminal oxidase 1 expressed in tobacco on photosynthetic electron transfer, 219–228. https://doi.org/10.1111/tpj.13101

Feller, U., Anders, I., & Mae, T. (2007). Rubiscolytics: fate of Rubisco after its enzymatic function in a cell is terminated. *Journal of Experimental Botany*, *59*(7), 1615–1624. https://doi.org/10.1093/jxb/erm242

Field, C. B., Behrenfeld, M. J., Randerson, J. T., & Falkowski, P. (1998). Primary Production of the Biosphere: Integrating Terrestrial and Oceanic Components. *Biogeosciences*, *8*(6), 1477–1486. https://doi.org/10.5194/bg-8-1477-2011

Finazzi, G. (2005). The central role of the green alga Chlamydomonas reinhardtii in revealing the mechanism of state transitions. *Journal of Experimental Botany*, *56*(411), 383–388. https://doi.org/10.1093/jxb/erh230

Finazzi, G., Furia, A., Barbagallo, R. P., & Forti, G. (1999). State transitions, cyclic and linear electron transport and photophosphorylation in Chlamydomonas reinhardtii. *Biochimica et Biophysica Acta (BBA) - Bioenergetics*, *1413*(3), 117–129. https://doi.org/https://doi.org/10.1016/S0005-2728(99)00089-4

Flori, S., Jouneau, P., Bailleul, B., Gallet, B., Estrozi, L. F., Moriscot, C., … Zeeman, S. (2017). Plastid thylakoid architecture optimizes photosynthesis in diatoms. *Nature Communications*, *8*(May), 15885. https://doi.org/10.1038/ncomms15885

Flori, S., Jouneau, P. H., Finazzi, G., Maréchal, E., & Falconet, D. (2016). Ultrastructure of the Periplastidial Compartment of the Diatom Phaeodactylum tricornutum. *Protist*, *167*(3), 254–267. https://doi.org/10.1016/j.protis.2016.04.001

Forti, G., & Ehrenheim, A. M. (1993). The role of ascorbic acid in photosynthetic electron transport. *Biochimica et Biophysica Acta (BBA) - Bioenergetics*, *1183*(2), 408–412. https://doi.org/https://doi.org/10.1016/0005-2728(93)90246-C

Fu, A., Liu, H., Yu, F., Kambakam, S., Luan, S., & Rodermel, S. (2012). Alternative oxidases (AOX1a and AOX2) can functionally substitute for plastid terminal oxidase in Arabidopsis chloroplasts. *The Plant Cell*, *24*(4), 1579–1595. https://doi.org/10.1105/tpc.112.096701

Fukasawa, Y., Tsuji, J., Fu, S.-C., Tomii, K., Horton, P., & Imai, K. (2015). MitoFates: improved prediction of mitochondrial targeting sequences and their cleavage sites. *Molecular & Cellular Proteomics : MCP*, *14*(4), 1113–1126. https://doi.org/10.1074/mcp.M114.043083

Gemmecker, S., Schaub, P., Koschmieder, J., Brausemann, A., Drepper, F., Rodriguez-Franco, M., … Beyer, P. (2015). Phytoene Desaturase from Oryza sativa: Oligomeric Assembly, Membrane Association and Preliminary 3D-Analysis. *PloS One*, *10*(7), e0131717–e0131717. https://doi.org/10.1371/journal.pone.0131717

Gerotto, C., Alboresi, A., Meneghesso, A., Jokel, M., Suorsa, M., Aro, E.-M., & Morosinotto, T. (2016). Flavodiiron proteins act as safety valve for electrons in Physcomitrella patens. *Proceedings of the National Academy of Sciences*, *113*(43), 12322 LP – 12327. https://doi.org/10.1073/pnas.1606685113

Gibson, D. G., Young, L., Chuang, R.-Y., Venter, J. C., Hutchison III, C. A., & Smith, H. O. (2009). Enzymatic assembly of DNA molecules up to several hundred kilobases. *Nature Methods*, *6*, 343.

Goss, R., Latowski, D., Grzyb, J., Vieler, A., Lohr, M., Wilhelm, C., & Strzalka, K. (2007). Lipid dependence of diadinoxanthin solubilization and de-epoxidation in artificial membrane systems resembling the lipid composition of the natural thylakoid membrane. *Biochimica et Biophysica Acta (BBA) - Biomembranes*, *1768*(1), 67–75. https://doi.org/https://doi.org/10.1016/j.bbamem.2006.06.006

Gould, S. B., Sommer, M. S., Kroth, P. G., Gile, G. H., Keeling, P. J., & Maier, U.-G. (2006). Nucleus-to-Nucleus Gene Transfer and Protein Retargeting into a Remnant Cytoplasm of Cryptophytes and Diatoms. *Molecular Biology and Evolution*, *23*(12), 2413–2422. https://doi.org/10.1093/molbev/msl113

Gould, S. B., Waller, R. F., & McFadden, G. I. (2008). Plastid Evolution. *Annual Review of Plant Biology*, *59*(1), 491–517. https://doi.org/10.1146/annurev.arplant.59.032607.092915

Grosche, C., Hempel, F., Bolte, K., Zauner, S., & Maier, U. G. (2014). The periplastidal compartment: a naturally minimized eukaryotic cytoplasm. *Current Opinion in Microbiology*, *22*, 88–93. https://doi.org/https://doi.org/10.1016/j.mib.2014.09.017

Grouneva, I., Rokka, A., & Aro, E.-M. (2011). The Thylakoid Membrane Proteome of Two Marine Diatoms Outlines Both Diatom-Specific and Species-Specific Features of the Photosynthetic Machinery. *Journal of Proteome Research*, *10*(12), 5338–5353. https://doi.org/10.1021/pr200600f

Gruber, A., Rocap, G., Kroth, P. G., Armbrust, E. V., & Mock, T. (2015). Plastid proteome prediction for diatoms and other algae with secondary plastids of the red lineage, 519–528. https://doi.org/10.1111/tpj.12734

Gruber, A., Vugrinec, S., Hempel, F., Gould, S. B., Maier, U.-G., & Kroth, P. G. (2007). Protein targeting into complex diatom plastids: functional characterisation of a specific targeting motif. *Plant Molecular Biology*, *64*(5), 519–530. https://doi.org/10.1007/s11103-007-9171-x

Gschloessl, B., Guermeur, Y., & Cock, J. M. (2008). HECTAR: a method to predict subcellular targeting in heterokonts. *BMC Bioinformatics*, *9*, 393. https://doi.org/10.1186/1471-2105-

Haferkamp, I. (2007). The diverse members of the mitochondrial carrier family in plants. *FEBS Letters*, *581*(12), 2375–2379. https://doi.org/10.1016/j.febslet.2007.02.020

Harrison, P. J., Waters, R. E., & Taylor, F. J. R. (1980). A broad spectrum artificial sea water medium for coastal and open ocean phytoplankton. *Journal of Phycology*, *16*(1), 28–35. https://doi.org/10.1111/j.0022-3646.1980.00028.x

Henderson, P., & Lardy, H. (1970). Bongkrekic acid. An inhibitor of the adenine nucleotide translocase of mitochondria. *The Journal of Biological Chemistry*, *245*, 1319–1326.

Huang, W., Yang, Y.-J., Zhang, S.-B., & Liu, T. (2018). Cyclic Electron Flow around Photosystem I Promotes ATP Synthesis Possibly Helping the Rapid Repair of Photodamaged Photosystem II at Low Light. *Frontiers in Plant Science*, *9*. https://doi.org/10.3389/fpls.2018.00239

Huesgen, P. F., Alami, M., Lange, P. F., Foster, L. J., Schröder, W. P., Overall, C. M., & Green, B. R. (2013). Proteomic amino-termini profiling reveals targeting information for protein import into complex plastids. *PloS One*, *8*(9), e74483–e74483. https://doi.org/10.1371/journal.pone.0074483

Inoue, K. (2011). Emerging roles of the chloroplast outer envelope membrane. *Trends in Plant Science*, *16*(10), 550–557. https://doi.org/10.1016/j.tplants.2011.06.005

Iwai, M., Takizawa, K., Tokutsu, R., Okamuro, A., Takahashi, Y., & Minagawa, J. (2010). Isolation of the elusive supercomplex that drives cyclic electron flow in photosynthesis. *Nature*, *464*(7292), 1210–1213. https://doi.org/10.1038/nature08885

Jans, F., Mignolet, E., Houyoux, P., Cardol, P., Ghysels, B., Cournac, L., … Franck, F. (2008). A type II NAD (P) H dehydrogenase mediates light-independent plastoquinone reduction in the chloroplast of Chlamydomonas. *Proceedings of the National Academy of Sciences USA*, *105*(51).

Jarvis, P., Dörmann, P., Peto, C. A., Lutes, J., Benning, C., & Chory, J. (2000). Galactolipid deficiency and abnormal chloroplast development in the Arabidopsis MGD synthase 1 mutant. *Proceedings of the National Academy of Sciences of the United States of America*, *97*(14), 8175–8179. https://doi.org/10.1073/pnas.100132197

Jinek, M., Chylinski, K., Fonfara, I., Hauer, M., Doudna, J. A., & Charpentier, E. (2012). A programmable dual-RNA-guided DNA endonuclease in adaptive bacterial immunity. *Science (New York, N.Y.)*, *337*(6096), 816–821. https://doi.org/10.1126/science.1225829

Johnson, G. N. (2005). Cyclic electron transport in C3 plants: Fact or artefact? *Journal of Experimental Botany*, *56*(411), 407–416. https://doi.org/10.1093/jxb/eri106

Jokel, M., Peltier, G., Aro, E.-M., & Allahverdiyeva, Y. (2018). Hunting the main player enabling Chlamydomonas reinhardtii growth under fluctuating light. *The Plant Journal*, *94*. https://doi.org/10.1111/tpj.13897

Joliot, P., Béal, D., & Joliot, A. (2004). Cyclic electron flow under saturating excitation of dark-adapted Arabidopsis leaves. *Biochimica et Biophysica Acta*, *1656*, 166–176. https://doi.org/10.1016/j.bbabio.2004.03.010

Joliot, P., & Delosme, R. (1974). Flash-induced 519 nm absorption change in green algae. *Biochimica et Biophysica Acta (BBA) - Bioenergetics*, *357*(2), 267–284.

https://doi.org/https://doi.org/10.1016/0005-2728(74)90066-8

Joliot, P., & Joliot, A. (1989). Characterization of linear and quadratic electrochromic probes in Chlorella sorokiniana and Chlamydomonas reinhardtii. *Biochimica et Biophysica Acta (BBA) - Bioenergetics*, *975*(3), 355–360. https://doi.org/https://doi.org/10.1016/S0005-2728(89)80343-3

Joliot, P., & Joliot, A. (2002). Cyclic electron transfer in plant leaf. *Proceedings of the National Academy of Sciences of the United States of America*, *99*, 10209–10214. https://doi.org/10.1073/pnas.102306999

Karas, B. J., Diner, R. E., Lefebvre, S. C., Mcquaid, J., Phillips, A. P. R., Noddings, C. M., … Weyman, P. D. (2015). Designer diatom episomes delivered by bacterial conjugation. *Nature Communications*, *6*, 1–10. https://doi.org/10.1038/ncomms7925

Katoh, K., Rozewicki, J., & Yamada, K. D. (2017). MAFFT online service: multiple sequence alignment, interactive sequence choice and visualization. *Briefings in Bioinformatics*. https://doi.org/10.1093/bib/bbx108

Kearse, M., Moir, R., Wilson, A., Stones-Havas, S., Cheung, M., Sturrock, S., … Drummond, A. (2012). Geneious Basic: an integrated and extendable desktop software platform for the organization and analysis of sequence data. *Bioinformatics (Oxford, England)*, *28*(12), 1647–1649. https://doi.org/10.1093/bioinformatics/bts199

Keeling, P. J. (2010). The endosymbiotic origin, diversification and fate of plastids. *Philosophical Transactions of the Royal Society B: Biological Sciences*, *365*(1541), 729–748. https://doi.org/10.1098/rstb.2009.0103

Keeling, Patrick J. (2004). Diversity and evolutionary history of plastids and their hosts. *American Journal of Botany*, *91*(10), 1481–1493. https://doi.org/10.3732/ajb.91.10.1481

Keeling, Patrick J, Burki, F., Wilcox, H. M., Allam, B., Allen, E. E., Amaral-Zettler, L. A., … Worden, A. Z. (2014). The Marine Microbial Eukaryote Transcriptome Sequencing Project (MMETSP): illuminating the functional diversity of eukaryotic life in the oceans through transcriptome sequencing. *PLoS Biology*, *12*(6), e1001889–e1001889. https://doi.org/10.1371/journal.pbio.1001889

Kilian, O., & Kroth, P. (2005). Identification and characterization of a new conserved motif within the presence of proteins targeted into complex diatom plastids. *The Plant Journal : For Cell and Molecular Biology*, *41*, 175–183. https://doi.org/10.1111/j.1365-313X.2004.02294.x

Kinoshita, H., Nagasaki, J., Yoshikawa, N., Yamamoto, A., Takito, S., Kawasaki, M., … Taniguchi, M. (2011). The chloroplastic 2-oxoglutarate/malate transporter has dual function as the malate valve and in carbon/nitrogen metabolism. *The Plant Journal*, *65*(1), 15–26. https://doi.org/10.1111/j.1365-313X.2010.04397.x

Klingenberg, M. (2008). The ADP and ATP transport in mitochondria and its carrier. *Biochimica et Biophysica Acta*, *1778*, 1978–2021. https://doi.org/10.1016/j.bbamem.2008.04.011

Krogh, A., Larsson, B., von Heijne, G., & Sonnhammer, E. L. L. (2001). Predicting transmembrane protein topology with a hidden markov model: application to complete genomes11Edited by F. Cohen. *Journal of Molecular Biology*, *305*(3), 567–580. https://doi.org/https://doi.org/10.1006/jmbi.2000.4315

Kuntz, M. (2004). Plastid terminal oxidase and its biological significance. *Planta*, *218*, 896–899. https://doi.org/10.1007/s00425-004-1217-6

Larosa, V., Meneghesso, A., La Rocca, N., Steinbeck, J., Hippler, M., Szabo, I., & Morosinotto, T. (2017). Mitochondria Affect Photosynthetic Electron Transport and Photosensitivity in a Green Alga. *Plant Physiology*, *176*, pp.01249.2017. https://doi.org/10.1104/pp.17.01249

Lau, J. B., Stork, S., Moog, D., Schulz, J., & Maier, U. G. (2016). Protein-protein interactions indicate composition of a 480 kDa SELMA complex in the second outermost membrane of diatom complex plastids. *Molecular Microbiology*, *100*(1), 76—89. https://doi.org/10.1111/mmi.13302

Lavergne, J. (1989). Mitochondrial responses to intracellular pulses of photosynthetic oxygen. *Proceedings of the National Academy of Sciences*, *86*(November), 8768–8772.

Lemaire, C., Wollman, F. A., & Bennoun, P. (1988). Restoration of phototrophic growth in a mutant of Chlamydomonas reinhardtii in which the chloroplast atpB gene of the ATP synthase has a deletion: an example of mitochondria-dependent photosynthesis. *Proceedings of the National Academy of Sciences of the United States of America*, *85*(5), 1344–1348. https://doi.org/10.1073/pnas.85.5.1344

Lewin, J. C., Lewin, R. A., & Philpott, D. E. (1958). Observations on Phaeodactylum tricornutum. *Journal of General Microbiology*, *18*(2), 418–426. https://doi.org/10.1099/00221287-18-2-418

Li, L., Aro, E., & Millar, A. H. (2018). Mechanisms of Photodamage and Protein Turnover in Photoinhibition. *Trends in Plant Science*, *23*(8), 667–676. https://doi.org/10.1016/j.tplants.2018.05.004

Lim, L., & Mcfadden, G. (2010). The Evolution, Metabolism and Functions of the Apicoplast. *Philosophical Transactions of the Royal Society of London. Series B, Biological Sciences*, *365*, 749–763. https://doi.org/10.1098/rstb.2009.0273

Losh, J. L., Young, J. N., & Morel, F. M. M. (2013). Rubisco is a small fraction of total protein in marine phytoplankton. *New Phytologist*, *198*(1), 52–58. https://doi.org/10.1111/nph.12143

Ludwig, O., De Pinto, V., Palmieri, F., & Benz, R. (1986). Pore formation by the mitochondrial porin of rat brain in lipid bilayer membranes. *Biochimica et Biophysica Acta (BBA) - Biomembranes*, *860*(2), 268–276. https://doi.org/https://doi.org/10.1016/0005-2736(86)90523-7

Marchand, J., Heydarizadeh, P., Schoefs, B., & Spetea, C. (2018). Ion and metabolite transport in the chloroplast of algae : lessons from land plants. *Cellular and Molecular Life Sciences*, *75*(12), 2153–2176. https://doi.org/10.1007/s00018-018-2793-0

Maxwell, K., & Johnson, G. (2000). Chlorophyll fluorescence - a practical guide. *J Exp Bot*, *51*. https://doi.org/10.1093/jxb/51.345.659

McDonald, A., Ivanov, A., Bode, R., Maxwell, D., Rodermel, S., & Huner, N. (2010). Flexibility in photosynthetic electron transport: The physiological role of plastoquinol terminal oxidase (PTOX). *Biochimica et Biophysica Acta*, *1807*, 954–967. https://doi.org/10.1016/j.bbabio.2010.10.024

Mcfadden, G. (2014). Origin and Evolution of Plastids and Photosynthesis in Eukaryotes. *Cold*

Spring Harbor Perspectives in Biology, *6*. https://doi.org/10.1101/cshperspect.a016105

McMillin, J. B., & Dowhan, W. (2002). Cardiolipin and apoptosis. *Biochimica et Biophysica Acta (BBA) - Molecular and Cell Biology of Lipids*, *1585*(2), 97–107. https://doi.org/https://doi.org/10.1016/S1388-1981(02)00329-3

Mehler, A. H. (1951). Studies on reactions of illuminated chloroplasts: I. Mechanism of the reduction of oxygen and other hill reagents. *Archives of Biochemistry and Biophysics*, *33*(1), 65–77. https://doi.org/https://doi.org/10.1016/0003-9861(51)90082-3

Meneghesso, A., Simionato, D., Gerotto, C., La Rocca, N., Finazzi, G., & Morosinotto, T. (2016). Photoacclimation of photosynthesis in the Eustigmatophycean Nannochloropsis gaditana. *Photosynthesis Research*, *129*(3), 291–305. https://doi.org/10.1007/s11120-016-0297-z

Merchant, S. S., Prochnik, S. E., Vallon, O., Harris, E. H., Karpowicz, S. J., Witman, G. B., … Grossman, A. R. (2007). The Chlamydomonas Genome Reveals the Evolution of Key Animal and Plant Functions. *Science*, *318*(5848), 245 LP – 250. https://doi.org/10.1126/science.1143609

Miller, M. A., Schwartz, T., Pickett, B. E., He, S., Klem, E. B., Scheuermann, R. H., … O'Leary, M. A. (2015). A RESTful API for Access to Phylogenetic Tools via the CIPRES Science Gateway. *Evolutionary Bioinformatics Online*, *11*, 43–48. https://doi.org/10.4137/EBO.S21501

Miyake, C., & Asada, K. (1992). Thylakoid-Bound Ascorbate Peroxidase in Spinach Chloroplasts and Photoreduction of Its Primary Oxidation Product Monodehydroascorbate Radicals in Thylakoids. *Plant and Cell Physiology*, *33*(5), 541–553. https://doi.org/10.1093/oxfordjournals.pcp.a078288

Müller, D. J., Wu, N., & Palczewski, K. (2008). Vertebrate Membrane Proteins: Structure, Function, and Insights from Biophysical Approaches. *Pharmacological Reviews*, *60*(1), 43 LP – 78. https://doi.org/10.1124/pr.107.07111

Munekage, Y., Hashimoto, M., Miyake, C., Tomizawa, K.-I., Endo, T., Tasaka, M., & Shikanai, T. (2004). Cyclic electron flow around photosystem I is essential for photosynthesis. *Nature*, *429*(6991), 579–582. https://doi.org/10.1038/nature02598

Murik, O., Tirichine, L., Prihoda, J., Thomas, Y., Araújo, W. L., Allen, A. E., … Bowler, C. (2019). Downregulation of mitochondrial alternative oxidase affects chloroplast function, redox status and stress response in a marine diatom. *New Phytologist*, *221*(3), 1303–1316. https://doi.org/10.1111/nph.15479

Nakamura, Y., Kanakagiri, S., Van, K., He, W., & Spalding, M. H. (2005). Disruption of the glycolate dehydrogenase gene in the high-CO2-requiring mutant HCR89 of Chlamydomonas reinhardtii. *Canadian Journal of Botany*, *83*(7), 820–833. https://doi.org/10.1139/b05-067

Nakano, Y., & Asada, K. (1987). Purification of Ascorbate Peroxidase in Spinach Chloroplasts; Its Inactivation in Ascorbate-Depleted Medium and Reactivation by Monodehydroascorbate Radical. *Plant and Cell Physiology*, *28*(1), 131–140. https://doi.org/10.1093/oxfordjournals.pcp.a077268

Nandha, B., Finazzi, G., Joliot, P., Hald, S., & Johnson, G. (2007). The role of PGR5 in the redox poising of photosynthetic electron transport. *Biochimica et Biophysica Acta*, *1767*,

1252–1259. https://doi.org/10.1016/j.bbabio.2007.07.007

Nawrocki, W. J., Bailleul, B., Cardol, P., Rappaport, F., Wollman, F.-A., & Joliot, P. (2017). Cyclic electron flow in Chlamydomonas reinhardtii. *BioRxiv*, 153288. https://doi.org/10.1101/153288

Nawrocki, W. J., Tourasse, N. J., Taly, A., Rappaport, F., & Wollman, F.-A. (2015). The plastid terminal oxidase: its elusive function points to multiple contributions to plastid physiology. *Annu. Rev. Plant Biol. 66*, 49–74.

Nymark, M., Sharma, A. K., Sparstad, T., Bones, A. M., & Winge, P. (2016). A CRISPR/Cas9 system adapted for gene editing in marine algae. *Scientific Reports*, *6*, 24951. https://doi.org/10.1038/srep24951

Ort, D. R., & Baker, N. R. (2002). A photoprotective role for O2 as an alternative electron sink in photosynthesis? *Current Opinion in Plant Biology*, *5*(3), 193–198. https://doi.org/https://doi.org/10.1016/S1369-5266(02)00259-5

Palmieri, F. (2013). Molecular Aspects of Medicine The mitochondrial transporter family SLC25: Identification, properties and physiopathology. *Molecular Aspects of Medicine*, *34*(2–3), 465–484. https://doi.org/10.1016/j.mam.2012.05.005

Palmieri, F., Pierri, C. L., De Grassi, A., Nunes-Nesi, A., & Fernie, A. (2011). Evolution, structure and function of mitochondrial carriers: A review with new insights. *The Plant Journal : For Cell and Molecular Biology*, *66*, 161–181. https://doi.org/10.1111/j.1365-313X.2011.04516.x

Pebay-Peyroula, E., Dahout-Gonzalez, C., Kahn, R., Trézéguet, V., Lauquin, G. J.-M., & Brandolin, G. (2003). Structure of mitochondrial ADP/ATP carrier in complex with carboxyatractyloside. *Nature*, *426*(6962), 39–44. https://doi.org/10.1038/nature02056

Peltier, G., & Thibault, P. (1985). O2 uptake in the light in chlamydomonas: evidence for persistent mitochondrial respiration. *Plant Physiology*, *79*(1), 225–230. https://doi.org/10.1104/pp.79.1.225

Petersen, J., Förster, K., Turina, P., & Gräber, P. (2012). Comparison of the H+/ATP ratios of the H+-ATP synthases from yeast and from chloroplast. *Proceedings of the National Academy of Sciences of the United States of America*, *109*(28), 11150–11155. https://doi.org/10.1073/pnas.1202799109

Petersen, T. N., Brunak, S., von Heijne, G., & Nielsen, H. (2011, September). SignalP 4.0: discriminating signal peptides from transmembrane regions. *Nature Methods*. United States. https://doi.org/10.1038/nmeth.1701

Petroutsos, D., Amiar, S., Abida, H., Dolch, L.-J., Bastien, O., Rébeillé, F., … Maréchal, E. (2014). Evolution of galactoglycerolipid biosynthetic pathways – From cyanobacteria to primary plastids and from primary to secondary plastids. *Progress in Lipid Research*, *54*, 68–85. https://doi.org/https://doi.org/10.1016/j.plipres.2014.02.001

Prihoda, J., Tanaka, A., de Paula, W., Allen, J., Tirichine, L., & Bowler, C. (2012). Chloroplast-mitochondria cross-talk in diatoms. *Journal of Experimental Botany*, *63*, 1543–1557. https://doi.org/10.1093/jxb/err441

Radmer, R. J., & Kok, B. (1976). Photoreduction of O2 Primes and Replaces CO2 Assimilation. *Plant Physiology*, *58*(3), 336 LP – 340. https://doi.org/10.1104/pp.58.3.336

Rastogi, A., Maheswari, U., Dorrell, R. G., Vieira, F. R. J., Maumus, F., Kustka, A., … Tirichine, L. (2018). Integrative analysis of large scale transcriptome data draws a comprehensive landscape of Phaeodactylum tricornutum genome and evolutionary origin of diatoms. *Scientific Reports*, *8*(1), 4834. https://doi.org/10.1038/s41598-018-23106-x

Rastogi, A., Murik, O., Bowler, C., & Tirichine, L. (2016). PhytoCRISP-Ex: a web-based and stand-alone application to find specific target sequences for CRISPR/CAS editing. *BMC Bioinformatics*, *17*(1), 261. https://doi.org/10.1186/s12859-016-1143-1

Riazunnisa, K., Padmavathi, L., Bauwe, H., & Raghavendra, A. S. (2006). Markedly low requirement of added CO_2 for photosynthesis by mesophyll protoplasts of pea (Pisum sativum): possible roles of photorespiratory CO_2 and carbonic anhydrase. *Physiologia Plantarum*, *128*(4), 763–772. https://doi.org/10.1111/j.1399-3054.2006.00803.x

Río Bártulos, C., Rogers, M. B., Williams, T. A., Gentekaki, E., Brinkmann, H., Cerff, R., … van der Giezen, M. (2018). Mitochondrial Glycolysis in a Major Lineage of Eukaryotes. *Genome Biology and Evolution*, *10*(9), 2310–2325. https://doi.org/10.1093/gbe/evy164

Roberty, S., Bailleul, B., Berne, N., Franck, F., & Cardol, P. (2014). PSI Mehler reaction is the main alternative photosynthetic electron pathway in Symbiodinium sp., symbiotic dinoflagellates of cnidarians. *New Phytologist*, *204*, 81–91. https://doi.org/10.1111/nph.12903

Robinson, A. J., Overy, C., & Kunji, E. R. S. (2008). The mechanism of transport by mitochondrial carriers based on analysis of symmetry. *Proceedings of the National Academy of Sciences*, *105*(46), 17766 LP – 17771. https://doi.org/10.1073/pnas.0809580105

Ronquist, F., Teslenko, M., van der Mark, P., Ayres, D. L., Darling, A., Höhna, S., … Huelsenbeck, J. P. (2012). MrBayes 3.2: efficient Bayesian phylogenetic inference and model choice across a large model space. *Systematic Biology*, *61*(3), 539–542. https://doi.org/10.1093/sysbio/sys029

Roy, A., Kucukural, A., & Zhang, Y. (2010). I-TASSER: a unified platform for automated protein structure and function prediction. *Nature Protocols*, *5*(4), 725–738. https://doi.org/10.1038/nprot.2010.5

Ruprecht, J. J., Hellawell, A. M., Harding, M., Crichton, P. G., McCoy, A. J., & Kunji, E. R. S. (2014). Structures of yeast mitochondrial ADP/ATP carriers support a domain-based alternating-access transport mechanism. *Proceedings of the National Academy of Sciences*, *111*(4), E426 LP-E434. https://doi.org/10.1073/pnas.1320692111

Ruprecht, J. J., & Kunji, E. R. (2019). Structural changes in the transport cycle of the mitochondrial ADP/ATP carrier. *Current Opinion in Structural Biology*, *57*, 135–144. https://doi.org/10.1016/j.sbi.2019.03.029

Sander, J. D., & Joung, J. K. (2014). CRISPR-Cas systems for editing, regulating and targeting genomes. *Nature Biotechnology*, *32*(4), 347–355. https://doi.org/10.1038/nbt.2842

Satre, M., Mattei, S., Aubry, L., Gaudet, P., Pelosi, L., Brandolin, G., & Klein, G. (2007). Mitochondrial carrier family: Repertoire and peculiarities of the cellular slime mould Dictyostelium discoideum. *Biochimie*, *89*(9), 1058–1069. https://doi.org/https://doi.org/10.1016/j.biochi.2007.03.004

Schleiff, E., Eichacker, L. A., Eckart, K., Becker, T., Mirus, O., Stahl, T., & Soll, J. (2003).

Prediction of the plant β-barrel proteome: A case study of the chloroplast outer envelope. *Protein Science*, *12*(4), 748–759. https://doi.org/10.1110/ps.0237503

Secq, M.-P. O.-L., & Green, B. R. (2011). Complex repeat structures and novel features in the mitochondrial genomes of the diatoms Phaeodactylum tricornutum and Thalassiosira pseudonana. *Gene*, *476*(1), 20–26. https://doi.org/https://doi.org/10.1016/j.gene.2011.02.001

Shao, N., Beck, C. F., Lemaire, S. D., & Krieger-Liszkay, A. (2008). Photosynthetic electron flow affects H2O2 signaling by inactivation of catalase in Chlamydomonas reinhardtii. *Planta*, *228*(6), 1055–1066. https://doi.org/10.1007/s00425-008-0807-0

Shikanai, T. (2007). Cyclic electron transport around photosystem I: genetic approaches. *Annual Review of Plant Biology*, *Annu. Rev.*, 199–217. https://doi.org/10.1146/annurev.arplant.58.091406.110525

Shimakawa, G., Matsuda, Y., Nakajima, K., & Tamoi, M. (2017). Diverse strategies of O 2 usage for preventing photo-oxidative damage under CO 2 limitation during algal photosynthesis. *Nature Publishing Group*, (April 2016), 1–9. https://doi.org/10.1038/srep41022

Sonoike, K. (2011). Photoinhibition of photosystem I. *Physiologia Plantarum*, *142*(1), 56–64. https://doi.org/10.1111/j.1399-3054.2010.01437.x

Spalding, M. H. (2009). The CO2-Concentrating Mechanism and Carbon Assimilation. In *The Chlamydomonas Sourcebook (Second Edition)* (pp. 257–301). https://doi.org/https://doi.org/10.1016/B978-0-12-370873-1.00016-2.

Spreitzer, R. J., & Salvucci, M. E. (2002). RUBISCO: Structure, Regulatory Interactions, and Possibilities for a Better Enzyme. *Annual Review of Plant Biology*, *53*(1), 449–475. https://doi.org/10.1146/annurev.arplant.53.100301.135233

Stamatakis, A. (2014). RAxML version 8: a tool for phylogenetic analysis and post-analysis of large phylogenies. *Bioinformatics (Oxford, England)*, *30*(9), 1312–1313. https://doi.org/10.1093/bioinformatics/btu033

Storti, M., Alboresi, A., Gerotto, C., Aro, E.-M., Finazzi, G., & Morosinotto, T. (2019). Role of cyclic and pseudo-cyclic electron transport in response to dynamic light changes in Physcomitrella patens. *Plant, Cell & Environment*, *42*(5), 1590–1602. https://doi.org/10.1111/pce.13493

Sugiyama, T., Mizuno, M., & Hayashi, M. (1984). Partitioning of Nitrogen among Ribulose-1,5-bisphosphate Carboxylase/Oxygenase, Phosphoenolpyruvate Carboxylase, and Pyruvate Orthophosphate Dikinase as Related to Biomass Productivity in Maize Seedlings. *Plant Physiology*, *75*(3), 665–669. https://doi.org/10.1104/pp.75.3.665

Sunil, B., Talla, S. K., Aswani, V., & Raghavendra, A. S. (2013). Optimization of photosynthesis by multiple metabolic pathways involving interorganelle interactions: resource sharing and ROS maintenance as the bases. *Photosynthesis Research*, *117*(1), 61–71. https://doi.org/10.1007/s11120-013-9889-z

Tanaka, A., Martino, A. De, Amato, A., Montsant, A., Mathieu, B., Rostaing, P., … Bowler, C. (2015). Ultrastructure and Membrane Traffic During Cell Division in the Marine Pennate Diatom Phaeodactylum tricornutum. *Annals of Anatomy*, *166*(5), 506–521. https://doi.org/10.1016/j.protis.2015.07.005

Terashima, M., Petroutsos, D., Hüdig, M., Tolstygina, I., Trompelt, K., Gäbelein, P., … Hippler, M. (2012). Calcium-dependent regulation of cyclic photosynthetic electron transfer by a CAS, ANR1, and PGRL1 complex. *Proceedings of the National Academy of Sciences*, *109*(43), 17717 LP – 17722. https://doi.org/10.1073/pnas.1207118109

Tesson, B., Cedric, G., & Veronique, M.-J. (2009). Insights into the polymorphism of the diatom Phaeodactylum tricornutum Bohlin. *Botanica Marina*. https://doi.org/10.1515/BOT.2009.012

Trouillard, M., Shahbazi, M., Moyet, L., Rappaport, F., Joliot, P., Kuntz, M., & Finazzi, G. (2012). Kinetic properties and physiological role of the plastoquinone terminal oxidase (PTOX) in a vascular plant. *BBA - Bioenergetics*, *1817*(12), 2140–2148. https://doi.org/10.1016/j.bbabio.2012.08.006

Tyra, H. M., Linka, M., Weber, A. P. M., & Bhattacharya, D. (2007). Host origin of plastid solute transporters in the first photosynthetic eukaryotes. *Genome Biology*, *8*(10), R212–R212. https://doi.org/10.1186/gb-2007-8-10-r212

Vandenhecke, J. M., Bastedo, J., Cockshutt, A. M., Campbell, D. A., & Huot, Y. (2015). Changes in the Rubisco to photosystem ratio dominates photoacclimation across phytoplankton taxa. *Photosynthesis Research*, 275–291. https://doi.org/10.1007/s11120-015-0137-6

Vieler, A., Wilhelm, C., Goss, R., Süß, R., & Schiller, J. (2007). The lipid composition of the unicellular green alga Chlamydomonas reinhardtii and the diatom Cyclotella meneghiniana investigated by MALDI-TOF MS and TLC. *Chemistry and Physics of Lipids*, *150*(2), 143–155. https://doi.org/https://doi.org/10.1016/j.chemphyslip.2007.06.224

Vignais, P. V, Vignais, P. M., & Defaye, G. (1973). Adenosine diphosphate translocation in mitochondria. Nature of the receptor site for carboxyatractyloside (gummiferin). *Biochemistry*, *12*(8), 1508–1519. https://doi.org/10.1021/bi00732a007

Villanova, V., Fortunato, A. E., Singh, D., Bo, D. D., Conte, M., Obata, T., … Finazzi, G. (2017). Investigating mixotrophic metabolism in the model diatom Phaeodactylum tricornutum. *Philosophical Transactions of the Royal Society B: Biological Sciences*, *372*(1728), 20160404. https://doi.org/10.1098/rstb.2016.0404

Wang, Y., Stessman, D. J., & Spalding, M. H. (2015). The CO_2 concentrating mechanism and photosynthetic carbon assimilation in limiting CO_2: how Chlamydomonas works against the gradient. *The Plant Journal*, *82*(3), 429–448. https://doi.org/10.1111/tpj.12829

Weber, A., & Flügge, U. (2002). Interaction of cytosolic and plastidic nitrogen metabolism in plants. *Journal of Experimental Botany*, *53*(370), 865–874. https://doi.org/10.1093/jexbot/53.370.865

Weber, A., Linka, M., & Bhattacharya, D. (2006). Single, Ancient Origin of a Plastid Metabolite Translocator Family in Plantae from an Endomembrane-Derived Ancestor. *Eukaryotic Cell*, *5*, 609–612. https://doi.org/10.1128/EC.5.3.609-612.2006

Weber, A. P. M., & Fischer, K. (2007). Making the connections – The crucial role of metabolite transporters at the interface between chloroplast and cytosol. *FEBS Letters*, *581*(12), 2215–2222. https://doi.org/10.1016/j.febslet.2007.02.010

Weber, A. P. M., & Linka, N. (2011). Connecting the Plastid: Transporters of the Plastid

Envelope and Their Role in Linking Plastidial with Cytosolic Metabolism. *Annual Review of Plant Biology*, *62*(1), 53–77. https://doi.org/10.1146/annurev-arplant-042110-103903

Wingler, A., Lea, P. J., Quick, W. P., & Leegood, R. C. (2000). Photorespiration: metabolic pathways and their role in stress protection. *Phil. Trans. R. Soc. Lond. B*, *355*(1402). https://doi.org/doi.org/10.1098/rstb.2000.0712

Wishnick, M., & Lane, M. D. (1969). Inhibition of ribulose diphosphate carboxylase by cyanide. Inactive ternary complex of enzyme, ribulose diphosphate, and cyanide. *The Journal of Biological Chemistry*, *244*(1), 55–59.

Witt, H. T. (1979). Energy conversion in the functional membrane of photosynthesis. Analysis by light pulse and electric pulse methods: The central role of the electric field. *Biochimica et Biophysica Acta (BBA) - Reviews on Bioenergetics*, *505*(3), 355–427. https://doi.org/https://doi.org/10.1016/0304-4173(79)90008-9

Wolfe, G. R., Cunningham, F. X., Durnfordt, D., Green, B. R., & Gantt, E. (1994). Evidence for a common origin of chloroplasts with light-harvesting complexes of different pigmentation. *Nature*, *367*(6463), 566–568. https://doi.org/10.1038/367566a0

Xie, X., Huang, A., Gu, W., Zang, Z., Pan, G., Gao, S., … Wang, G. (2016). Photorespiration participates in the assimilation of acetate in Chlorella sorokiniana under high light. *New Phytologist*, *209*(3), 987–998. https://doi.org/10.1111/nph.13659

Yi, Q., Li, Q., Yao, S., Chen, Y., Guan, M., & Cang, X. (2019). Mitochondrion Molecular dynamics simulations on apo ADP / ATP carrier shed new lights on the featured motif of the mitochondrial carriers. *Mitochondrion*, *47*(April), 94–102. https://doi.org/10.1016/j.mito.2019.05.006

Zehr, J. P., & Kudela, R. M. (2009). Photosynthesis in the Open Ocean. *Science*, *326*(5955), 945 LP – 946. https://doi.org/10.1126/science.1181277

Zeman, I., Schwimmer, C., Postis, V., Brandolin, G., David, C., Trezeguet, V., & Lauquin, G. (2003). Four Mutations in Transmembrane Domains of the Mitochondrial ADP/ATP Carrier Increase Resistance to Bongkrekic Acid. *Journal of Bioenergetics and Biomembranes*, *35*, 243–256. https://doi.org/10.1023/A:1024611731860

Zhang, C., & Hu, H. (2014). High-efficiency nuclear transformation of the diatom Phaeodactylum tricornutum by electroporation. *Marine Genomics*, *16*, 63–66. https://doi.org/https://doi.org/10.1016/j.margen.2013.10.003

Zhang, H., Whitelegge, J. P., & Cramer, W. A. (2001). *Ferredoxin : NADP + Oxidoreductase is a Subunit of the Chloroplast Cytochrome b 6 f Complex*.

Zhu, X.-G., Long, S. P., & Ort, D. R. (2010). Improving Photosynthetic Efficiency for Greater Yield. *Annual Review of Plant Biology*, *61*(1), 235–261. https://doi.org/10.1146/annurev-arplant-042809-112206

4.9 Acknowledgment